Cranfield University

Simon David Lazarus

Energy Absorption For Crashworthiness In Carbon Fibre Braided Composite Structures

School of Industrial and Manufacturing Science

PhD

Cranfield University

School of Industrial and Manufacturing Science

PhD THESIS

2004

Simon David Lazarus

Energy Absorption For Crashworthiness In Carbon Fibre Braided Composite Structures

Supervisors: Andrew Mills and Dr. J. Spurrier

Academic Year 2000 to 2004

© Cranfield University, 2004. All rights reserved. No part of this publication may be reproduced without the written permission of the copyright holder.

ABSTRACT

In this investigation the effects of material, structural and testing parameters of carbon epoxy braided composite tubes were analysed with respect to their performance in crush and impact conditions. An original method of manufacturing the composite tubes with vacuum infusion together with an expandable foam core to form multi-cellular structures was used. Low cost, 24k tow carbon fibre braids were used and their performance was compared with that of the more expensive 12k tow size fibres. The specimens produced were axially crushed at constant quasi-static low velocities and at higher impact velocities using an instrumented falling weight machine. Load displacement data gathered from such tests were used to evaluate the test specimens with respect to their specific energy absorption values. The effects of a number of parameters including fibre tow size, braid architecture, resin content and loading type were evaluated.

From the experimental results analysed from the test specimens it can be concluded that: -

- The 24k fibre showed lower specific energy absorption values than specimens made from 12k fibre.
- Epoxy resin content rather than epoxy resin type can significantly affect the specific energy absorption values.
- In general, specimens tested in impact loading exhibited lower specific energy absorption values than the same specimens test in quasi-static crush.
- A reasonably good correlation between global density and specific energy absorption for the type of structures examined was found

Keywords:

Crush, Impact, Coretex

ACKNOWLEDGEMENTS

Firstly, I would like to thank Andrew Mills for giving me the opportunity of this study and for his continued support, insight and ability to keep me focused throughout this period. Also, Dr. John Spurrier for his guidance, advice and careful review of this work.

I would also like to thank my friends and colleagues at the Centre for Lightweight Composites at Cranfield University, in particular, Matt Frost, Jim Hurley, Axel Castaños, Andrea Marasco and Denis Cartie for their friendship and advice, both personally and professionally.

I gratefully acknowledge the financial support of the EPSRC as well as my studentship industrial sponsors at Ford motor company.

I would also like to thank my family, especially my parents, for their continued support, both emotionally and sometimes financially.

Thank you to you all.

TABLE OF CONTENTS

ABSTRACT i

ACKNOWLEDGEMENTS ii

TABLE OF FIGURES vi

TABLE OF TABLES ix

TABLE OF EQUATIONS x

1 Introduction 11

1.1 Vehicle Crashworthiness 11

1.2 Background 13

1.3 Objectives 13

2 Literature Review 15

2.1.1 Composite Materials 17

2.1.2 Test Methodologies 18

2.1.3 Crushing Modes and Mechanisms 19

2.1.4 Calculation of Specific Energy Absorption 25

2.1.5 Effect of Fibre on Specific Energy Absorption 26

2.1.6 Effect of Matrix on Specific Energy Absorption 27

2.1.7 Effect of Fibre Architecture on Specific Energy Absorption 28

2.1.8 Effect of Specimen Geometry on Specific Energy Absorption 30

2.1.9 Effect of Fibre Volume Fraction on Specific Energy Absorption 31

2.1.10 Effect of Testing Speed on Specific Energy Absorption 32

2.1.11 Braided Composites 33

2.1.12 Multi-Cellular Braided Structures – Coretex 36

2.1.13 Comment 36

3 Materials 38

3.1 Introduction 38

3.2 Fibre 38

3.3 Braids 39

3.3.1 Nominal Braid Diameter 42

3.3.2 Calculation of Braid Mass 43

3.3.3 Number and Size of Tows 45

3.4 Foam 46
3.5 Matrix 46
4 Manufacture 48
4.1 Manufacturing Process Development 48
4.2 Choice of Dimension 52
4.2.1 Cross sectional geometry 52
4.2.2 Corner radii 53
4.3 Mould Making 53
4.3.1 Wet lay-up GRP mould 53
4.3.2 PVC mould 55
4.3.3 Aluminium Mould 57
4.4 Processing 57
4.4.1 Preparation of mould tool 57
4.4.2 Infusion 58
4.4.3 De-moulding 59
4.5 Specimens for testing 60
4.5.1 Chosen Trigger 60
4.5.2 Length 61
5 Experimental 62
5.1 Introduction 62
5.2 Quasi-static Testing 64
5.2.1 Procedure 64
5.3 Impact Testing 66
5.3.1 Procedure 66
5.4 Bend Testing 69
6 Test Programme 70
6.1 Introduction 70
6.2 Test Matrix 70
7 Results 72
7.1 Introduction 72
7.2 Quality assessment of samples 72
7.3 Effect of tow size 73

7.4 Effect of original braid diameter (braid angle)....74
7.5 Effect of number of tow ends....76
7.6 Effect of internal structure....78
7.7 Effect of loading condition....80
7.8 Effect of Resin Type....82
8 Discussion....85
8.1 Tow size effects....85
8.2 Braid angle (diameter) effects....86
8.3 Effects of number of tow bundles in braid....87
8.4 Effect of internal structure....87
8.5 Resin effects....91
8.6 Effect of loading....93
8.7 3-Point Bend Tests....94
8.8 Mould Tooling....98
8.9 Summary....99
9 Conclusions....100
10 FUTURE WORK....102
11 REFERENCES....103
12 APPENDICES....109
Appendix A: Specific Energy Absorption Table....110
Appendix B: Table of Manufacturing and Testing Results Data for all Test Samples.113
Key for Manufacturing and Results Data Table....117
Appendix C: Tabulated data for each braid type showing braid mass per metre....117
Appendix D: Wall Thickness Data....118
Appendix E: Fibre, Resin and Foam data sheets....132

TABLE OF FIGURES

Figure 1 Shows (a) progressive folding of axially compressed metal tube and (b) its force-displacement curve [5].....15

Figure 2 Typical load displacement curve of a glass polyester composite tube tested axially in compression as it is crushed [6] 17

Figure 3 Typical load-displacement curve of a catastrophically failed composite tube [5] 20

Figure 4 Transverse shearing or Fragmentation mode[9] 21

Figure 5 Lamina Bending or Splaying Mode [9] 23

Figure 6 Brittle Fracturing [9] 24

Figure 7 Local Buckling or Progressive Folding [9].....25

Figure 8 Schematic illustrating Braider with braid nomenclature [35].....34

Figure 9 Geometric schematic drawing of different configurations of braided preforms [37] 35

Figure 10 Schematic illustrating plain and twill weave braid biaxial architectures.....40

Figure 11 Schematic illustrating triaxial braid architecture. 41

Figure 12 Chart illustrating the percentage change in length of a braid as a function of its braid diameter 44

Figure 13 Chart illustrating braid mass per metre with various braid parameters 45

Figure 14 Schematic illustrating coretex preform before a) and during b) an applied vacuum. 48

Figure 15 Schematic illustrating experimental set-up for coretex vacuum infusion.....49

Figure 16 Photograph illustrating fibre and resin distribution on an inner wall of a 9 cell coretex beam.....50

Figure 17 Photograph illustrating voids found between the inner walls in a 9 cell coretex beam 51

Figure 18 GRP mould closed, sealed and ready for infusion.....55

Figure 19 PVC mould showing coretex preform inside.....56

Figure 20 PVC mould with aluminium End Tabs.....56

Figure 21 Aluminium mould with no lid.....57

Figure 22 Schematic illustrating the effect of pressure on PVC mould walls at different temperatures when a vacuum is applied inside the mould. 59
Figure 23 Photo illustrating PVC mould after demoulding 60
Figure 24 a) Schematic of triggered specimen between loading platens, b) Top view of triggered specimen where dotted lines indicate chamfered walls and solid lines indicate non chamfered walls. 61
Figure 25 Chart illustrating breakdown of investigated coretex parameters.....63
Figure 26 Hydraulic Instron test machine with 250kN load cell. 65
Figure 27 A four-cell coretex beam undergoing quasi-static crush loading 65
Figure 28 Schematic of load displacement curve showing calculation of area.....66
Figure 29 Photograph of drop tower impact machine.....67
Figure 30 Coretex beam undergoing impact crush loading 68
Figure 31 Chart illustrating a typical example of an impact trace 68
Figure 32 Photo illustrating set-up of the 3-point bend test used.....69
Figure 33 Load versus displacement chart illustrating effect of tow size 73
Figure 34 Bar chart illustrating the effect of varying the original braid diameter and therefore braid angle for coretex beams tested at 10mm/min crush. Each bar shows the mean value with the error bars indicating the maximum and minimum values. 75
Figure 35 Bar chart illustrating the effect of varying the number of tow ends in a braid on specific energy absorption when tested in crush at 10mm/min. Each bar shows the mean value with the error bars indicating the maximum and minimum values. 77
Figure 36 Bar chart illustrating the effect of varying the internal structure from 4 cells to 9 cells on specific energy absorption when tested in crush at 10mm/min. Each bar shows the mean value with the error bars indicating the maximum and minimum values.....79
Figure 37 Photographs illustrating the cross section of a four-cell and nine-cell beam .80
Figure 38 '3-D' column bar chart illustrating the effect of varying the loading condition from quasi-static to impact on the specific energy absorption. 81
Figure 39 Bar chart illustrating the effect of resin type on beam type 'a' with specific energy absorption under both loading conditions. 83

Figure 40 Scatter chart plotting specific energy absorption values against global density for all coretex test specimens 89
Figure 41 Beam type ‘o’ undergoing quasi-static crush showing a progressive crush failure mode.....90
Figure 42 Beam type ‘n’ after a quasi-static crush showing accordion-type buckling failure mode.....91
Figure 43 Bar chart illustrating the effect of variation in resin mass on the density, volume fraction and specific energy absorption in beam type ‘a’ specimens.....92
Figure 44 Chart illustrating load deflection data of FMVSS 214 3-point bend test including the plan and side view of FMVSS 214 door crush test with force deflection criteria displayed graphically. 95
Figure 45 Chart displaying load displacement data for steel and glass-epoxy side impact beams [47] 96

TABLE OF TABLES

Table 1 Typical mechanical properties of STS, HTS, T700 carbon fibres with E-glass fibre. Properties selected from data published in Appendix B.....39

Table 2 Material characterisation of each braid used.....42

Table 3 Selected Material Properties of LY3505 and XU3508 epoxy resins. The full data sheet for these resins can be found in appendix section.....47

Table 4 Table illustrating combination of various parameters for test matrix.....70

Table 5 Typical data for beam type 'e'- 24K STS (48E, 40mm) and beam type 'p' - 12K HTS (48E, 40mm).....74

Table 6 Shows specific energy absorption values of a selection of polymer composite and metallic materials found in the literature.....112

TABLE OF EQUATIONS

Equation 1 Specific Energy Absorption.....26
Equation 2 Mass of braid per metre at original diameter.....43
Equation 3 Mass of braid per square metre at original diameter.....43
Equation 4 Mass of braid per metre at the diameter of use.....44
Equation 5 Equation for the total energy under load displacement graph 66

1 Introduction

Crashworthiness is of vital importance in the design of automobiles. During a crash, a properly designed structure will absorb the impact energy in a controlled manner, such that the passenger cell is brought to rest safely and the occupants are protected from exposure to dangerous decelerations.

1.1 Vehicle Crashworthiness

The techniques for providing direct human protection in vehicles are strongly related to the efficacy of the passenger cell in preventing damage to the occupant in vehicular collisions. Over the last thirty years substantial efforts have been made by manufacturers, research and design engineers to improve the crash resistance, that is, the 'crashworthiness' of their vehicles. General reference texts such as books by Johnson [1] and Mamalis [2] cover most aspects of crashworthy impact situations.

Crashworthiness can be achieved by maximising the deformation of the structural element or system up to a specified limit. A vehicle may be subjected to large load levels which consequently cause large, irreversible displacements of a part or all of the structure, but the degree of force and momentum transmitted to the protective passenger cell and its contents is significantly reduced. The use of suitable energy absorbing devices in strategic places of the vehicle is an optimal way to achieve this. The aim is to dissipate the kinetic energy irreversibly rather than convert and store it elastically.

Metals work well for energy absorption and are commonly used, but designs incorporating metallic structures tend to be rather heavy crash structures. Recently, there has been an increasing demand for lightweight, fuel-efficient vehicles, and therefore engineers are reviewing their options and designs, and composite materials are now of increased interest.

It therefore appears timely to investigate the suitability of composite materials as energy-absorbing devices for application in the automotive industry. There may be advantages in terms of initial costs and/or whole-life costs.

However, it is necessary to establish relevant test procedures, as well as choice of material, geometric structure, manufacturing methods and reliability. In particular, this work will study polymer composites and their response to impact and quasi- static loading and crushing conditions.

The structure of this thesis is described as follows.

Chapter 1 includes introduction, structure, background and objectives of thesis

Chapter 2 is a review of the current literature outlining the differences between metals and composites in the way they absorb energy under crush conditions. A description of crush failure modes found in composites is presented. A definition of specific energy absorption is illustrated together with test methodologies in obtaining this parameter. The effects of various material, architectural and geometrical parameters are reviewed. A description of braided composites and multi-cellular braided structures – Coretex is introduced.

Chapter 3 describes the materials used in the research and their typical mechanical properties. Reasons for the materials selected are given together with equations used for calculating braid characteristics

Chapter 4 details the manufacturing process used to produce 'Coretex' test samples. This includes a description of the process development undertaken in manufacturing outlining difficulties encountered with mould tool design and a modified version of vacuum infusion liquid composite processing uniquely used to make structures – Coretex – is introduced. Choice of dimensions and test sample size are also described.

Chapter 5 Describes the procedures used in testing the manufactured samples detailing methods and calculations used to determine the energy absorbed under impact and quasi-static axial loading conditions as well as in bending. A chart

illustrating how the various material parameters involved in coretex structures are categorized.

Chapter 6 Illustrates how the various material parameters are organized into different beam types which form an organized testing matrix used. A list of effects of particular parameters that can be examined due to the testing matrix is presented.

Chapter 7 Graphically states the results obtained from the experimental testing with a discussion of these results detailed in chapter 8.

Chapter 9 states the conclusions from this research with chapter 10 outlining future work. Data characterizing each test sample including their performance in testing is recorded in tabulated form and shown in the appendix together with company data sheets for the materials used. Photographs of typical beam cross sections are illustrated with measured values of wall thickness for each cross section shown.

1.2 Background

DTI funded research programmes conducted at Cranfield University [3, 4] prior to this thesis in order to attempt to develop a manufacturing technology for lightweight vehicle structures and components saw the conception and initial development of a novel design and materials approach using a braided textile preform to form a single integrated frame structure. The potential use of these braided structures as crashworthy energy absorbing structures was identified as a result of this work.

1.3 Objectives

Following the above research a review of the current published literature was conducted and the following objectives were identified for this research.

1. Examine the properties of manufacture of carbon fibre coretex composite beams in terms of time, temperature and pressure with particular reference to foam stability and resin flow.

2. Investigate various designs and materials for use in mould tools to minimize time and cost factors in the manufacturing process.
3. Look into the effect that fibre angle and number of tows of a braided preform has on the energy absorbing performance of coretex structures in axially loaded crushing to identify the most efficient fibre architecture.
4. Determine whether a change from low (crush) to high (impact) loading rates has any effect on the specific energy absorption of the beams when subjected to axial crush loading.
5. Identify whether the internal geometry of a multi cellular beam has an effect on the energy absorption characteristics of that beam when tested under axial crush loading.
6. Investigate the effect of changing the tow size and fibre type in the coretex beams with respect to their performance in absorbing energy, while being aware of the cost factors involved.
7. Identify the effects of amount and type of resin used on the specific energy absorption capability of the beams.

2 Literature Review

Traditionally, metals have been used for crashworthy structural applications. Although small amounts of energy are stored elastically, their benefit is that they can absorb considerable impact energy by plastic deformation. Figure 1a shows the progressive folding of a metal tube by plastic deformation when it is compressed axially. A typical force-displacement response is shown in Figure 1b, where the area underneath the curve indicates the energy absorbed for the specified length.

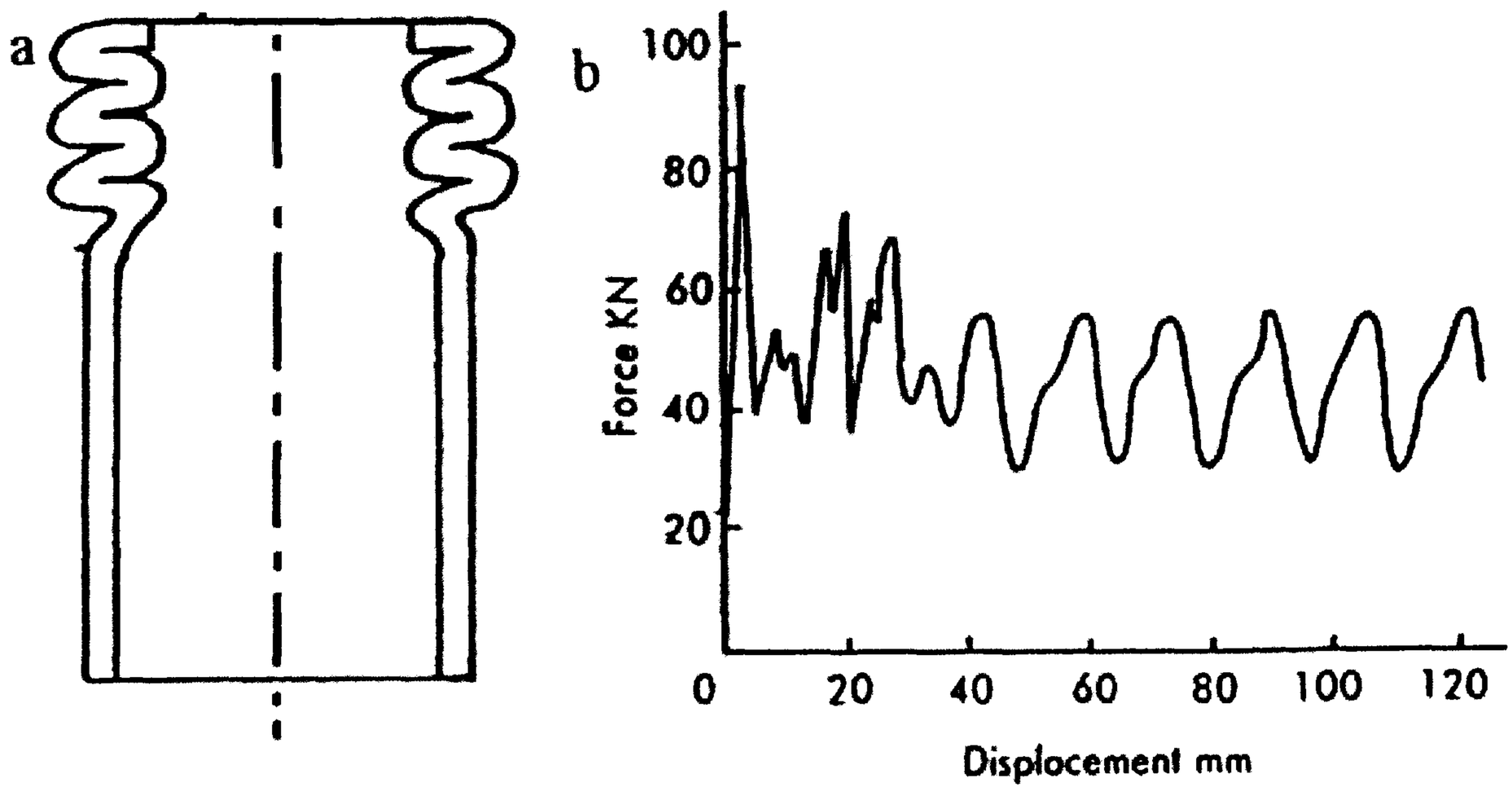


Figure 1 Shows (a) progressive folding of axially compressed metal tube and (b) its force-displacement curve [5]

Unlike metals, brittle fibre reinforced polymer composites typically display little plastic deformation characteristics. Carbon fibre reinforced epoxy composites are inherently brittle and typically fail after elastic deformation of about 2% strain. The stored elastic energy before fracture is converted into the surface energy of the fractured parts and kinetic energy. If poorly designed, these processes absorb little energy and fracture is invariably uncontrolled and catastrophic. A typical load-displacement curve of a

catastrophically failed composite tube is illustrated in Figure 3, and will be discussed in section 2.1.3.

However, properly designed polymer composite materials absorb more energy per unit mass of material than conventional metals. That is they exhibit higher values of specific energy absorption or SEA. The calculation and data for this will be presented in section 2.1.4. A table displaying specific energy absorption values of a selection of composite and metallic materials can be found in Appendix A. It is noted that in some cases, specific energy absorption values quoted from the literature show an extremely wide range of values for a given material. However, this does not mean that any values are particularly right or wrong but emphasises the fact that there are many factors which control the energy absorption capability of materials, especially composites. It is noted here that the specific energy absorption values given for aluminium are higher than some of those given for some composite materials. However, there are a number of carbon-PEEK and carbon-epoxy composites that show higher specific energy absorption values than those found in metallic structures. Glass-polyester and Kevlar-epoxy composite materials show relatively low values of specific energy absorption, some of which are values lower than that found for mild steel. This highlights how the choice of fibre and matrix material in a composite structure can greatly affect its efficiency in absorbing energy.

The following chart, Figure 2, illustrates a typical load displacement curve of a glass polyester composite tube loaded axially in compression until it is crushed [6].

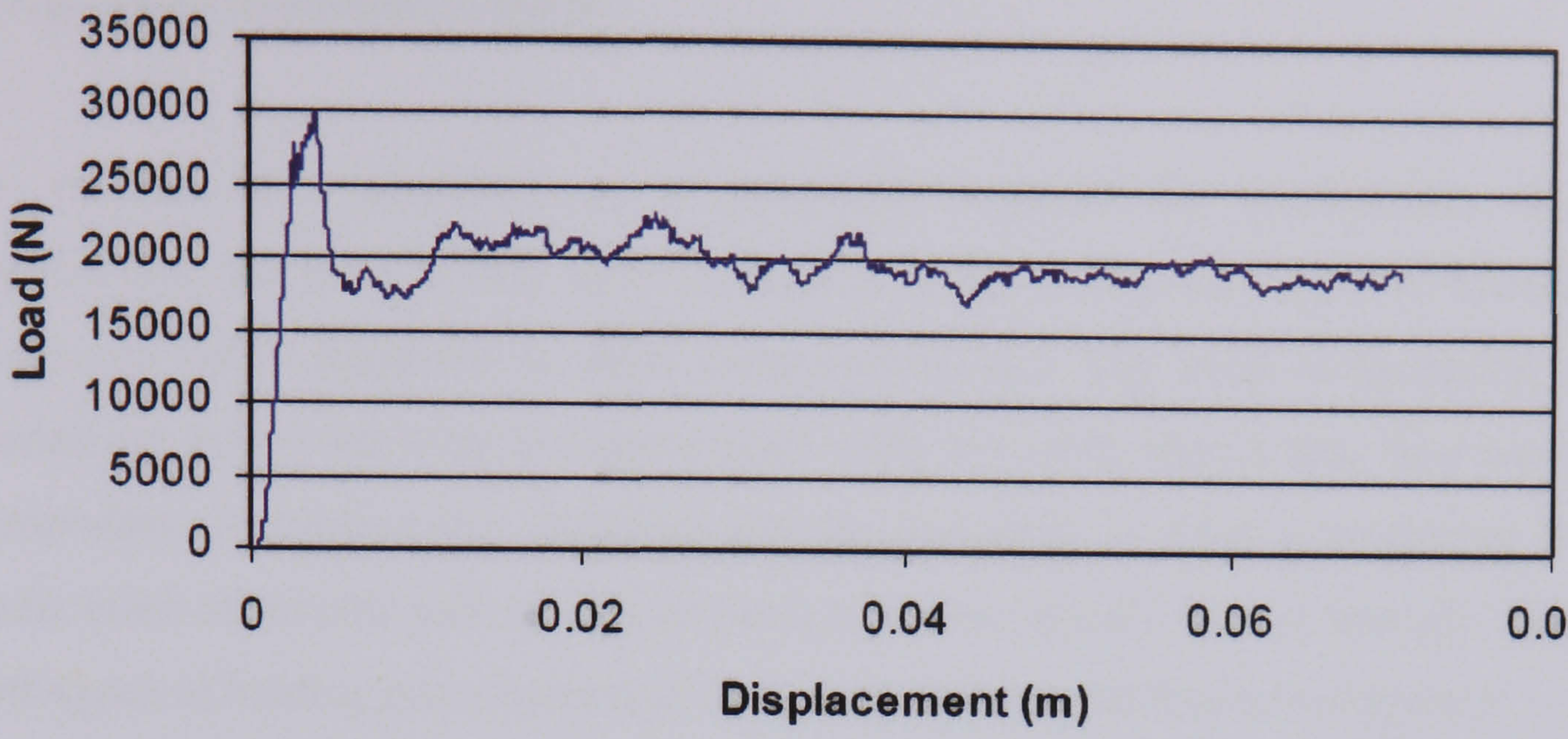


Figure 2 Typical load displacement curve of a glass polyester composite tube tested axially in compression as it is crushed [6]

This curve displays a relatively smooth crush load along the displacement compared to the metal structure shown in Figure 1. This aspect is attractive for designing crashworthy vehicle structures as a fairly constant crush load means that the decelerations on the passenger cell of a car are relatively constant and do not oscillate as they can in metal structures.

2.1.1 Composite Materials

Generally composite materials consist of two distinct constituents. One of these, the reinforcement, is said to enhance the properties of the other constituent which is known as the matrix. Most man-made composites in industrial use are based on polymeric matrices such as thermosets and thermoplastics. Typically, the reinforcement used in these types of composites is aligned synthetic inorganic fibres such as carbon and glass. The significant difference in material properties, such as stiffness, between the fibres and matrix allows for marked anisotropy. That is to say, their properties vary significantly when measured in different directions. In the manufacture of composites, the potential for controlled anisotropy - that is the ability to place and orientate the fibres preferentially within the matrix - offers considerable scope for integration between the processes of material specification and material design.

2.1.2 Test Methodologies

To evaluate the suitability of a composite material for crashworthy structural applications, the most widely used practice is to understand the crushing behaviour of composite tubes subjected to axial compressive load. The axial compression can be carried out in two ways: by low speed quasi-static test or by impact test. However, not all composites in crashworthy situations can be evaluated in axial compressive loading. Some crash structures such as side impact protection bars are loaded laterally. Details of both types of loading procedures used in this research can be found in chapter 5.

2.1.2.1 Quasi-Static Testing

In quasi-static testing specimens are crushed at a constant speed. This, however, may not be a true simulation of a real crash condition. This is because in an actual crash scenario the structure would undergo an initial impact velocity, which would then reduce to zero. As the structure's material may be strain rate sensitive the speed of the impact may also be a factor in the energy absorbing ability of the structure. Therefore a structure exhibiting good energy absorption behaviour under quasi-static crush conditions does not ensure satisfactory performance in an actual crash.

However quasi-static tests do have their advantages. They are easy and simple to control. As a result they are simpler and less expensive than impact tests [7].

2.1.2.2 Impact Testing

As discussed above, impact testing is a true simulation of a crash condition as it includes the factor of strain rate with a decreasing velocity to rest.

However, impact test equipment is relatively expensive and is coupled with the need for high-speed data recording devices such as high-speed video cameras to capture failure mechanisms. Typically impact test machines found in research establishments such as

universities are capable of achieving impact velocities from 1 to 10m/s. However, it is noted that in a real crash situation velocities far exceeding that capable of common impact test machines could be observed. For comparison 30 miles per hour equates to 13.3 metres per second

2.1.3 Crushing Modes and Mechanisms

2.1.3.1 Catastrophic Failure Modes

A catastrophic failure mode is characterised by a sudden increase in load to a peak value followed by a low post failure load. This can take place when unstable intralaminar or interlaminar crack growth occurs. This leads to brittle fracture failure by compressive shear or axial splitting of the tube wall [5].

This has also been found to happen in long thin walled tubes due to the column instability.

As tubes undergoing catastrophic failure are relatively inefficient in absorbing energy, structures designed to fail in this mode are usually designed to be heavier than structures that fail progressively[7].

Furthermore the peak load tolerated in a catastrophic failure may well by too high to prevent injury to the occupants of an automobile.

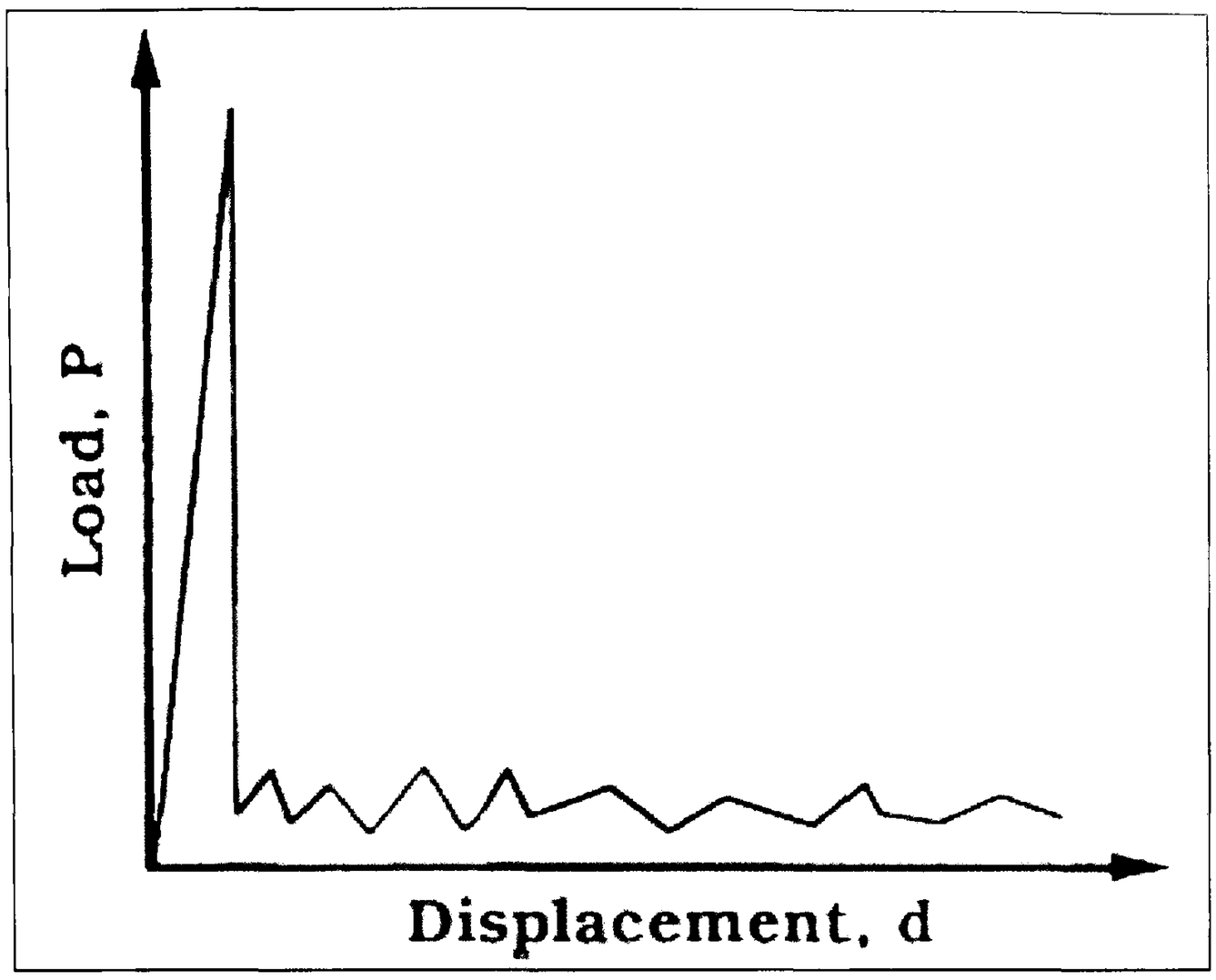


Figure 3 Typical load-displacement curve of a catastrophically failed composite tube [5]

2.1.3.2 Progressive Failure Modes

A progressive failure mode is characterized by energy being absorbed in a controlled manner. A common way to obtain this mode is to have a trigger; which is typically a machined chamfer on one end of the structure that reduces the initial load peak that accompanies failure initiation. Applying a load generates high stresses in the chamfered region forming local high stresses that initiate micro fractures in this region leading to the formation of a stable crush zone.

Energy absorbed in progressive crushing is larger than the energy absorbed in catastrophic failure. As a result progressively failing energy absorbers are lighter than structures designed to absorb energy catastrophically [7].

A number of other trigger geometries such as bevels, grooves and holes that have been investigated in laboratory specimens are not as easy to use in vehicle structures [8].

The following subheadings describe the various modes of progressive failure found in composite structures designed for axially loaded crash scenarios. Terms such as

'fragmentation mode', 'splaying mode' and 'local buckling' which are used later in the thesis are defined here.

2.1.3.3 Transverse Shearing or Fragmentation Mode

The transverse shearing and fragmentation mode is characterised by a wedge-shaped laminate cross section with one or multiple short interlaminar and longitudinal cracks, which form partial lamina bundles [9]. The main energy absorbing mechanism is fracturing of the lamina bundles, where the number, location and length of the cracks are a function of the material structure and its properties. The lamina bundles act as columns to resist the applied load. Interlaminar cracks grow until the edges of the column are fractured forming a wedge-shaped cross section, as illustrated in Figure 4.

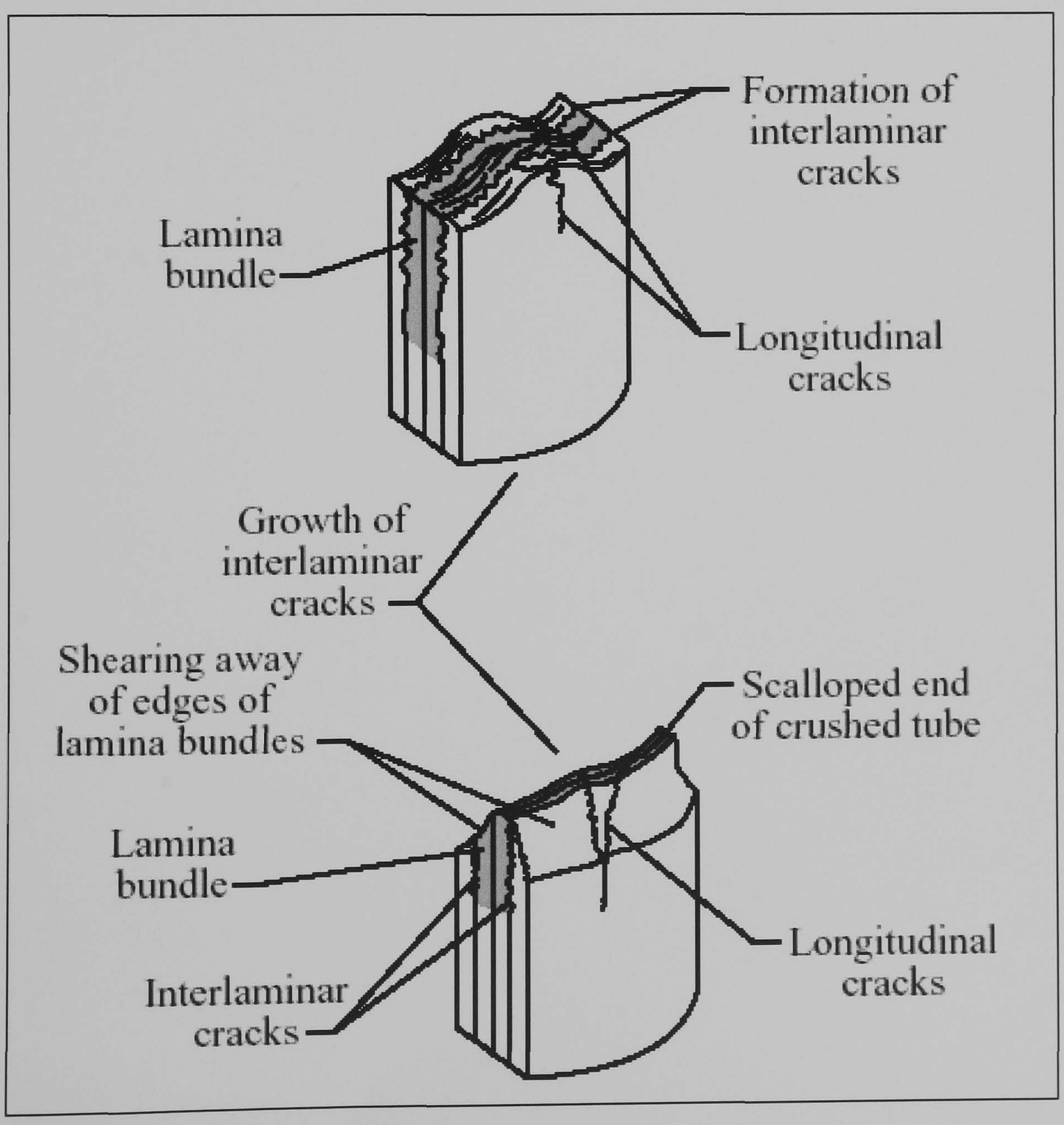


Figure 4 Transverse shearing or Fragmentation mode[9]

2.1.3.4 Lamina Bending or Splaying Mode

Long interlaminar, intralaminar and parallel to fibre cracks are characteristics of failure by lamina bending or splaying mode. The main energy absorbing mechanism is crack growth. The lamina bundles do not fracture but exhibit bending deformation or splaying [10], illustrated in Figure 5. Two secondary energy-absorbing mechanisms are also identified; these are associated with frictional forces [11]. As the bundles bend, friction occurs between the sliding bundle and the loading surface. Also friction occurs when the bundles slide over each other during bending.

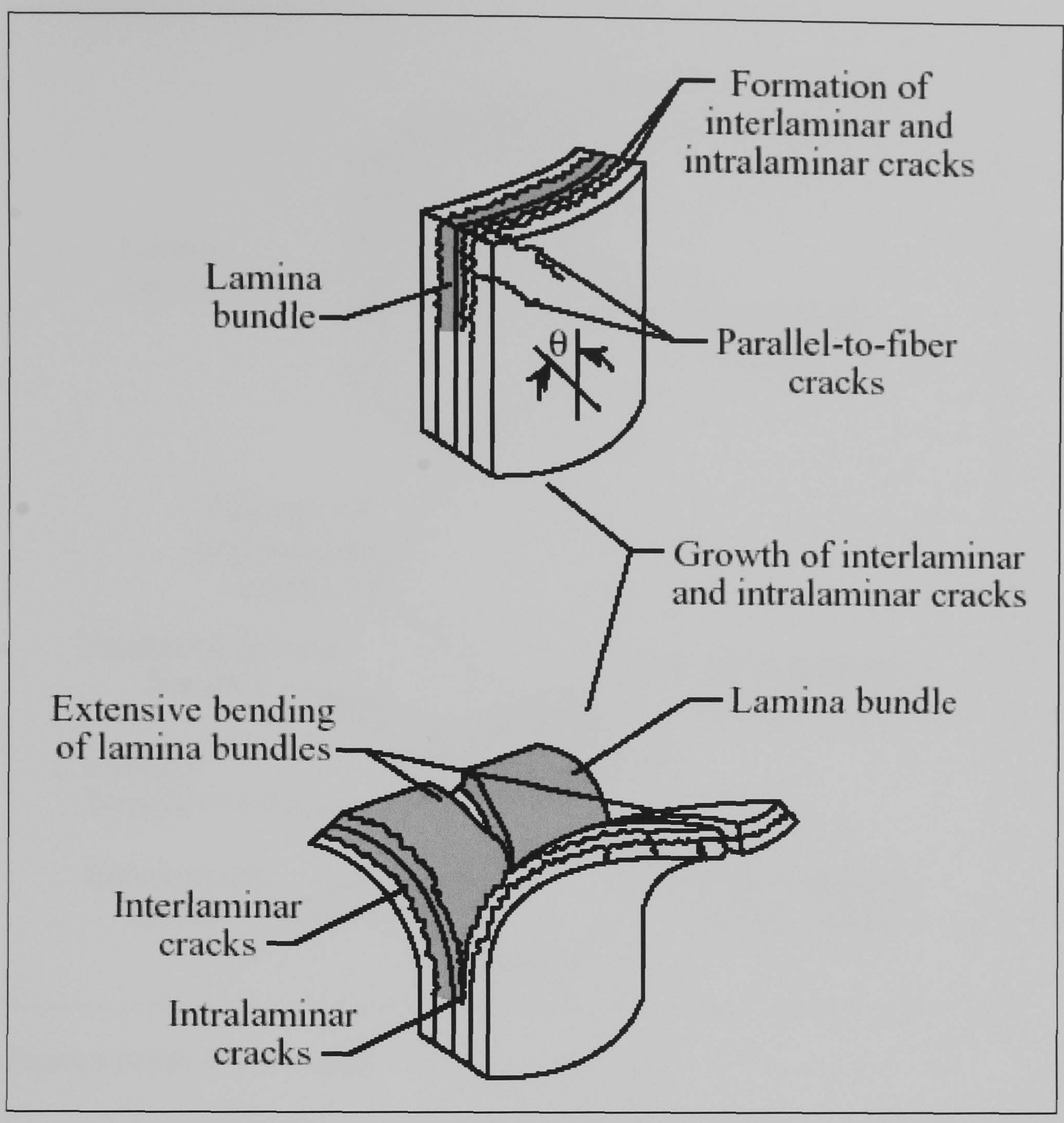


Figure 5 Lamina Bending or Splaying Mode [9]

2.1.3.5 Brittle Fracturing

Brittle fracturing in crushing mode is really a combination of the transverse shearing and lamina bending crushing modes [9] mentioned in the two previous paragraphs. The lengths of interlaminar cracks in brittle fracturing mode are larger than those exhibited in transverse shearing but smaller than those illustrated in lamina bending. Consequently their mechanism of energy absorption is a combination of the two. See Figure 7.

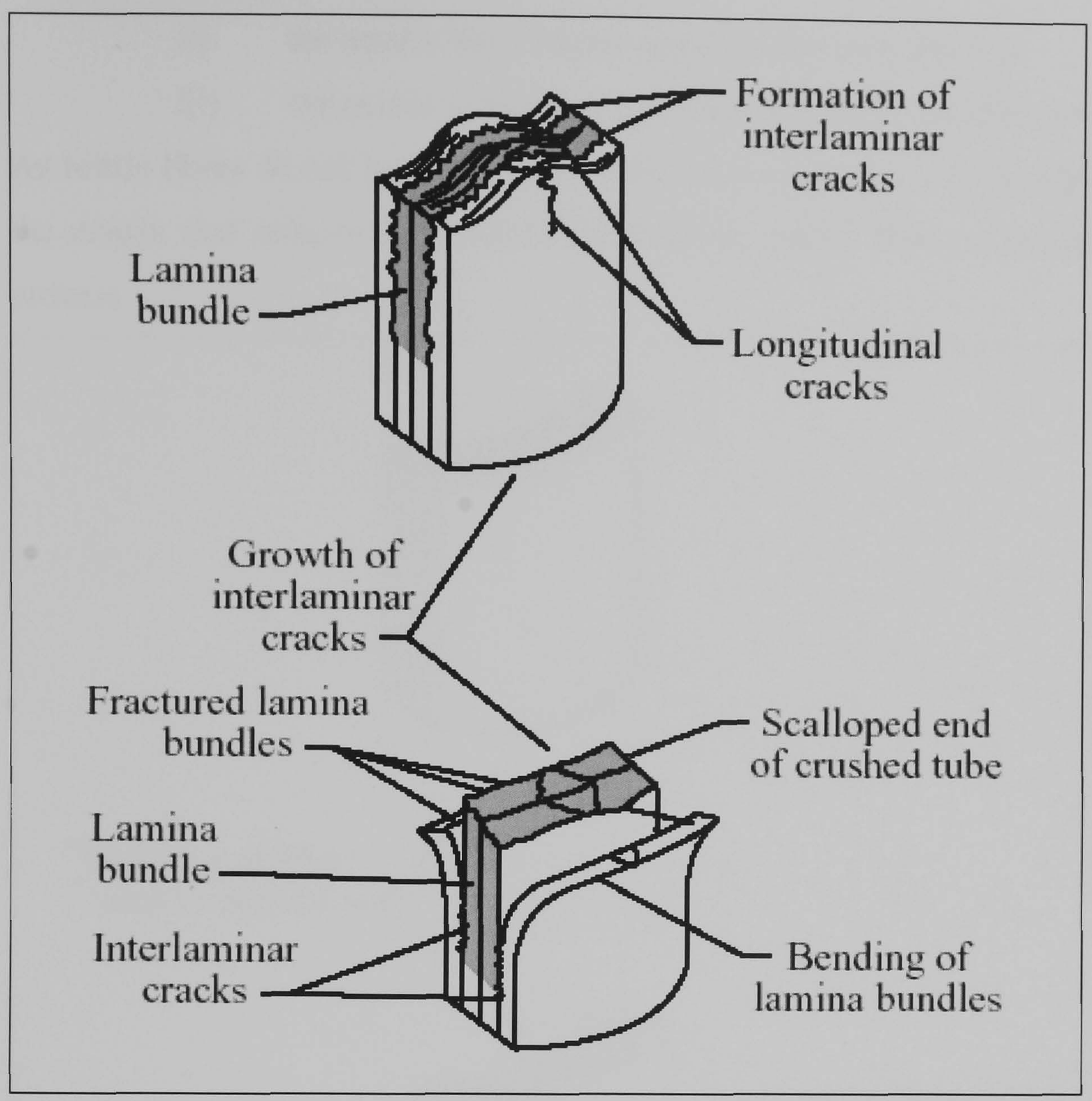


Figure 6 Brittle Fracturing [9]

2.1.3.6 Local Buckling or Progressive Folding

The local buckling mode exhibited by both brittle and ductile fibre reinforced composite materials is similar to that exhibited by ductile metals [9]. Here the crushing mode consists of the formation of local buckles by means of plastic deformation of the material as illustrated in Figure 7.

Ductile fibre reinforced materials, such as Kevlar, plastically deform at the buckle site along the compression side of the buckled fibres [12]. Ductile fibre reinforced composites remain intact after being crushed and thereby demonstrate post-crushing integrity. This is a result of fibre and matrix plasticity and fibre splitting.

Brittle fibre reinforced composites only exhibit local bucking crushing mode when

i) the interlaminar stresses are small relative to the strength of the matrix

ii) the matrix has a higher failure strain than the fibre

iii) the matrix exhibits plastic deformation under high stress

As brittle fibres do not have a plastic stress-strain response, it is the high failure strain of the matrix that reduces or prevents interlaminar cracks from occurring in the crushing process.

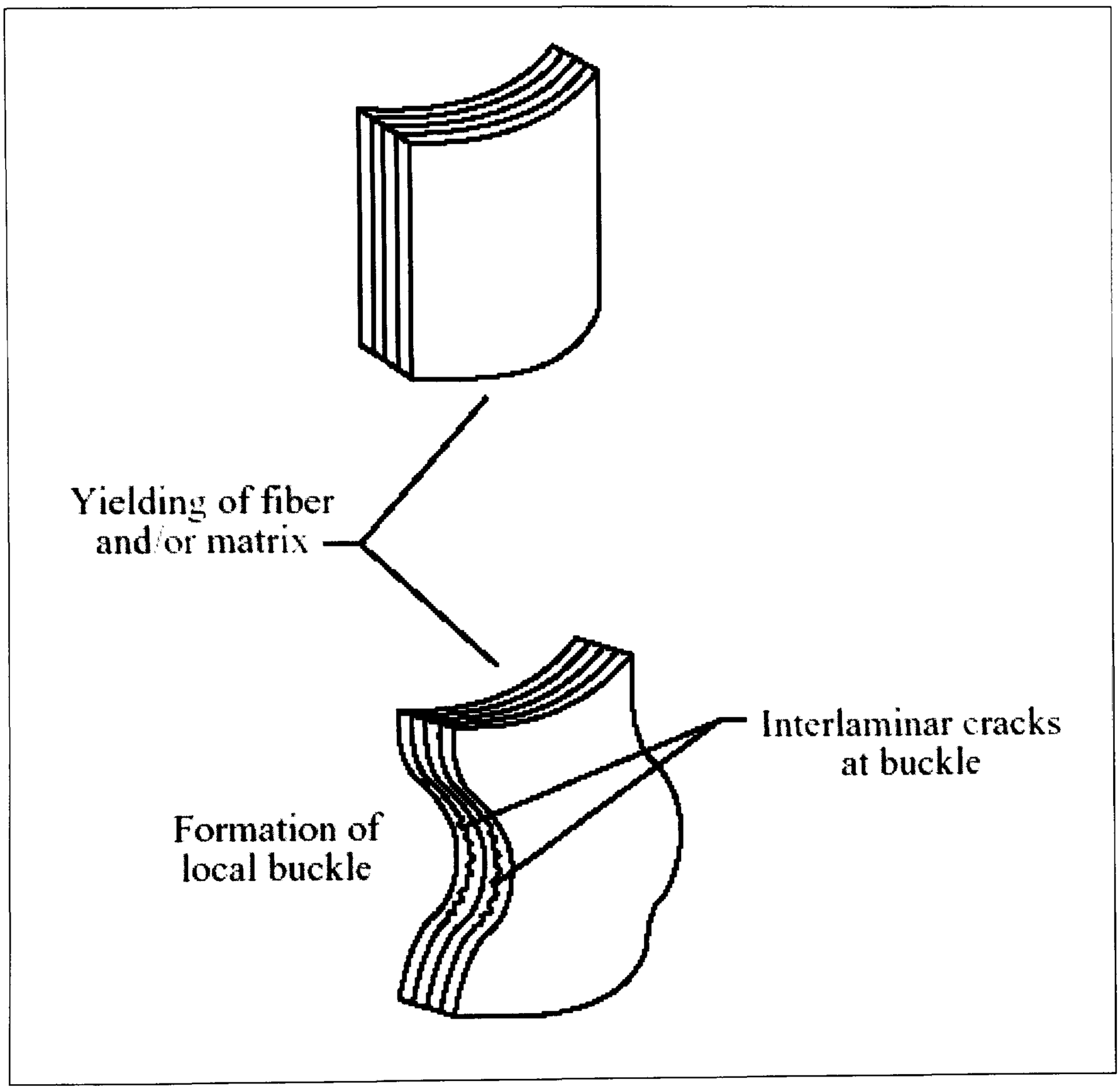


Figure 7 Local Buckling or Progressive Folding [9]

2.1.4 Calculation of Specific Energy Absorption

The crashworthiness of a material is expressed in terms of its specific energy absorption Es (SEA) that is characteristic to that particular material. It is defined as the energy absorbed per unit mass of crushed material.

Mathematically

$$SEA = W / m$$

$$W = \int_0^x P dx$$

$$m = Al\rho$$

$$SEA = \frac{\int_0^x P dx}{Al\rho}$$

Equation 1 Specific Energy Absorption

Where W, the total energy absorbed, is calculated by integrating the area under the load-deflection curve.

P is the load

x is the displacement

m is the mass

A is the cross-sectional area of crushed material

ρ is the density of the material, and

l is the length of the material crushed

2.1.5 Effect of Fibre on Specific Energy Absorption

The energy absorption characteristics of composite material are dependent on the type of matrix (see section 2.1.6) and the reinforcing fibres used. Glass and carbon fibre reinforced thermoset tubes were found to progressively crush in splaying and fragmentation modes [13-18], whereas aramid fibre reinforced thermoset tubes were found to crush by a progressive folding mode [19].

Schmuesser and Wickliffe [12] also noted a different failure behaviour of Kevlar/epoxy tubes compared to carbon and glass epoxy tubes when crushed statically. The graphite/epoxy and glass/epoxy tubes displayed brittle failure modes consisting of fibre tows splitting and ply delamination. Kevlar/epoxy composite tubes failed in an accordion-type buckling mode similar to that obtained by metals. As all the tubes tested in this study used a common matrix material, the differences in failure modes are directly related to the fibre failure characteristics where the Kevlar fibres had a more inelastic response with little fibre splitting.

Hamada [20] compared Carbon(AS4)/PEEK, Carbon(IM7)/PEEK and Glass(S2)/PEEK tubes under crushing tests. All tubes crushed progressively by the splaying mode. However, the specific energy absorption of the Glass(S2)/PEEK was 20% less than that of the Caron(AS4)/PEEK and Carbon(IM7)/PEEK tubes even though the mean crush stress of all the tubes was comparably the same. This indicates how the lower density carbon fibres display a higher specific energy absorption compared to the Glass(S2)/PEEK tubes.

Farley [14] noted that graphite/epoxy tubes which failed in a brittle mode had high specific energy absorption values compared to Kevlar/epoxy tubes. However, graphite/epoxy tubes exhibited negligible post crush integrity whereas Kevlar/epoxy tubes, failing in an accordion buckling mode exhibited post crush integrity. Post crushing structural integrity with respect to crashworthy structures is where the structure remains intact to provide protection for the occupants. Chiu [21] compared carbon/epoxy and kevlar/epoxy 3-D braided square tubes and also found that carbon/epoxy tubes had specific energy absorption values 24% higher than kevlar/epoxy tubes but the kevlar/epoxy tubes demonstrated good post structural integrity.

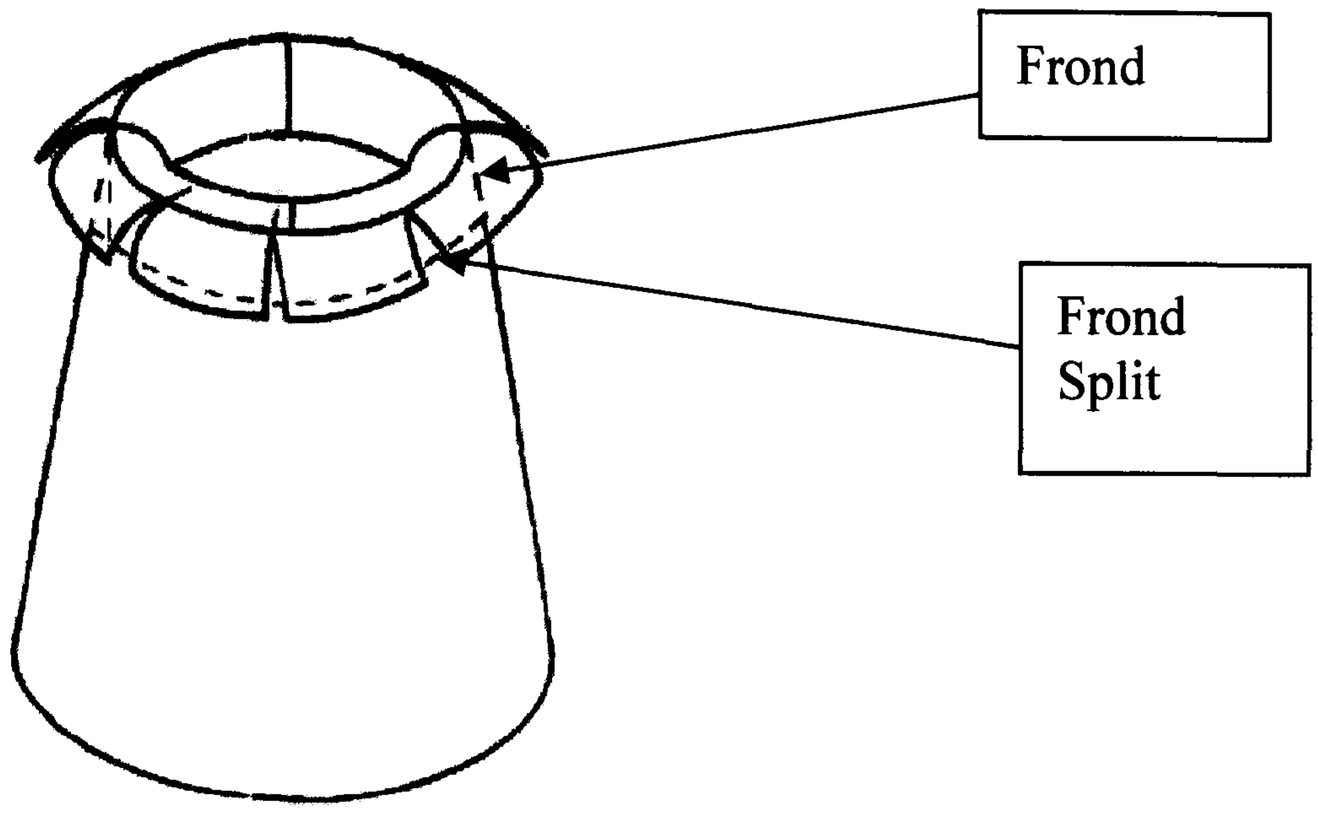
2.1.6 Effect of Matrix on Specific Energy Absorption

Higher interlaminar G_{IC} values of matrix cause an increase in energy absorption. An increase in matrix failure strain causes increased specific energy absorption with brittle fibres and decreased specific energy absorption with ductile fibres. [16]

Tao et al. [22] demonstrated that the specific energy absorption increases with matrix compressive strength for glass composite rods. Thornton and Jeryan [23] showed that specific energy absorption depends in a linear trend on the tensile strength and modulus of thermosetting resin, and, specifically, not on the fracture toughness of the resin. However, Ramakrishna [24] observed increasing specific energy absorptions for a range of high temperature thermoplastic matrices, which correlated with the increasing matrix fracture toughness. Warrior et al. [25] focused on the effect of thermoset resin-related parameters on the specific energy absorption of composite tubes. They found that the best indicator of specific energy absorption performance was the ultimate compressive strength of the composite.

2.1.7 Effect of Fibre Architecture on Specific Energy Absorption

Ramakrishna [26] found that the specific energy absorption of progressively crushed carbon fibre tubes with various thermoplastic matrices was a function of the angle of fibre lay up. In general, as the angle increases (from 0° to +/-15°) the lengths of the longitudinal cracks decrease. This was attributed to the increase in angle of fibre. This improved fracture toughness and offered more resistance to the crack growth process. Also micro fracture processes such as fibre fracture and frond splits increased with increasing angle. The following diagram illustrates a frond and frond split on an axial loaded circular cone.



However, in Farley's [16] carbon epoxy tubes with fibre architecture $[0\pm\theta]_4$, specific energy absorption decreased with an increasing θ from 0° up to 45°. The crushing mode is primarily brittle fracture and the decrease in specific energy absorption was attributed to the reduction in in-plane axial strength of the composite material. This caused a reduction in the average loads sustained during crush and so less energy was absorbed as a consequence.

Schumuser and Wickliffe [12] also found specific energy absorption values vary with ply orientation but found that $[0_2/\pm\theta]$ [1]carbon / epoxy specimens have *increased* specific energy absorption capability as θ is increased. However, testing conditions appear to be different from Farley's in that a drop tower dynamic impact was used as opposed to quasi-static testing. Furthermore, it appears that no collapsible trigger mechanism has been used to promote stable failure, unlike Farley's specimens.

Farley's glass and Kevlar epoxy specimens however show an increase in specific energy absorption with increasing fibre angle. This may be attributed to laminar bending and local buckling crushing modes observed in the glass/epoxy and Kevlar/epoxy tubes respectively as compared to brittle fracturing in carbon/epoxy specimens. Farley

---

[1] Where $[0_2/\pm\theta]$ denotes both lay-up and stacking sequence of a laminate thus showing $(0/0/+\theta/-\theta)$ where θ is a fibre angle between 0 and 90.

attributed this increase in energy to the increased lateral support to the axial fibres with increasing θ.

From the above literature reviewed on the effect of fibre architecture on specific energy absorption it is not clear whether increasing or decreasing fibre angle will improve the composite's specific energy absorption in crush. The idea that the type of loading subjected to the structure, that is quasi-static or impact loading, may influence this effect on weather it increases or decreases the structures energy absorption capability. The research found on effect of fibre angle on specific energy absorption has been conducted on laminated composite tubes. However, it is expected that angle effects in braided tubes will show similar trends as both processes use long continuous fibres. Due to the woven nature of braids, equivalent in-plane mechanical properties of braided structures are expected to be lower than those seen in laminated structures.

2.1.8 Effect of Specimen Geometry on Specific Energy Absorption

In 1986, Farley's published paper [13] reported his investigation into the influence of the ratio of the inside tube diameter to wall thickness (D/t) on the energy absorption of statically axially crushed carbon and Kevlar / epoxy circular laminate tubes. Specific energy absorption was found to fall non-linearly as D/t increases. In addition, Farley reported that the carbon-epoxy specimens exhibited different non-linear dependencies on D/t for specimens of different internal diameters. The Kevlar-epoxy tubes of all diameters exhibited no such diametrical dependence; implying that Kevlar-epoxy tubes can be geometrically scaled for energy absorption whilst carbon-epoxy tubes cannot. It is suspected that the lack of scalability for carbon-epoxy is partially due to a local instability mode reducing the buckling load of the lamina bundles. The Kevlar-epoxy tubes are geometrically scalable, as they have metallic like crushing characteristics. That is, the crushed region of the tube plastically deforms. The buckling of the lamina bundles and subsequent plastic deformation of the fibre causes the Kevlar composite to crush in an accordion-type manner.

Thornton and Edwards [17] reported large changes in the specific energy absorption characteristics of carbon-epoxy and glass-epoxy with a range of values of tube diameters, wall thickness and t/D ratio. They varied the relative density in the range from 0.01 to 1.0, where the relative density = (volume of the tube / volume of solid of the same external dimensions). They indicated that below a certain relative density (0.025 for carbon-epoxy and 0.045 for glass-epoxy) the tube crush would be unstable. They also reported that for tubes, which are crushed in a stable manner, the specific energy is essentially independent of the tube dimensions. However, details of the crush zone morphology are not available.

Hamada *et al.* [27] studied the crushing performance of carbon/PEEK tubes with different t and D values ranging from 35.5 to 96 mm for D and 0.28 to 10.54 mm for t. In the case of thermoplastic tubes, it was found that the specific energy absorption characteristics are mainly influenced by the absolute value of t rather than the t/D ratio.

Thornton and Edwards [17] report that the square and rectangular cross-section tubes are generally less effective at absorption energy than circular ones when tested axially. These finding are also supported by Mamalis *et al.* [28] who report that square and rectangular cross-sectioned tubes have, respectively, 0.8 and 0.5 times the S.E.A. of comparable circular tubes. This is generally attributed to the fact that the corners act as stress concentrations leading to the formation of splitting cracks. This tends to result in unstable collapse with low energy absorption. In addition Mamalis *et al.* [28] report that the axial length of the square tube does not affect the crashworthy capability when subjected to axial loading and collapsing in a stable manner.

2.1.9 Effect of Fibre Volume Fraction on Specific Energy Absorption

Findings from Ramakrishna, Hull and Thornton [29] indicate that specific energy absorption increases with increasing fibre content. One possible explanation for this is that a higher tube loading is associated with the generation of larger surfaces due to fibre/matrix de-bonding which results in increased specific energy absorption.

However, Farley's work [16] has found that increasing the fibre volume fraction of carbon/epoxy tubes from 40% to 70% resulted in a decrease in specific energy absorption. Farley attributed this to the decrease in interlaminar shear strength of the composite with an increase in fibre content. It should also be noted that increasing the fibre volume fraction of the composite would also increase the overall density of the composite assuming that the fibres have a higher density than the matrix, for example carbon fibre density is 1.75 g/cm^3 compared with epoxy with a density of 1.15g/cm^3. So if the specific energy absorption of the composite is to increase the crush load must increase by an amount that exceeds the increase in composite density.

2.1.10 *Effect of Testing Speed on Specific Energy Absorption*

Many researchers have investigated the influence of strain-rate on the energy absorbing capacity of composite shells subjected to axial loading. Experimental work has been carried out on static and dynamic crushing, but conflicting results have been produced. Energy absorption has been shown to increase [30], reduce [31] [12], and be independent of [14] an increase in velocity.

Farley [30] reported that matrix stiffness and failure strain can be a function of strain-rate and, therefore, the energy absorption associated with interlaminar crack growth may be considered as a function of crushing speed. However, he also reported that the mechanical properties of brittle fibres are generally insensitive to strain-rate and, therefore, the fracturing of the lamina bundles generally is not a function of crushing speed. Farley tested various circular tubes loaded axially and reported that the energy absorbing capability of the tubes was influenced by the crushing speed. Carbon-epoxy $[\pm\theta]_3$ specimens were crushed at constant speeds between 0.01m/s and 12m/s, where a weak function of crushing speed with specific energy absorption was found with an increase of 35%. However, the $[0/\pm\theta]_2$ carbon-epoxy tubes were not found to be a function of crushing speed. Earlier work by Farley [14]tested carbon-epoxy tubes with ply orientations of $[0/\pm\theta]_4$ dynamically and the results obtained also suggest that energy

absorption capability of the composite material was not a function of crushing speed. Hence, it may be assumed that with the $[0/\pm\theta]_2$ carbon-epoxy specimens, the fibre (whose mechanical properties are not a function of strain-rate) controls the crushing process, whilst with the $[\pm\theta]_3$ carbon-epoxy tubes, the matrix (whose mechanical properties are a function of strain-rate) is the primary influence [30].

Thornton [32] reports a 20% increase in specific energy absorption with test speed for glass-polyester tubes and a 10% decrease in specific energy absorption for glass-vinyl ester specimens. This indicates the significance of the choice of matrix to be used in energy absorbing specimens.

Ramakrishna [20] reports specific energy absorption values of carbon-PEEK tubes to be reduced by 50% under impact conditions compared to quasi-static conditions with the same progressively crushed splaying mode being observed in both loading conditions.

From these findings it is difficult to predict the effect of loading rate on braided carbon epoxy tubes.

2.1.11 Braided Composites

Braiding is a technique that is most probably the oldest textile technology known to humans. It is known for its simplicity and versatility and has been used for a variety of applications in many different areas[33].

The commercial textile process of braiding dates back to the early 1800s. In braiding, a mandrel is fed through the centre of the machine at a uniform rate, and fibre yarns from the moving carriers on the machine braid over the mandrel at a controlled rate. The carriers work in pairs to accomplish an over/under braiding sequence [34].

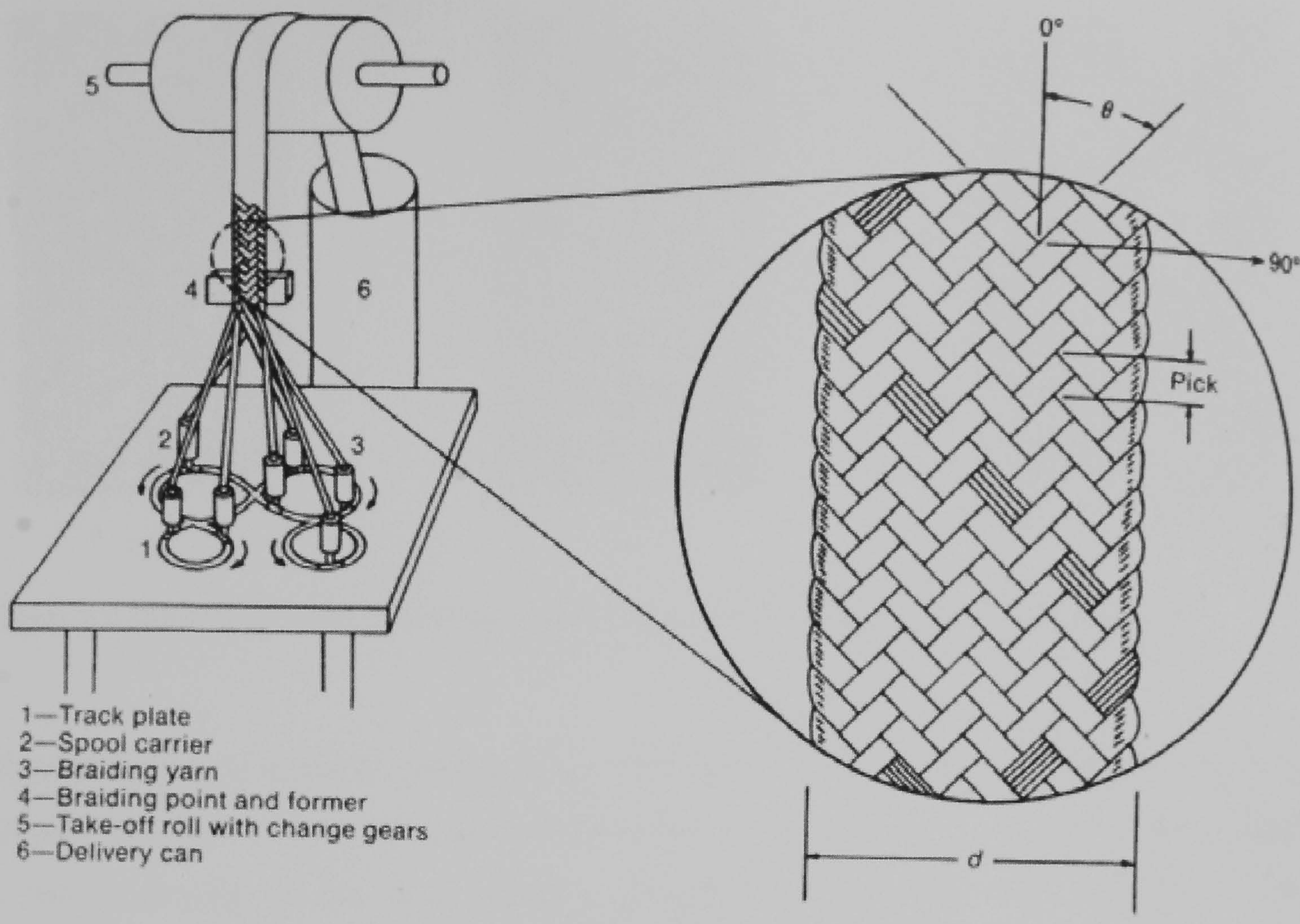


Figure 8 Schematic illustrating Braider with braid nomenclature [35]

Braids are formed by interlacing three or more yarns so that each yarn passes over and under one or more of the others. Braids are divided into two types: (i) flat braids, in the form of narrow flat tapes and (ii) tubular braids, which may be hollow or have a centre core.

The geometric configurations of some 2-D braids are given in Figure 9 below. The first one (a) shows the braid with a 2/2 repeat of intersecting pattern, and it is known as a regular, plain or standard braid. Figure (b) gives a diamond or basket braid, which is characterized by a 1/1 repeating pattern. Figure (c) is a regular braid with longitudinal in-laids, and it is also called a triaxial braid because of the three directional fibre orientations.[36]

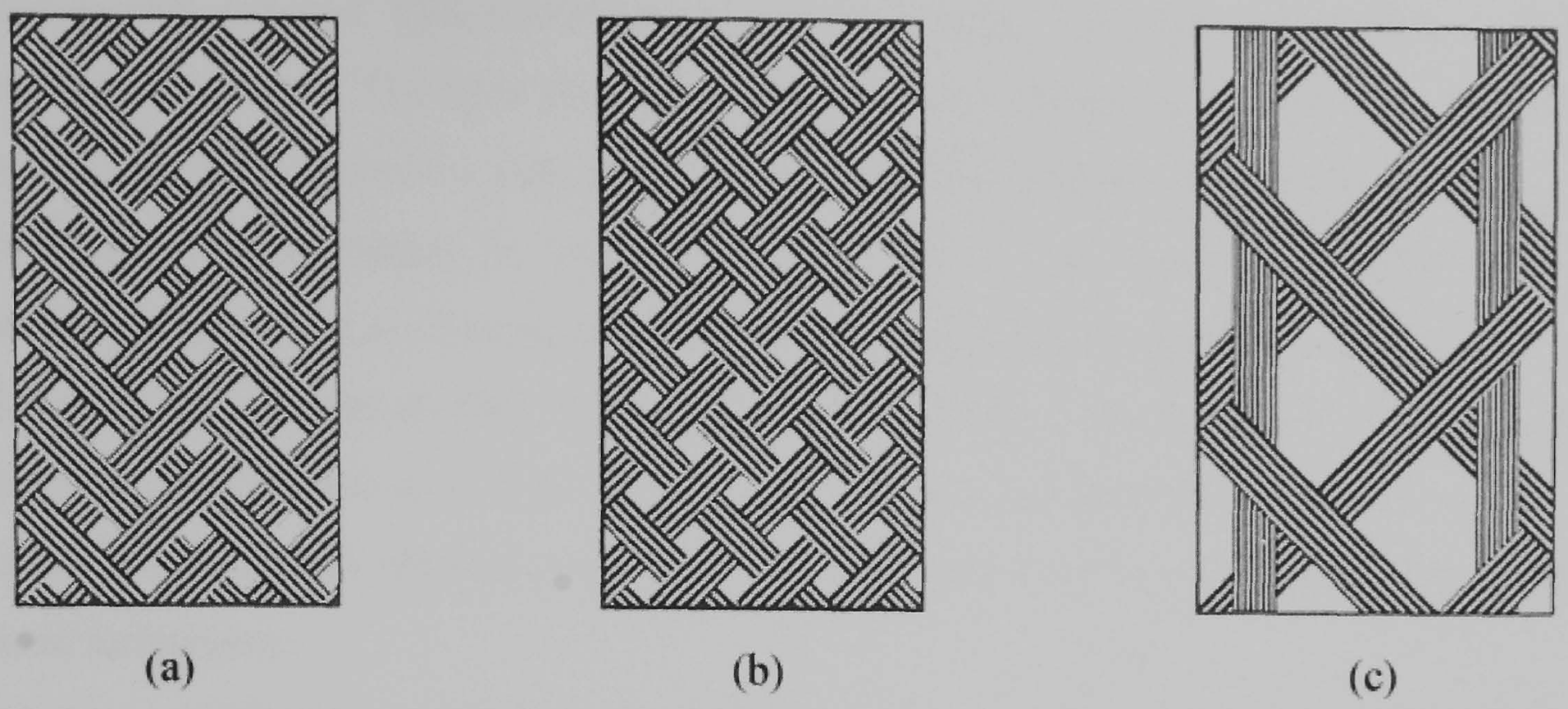


Figure 9 Geometric schematic drawing of different configurations of braided preforms [37]

Braided fabric is a good candidate for reinforcement of composite materials such as tubular structures. When compared to laminates the superior point of braided composites is the continuity of the fibre bundles through the composite. For example a tube manufactured from laminate plies made by wrapping a sheet around to form a cylinder would have areas where one ply finished and another ply starts thus having areas of cut fibres in the structure. Each fibre can sustain applied load and this mechanism brings about high-performance composites.

Compared to the research on the crush behaviour of the laminated, woven and knitted composite tubes, very little work has been done on the crush behaviour of braided composite tubes. Chiu et al. [21] studied the crushing characteristics of 3D braided composite square tubes. They found that the failure modes of the crush tests of 3D carbon/epoxy braided composite tubes included compressive shear failure, bending and local buckling of the axial fibres, shear and tensile failure of the braiders. In their work the axial yarns were found to dominate the energy absorption, whereas the braiding yarns control the crushing failure mode.

A disadvantage of braided composites compared to unidirectional fabrics and prepreg tape is their mechanical properties. Falzon et al. [38] showed that while braided composites show tension and compression stiffness values comparable to that of unidirectional fabrics and prepreg tape, values for tension and compression strength were

considerably reduced. This was attributed to fibre damage and fibre tow waviness of the braided composites. The fibre damage was caused during the braiding process and fibre tow tension tests showed a reduction of 20% in tensile strength of the fibres. Fibre tow waviness or crimp cannot be avoided in braids and is also seen as a disadvantage in woven fabrics which are formed by introducing warp fibres by weaving.

However, Karbhari et al. [39] indicated that the braiding of preforms for crash energy absorbing structures is seen to be a very effective means of fabrication and the response is comparable to results obtained from specimens using conventional unidirectional prepreg based techniques.

For mass production vehicles, all parts must be made quickly and cheaply, but manufacturing of composite structures with conventional (tape lay) laminated composites is time consuming and expensive. Braided composites offer a reduced fabrication time at a relatively low cost, and thus show great promise for use in the automotive industry [40].

2.1.12 Multi-Cellular Braided Structures – Coretex

A process, developed at Cranfield University, which uses low cost carbon fibre braid is known as 'coretex' [3, 41].

The coretex approach offers the potential for affordable manufacture of lightweight carbon fibre composite vehicle frame like structures as the manufacturing process can be tailored to suit automated deposition of reinforcement and resin impregnation. This approach of using multiple braided tubes was also seen potentially, as an original way of absorbing energy in impact and collision scenarios.

2.1.13 Comment

After conducting a review of the literature based on energy absorption in composites, the benefit of composites coupled with the process technology of coretex was deemed worth investigating for crashworthy energy absorbing structures. This included the development of the techniques of moulding in order to try to give reproducibility of properties.

The manufacture of several series of composite beams for this purpose is outlined in the experimental section. The beams were then tested in static loading or impact loading, and the results are analysed in terms of the tow size, braid angle, internal geometry and number of ends.

3 Materials

3.1 Introduction

In this chapter, the various materials that are used in coretex structures are described. Furthermore reasons for a number of material choices are outlined.

3.2 Fibre

Due to findings in the review of the literature (see section 2.1.5) it was decided to evaluate carbon fibres to be used to form the braids. Braided composite tubes offer better energy management characteristics than laminated composites because the intertwining fibre architecture prevents gross delamination.

Tenax® STS carbon fibre is a newly developed low cost yarn, suitable for modern industrial applications. The STS fibre yarn was chosen primarily due to its price and process ability for all common fibre processing methods. It has similar properties to other fibres from Tenax such as HTS. However, STS is manufactured only at a relatively large tow size of 24K, where the tow size is the number of fibre filaments (24,000 in this case) bundled to form one 'tow' or 'end'. This factor allows the price to be lowered.

Carbon fibre from the company Toray Industries was also used. T700SC-24000 is also a 24K tow fibre with increased tensile strength and strain to failure compared with the STS fibre.

Table 1, illustrates typical values for some of the mechanical properties of STS, HTS and T700 fibres.

	STS	HTS	T700SC-24000	E-glass	Units
Filament Diameter	7	7	7	8-15	μm
No. of Filaments (Tow Size)	24000 (24K)	12000 (12K)	24000 (24K)	8 x 300 tex	No units
Density	1.77	1.76	1.79	2.56	g/cm^3
Tensile Strength	4000	4300	4900	2000	MPa
Tensile Modulus	240	238	230	76	GPa
Elongation at break	1.5	1.8	2.1	2.6	%

Table 1 Typical mechanical properties of STS, HTS, T700 carbon fibres with E-glass fibre. Properties selected from data published in Appendix B

One glass fibre braid was also included in the test programme for comparison. E-glass was used as the fibre with a tow size of 8 bundles of 300 tex per tow (see section 3.3.2 for definition of tex).

3.3 Braids

Braids are manufactured as preforms using a braiding machine. The machine has a ring of spools, which hold bundles of fibres known as tows. The spools follow intersecting circular paths so that the tows interlace together over a mandrel to form a tubular fabric. This forms a biaxial braided fabric with braider tows following the $+\theta$ and $-\theta$ directions and are braided in a 1x1 (plain weave) pattern or a 2x2 (twill weave) pattern. Examples of these braid architectures are shown in Figure 10.

The braid angle, θ, is controlled by the rotational speed of the spools on the braiding machine and the transverse speed of the mandrel moving though the centre of the ring of spools.

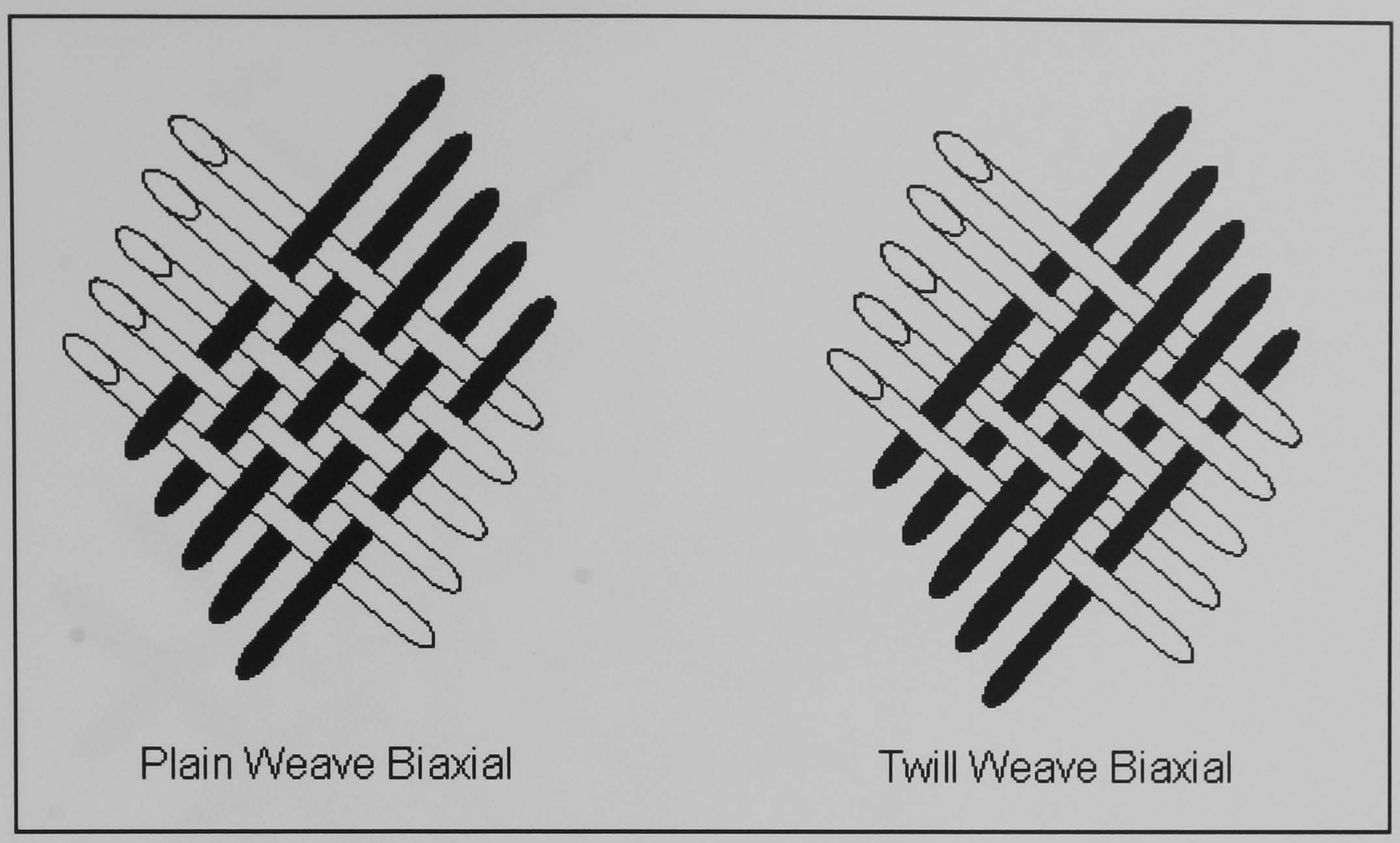


Figure 10 Schematic illustrating plain and twill weave braid biaxial architectures

Due to the inherent structure of braids they can be classified into two different fibre architectures, which are biaxial and triaxial. Triaxial braids have a third set of tows that are introduced in the axial direction and follow the zero degree (axial) direction. See Figure 11 below.

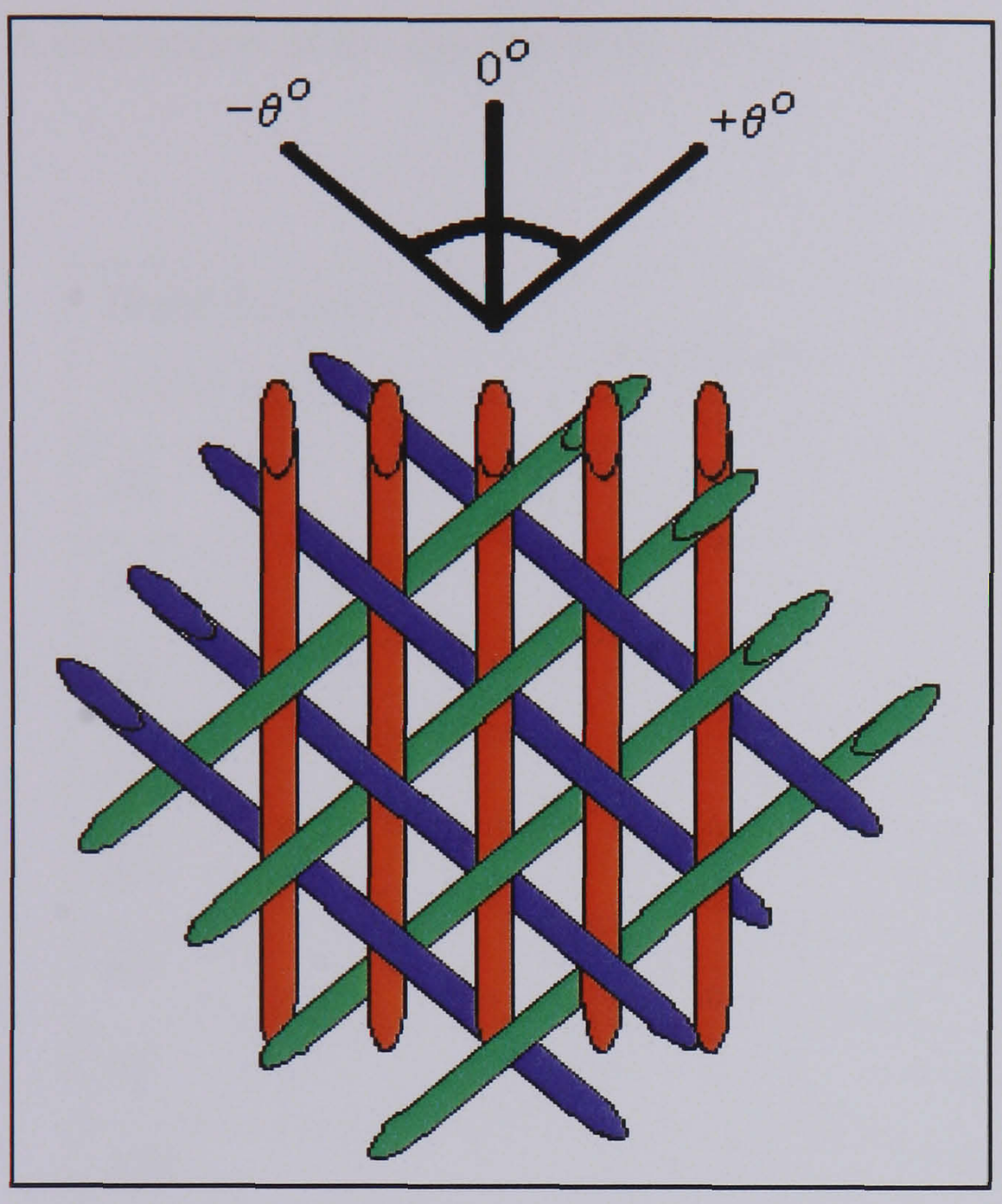


Figure 11 Schematic illustrating triaxial braid architecture.

Although findings in the literature suggests increased axial properties may increase specific energy absorption, attempts in using triaxial braid architecture were found to be too complicated and time consuming in trying to over-braid this type of reinforcement on to the foam manually. Consequently triaxial braided preforms have not been used in manufacturing multi-cellular beams. Another reason for not using triaxial braids is that the foam material used in the coretex process expands outwards onto the walls of the braided sleeve (see section 3.4 for further details on the foam). A triaxial braid will not allow its diameter to dilate without the axial fibres becoming kinked or wrinkled thus compromising its structure. In biaxial braids, the diameter can be dilated without structural compromise. However it is noted that an increase in braid angle will occur when the biaxial braid is dilated. It is also noted that if the over-braiding of the foam process was automated or included as part of steps when forming the braids from fibres, using triaxial braids would be worth re-consideration.

A description of the specific braid choices is presented in Table 2.

Braid Diameter at +/-45° angle, mm	No. of Ends	Fibre Type	Tow Size
40	48	Tenax HTS Carbon	12K
40	34	Tenax STS Carbon	24K
40	42	Tenax STS Carbon	24K
40	48	Tenax STS Carbon	24K
60	34	Tenax STS Carbon	24K
60	42	Tenax STS Carbon	24K
60	48	Tenax STS Carbon	24K
100	84	Tenax STS Carbon	24K
100	84	Toray T700SC Carbon	24K
40	42	E-Glass	8x300tex

Table 2 Material characterisation of each braid used

3.3.1 Nominal Braid Diameter

The braids were manufactured to give an angle of +/- 45° at a specified diameter. To change the fibre angle of the braid the diameter of the braid must change. This concept is used to change the final fibre angle used in the beam.

In manufacturing a beam of 4 braided sleeves, that is a 4 cell or 2x2 array, each braid will be sleeved over foam of cross section 29x29mm. This will result in a braid, whose original diameter of 40mm, will be pulled down to a smaller diameter and subsequently give a smaller fibre angle of about 32°. The same braid used in a 3x3 array will be

sleeved over foam of cross-section 19x19mm. Consequently a fibre angle of about 21° is achieved.

An original braid diameter of 60mm will result in even smaller fibre angles for the 2x2 and 3x3 arrays of 21° and 15° respectively.
The single glass braid was used as a comparative braid and is most similar in volume and architecture to the 40mm diameter carbon braid with 42 ends.

3.3.2 Calculation of Braid Mass

Differences in braid mass per metre when the original braid diameter is increased or reduced are calculated and shown below
In order to calculate the mass per meter, W_b, of a braid at ±45°, two variables are required. The number of ends, n and the 'tex' number, tex, where tex is defined as the mass in grams of a 1km length of fibre.

$$W_b = \sqrt{2}\left(n.\frac{tex}{1000}\right) \qquad \text{(Units g/m)} \qquad \text{Ref [42]}$$

Equation 2 Mass of braid per metre at original diameter

Using the original braid diameter, d_0, the mass per square metre, W_a, can be calculated as follows.

$$W_a = \left(\frac{1000}{\pi d_0}\right).W_b \qquad \text{(Units g/m}^2\text{)} \qquad \text{Ref[42]}$$

Equation 3 Mass of braid per square metre at original diameter

To calculate the mass per metre, W_b, at a diameter other than the original diameter the following graph was used to obtain the percentage change in length with a percentage increase or decrease in braid diameter.

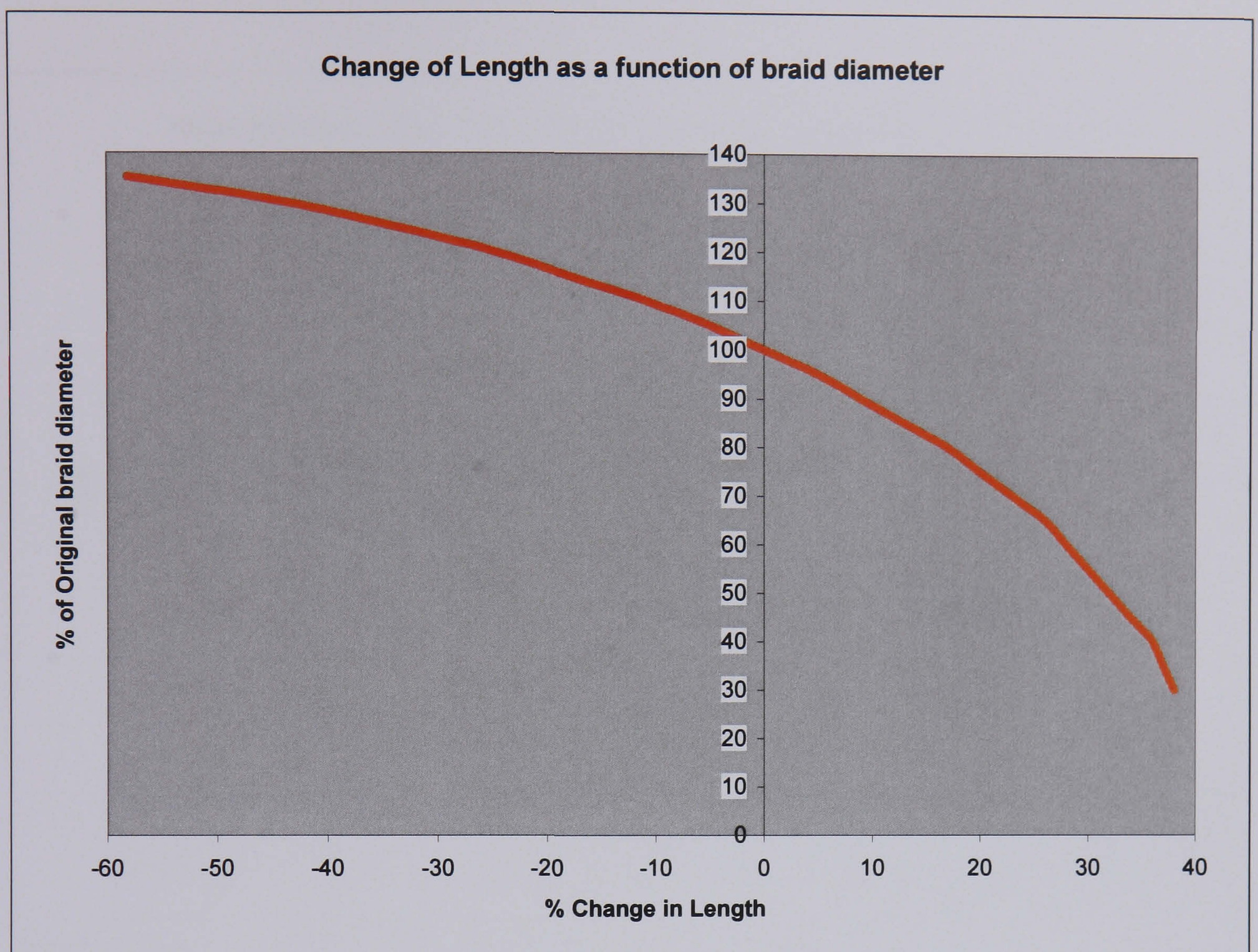


Figure 12 Chart illustrating the percentage change in length of a braid as a function of its braid diameter

So, the mass per metre of the braid at the use diameter, W_{usedia}, can be expressed as

$$W_{usedia} = \frac{W_b}{100 + \omega} \qquad \text{(Units g/m)} \qquad \text{Ref [42]}$$

Equation 4 Mass of braid per metre at the diameter of use

Where ω is the percentage change in length.

The following bar chart, Figure 13, displays the braid mass per metre for each particular braid type and dimension. A tabulated version of these data is displayed in section B of the Appendix.

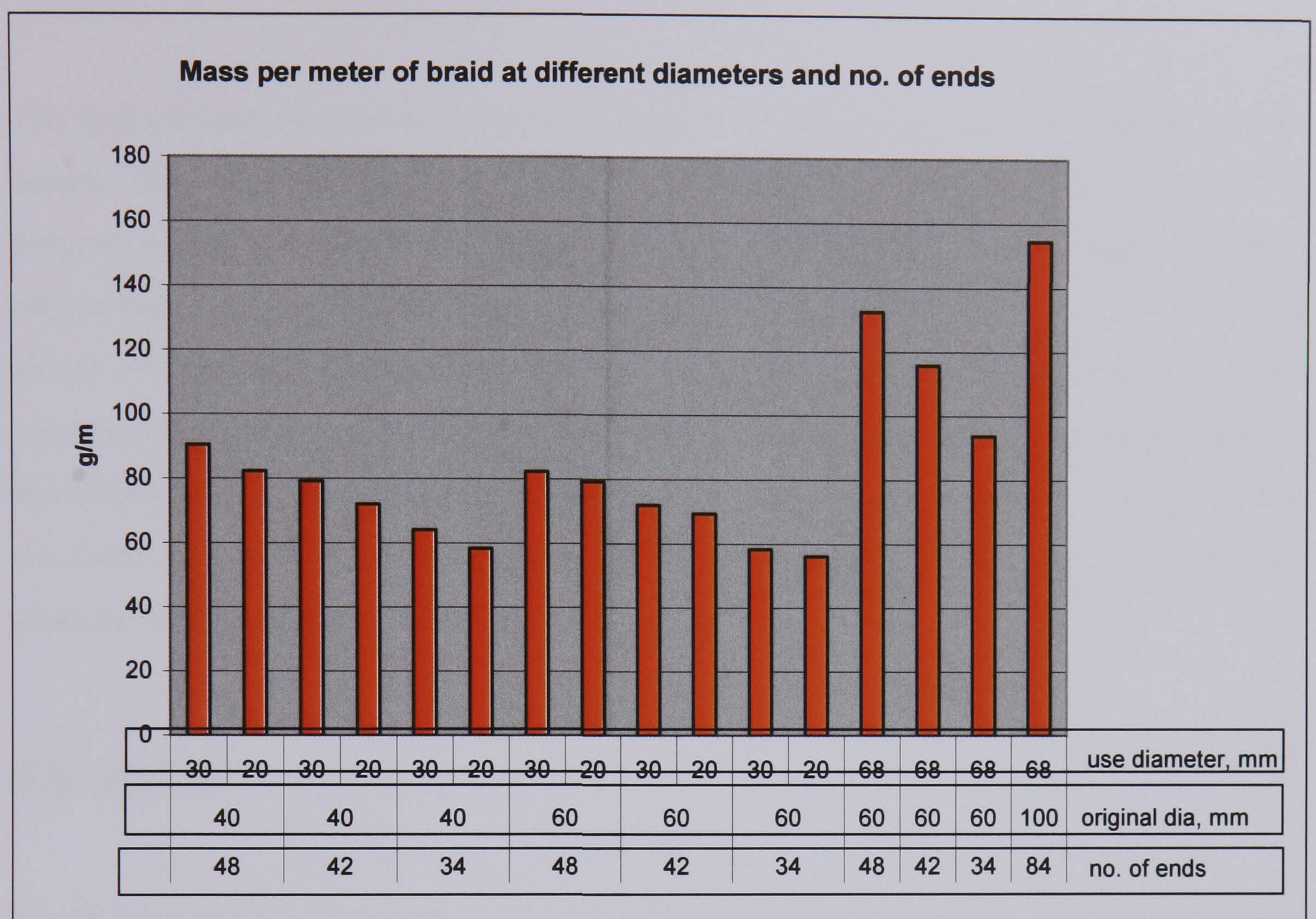


Figure 13 Chart illustrating braid mass per metre with various braid parameters

3.3.3 Number and Size of Tows

Varying the number of tows in a braid will affect the thickness and cover factor of the braid. Generally, increasing the number of tows will increase the thickness and reduce gaps in the braid; hence surface coverage will also increase.

Two tow sizes have been investigated in the study, namely a 12K and a 24K tow size. The 24K tow has of course double the cross-sectional area than the 12K. This causes an increase in the waviness of the braid. Also the braid structure as a whole is coarser.

3.4 Foam

The type of foam used plays a crucial part in the manufacturing process of multi-cellular beams. The foam selected is a closed cell cross-linked ethylene methyl acryalate co-polymer called Supazote®. It is a soft non-structural foam produced in sheet form by a unique high pressure nitrogen gas solution process giving a density of 26 kg/m^3. Due to its closed cell structure the gas enclosed within the cells is at atmospheric pressure. Under vacuum, the foam expands, due to the pressure difference, exerting a force on the walls of the closed cells. Such a phenomenon allows the foam to expand under a vacuum. When the foam is not constricted an increase in volume of about 100% is observed at 80mbar pressure and 50°C temperature.

3.5 Matrix

Epoxy resin systems were chosen as a matrix material for a number of reasons. Firstly and most importantly, some thermoset epoxy systems can be infused at room or low temperature due to their low viscosities. This is another key factor in the low cost manufacturing of multi-cellular beams as no high pressures or high temperatures are required which are an expensive feature of autoclaved manufactured composites.

Vantico's Araldite® LY3505 resin coupled with XB3403 hardener was used as the baseline resin system. Its properties of very low viscosity and low curing temperature made this a suitable choice. One other resin, namely 'Resin XU3508' coupled with the same hardener XB3403 was used as a comparative resin. It was chosen due to its fracture energy value, G_{1C}, being about 5 times more than the fracture energy value for the baseline LY3505 resin. This is due to XU3508 resin being toughened. It is also noted that the viscosity of XU3508 is higher than LY3505.

Key mechanical and physical property data obtained from the manufactures for the two resin systems are tabulated below, see Table 3.

Resin	LY3505	XU3508	*UNITS*
Hardener	XB3403	XB3403	
Initial mix viscosity @25°C	300-400	650-800	*mPa s*
Cure Cycle	15hours @ 50°C	15hours @ 50°C	
Tensile Strength, σ_T	70-74	----	*MPa*
(Tensile) Ultimate Elongation, ε_T	10-13	----	*%*
Tensile Modulus, E_T	3180-3280	----	*MPa*
Flexural Strength, σ_{FL}	85-93	100-125	*MPa*
(Flexural) Ultimate Elongation, ε_{FL}	11.0-13.0	9.0-11.0	*%*
Flexural Modulus, E_{FL}	3400-3550	2900-3100	*MPa*
Fracture Toughness, K_{1C}	0.95-1.05	2.1-2.3	*MPa$\sqrt{m}$*
Fracture Energy, G_{1C}	0.25-0.28	1.25-1.4	*kJ/m^2*

Table 3 Selected Material Properties of LY3505 and XU3508 epoxy resins. The full data sheet for these resins can be found in appendix section

4 Manufacture

In this chapter, reasons and decisions for various manufacturing choices are described. The various manufacturing processes are also discussed outlining their respective advantages and disadvantages.

4.1 Manufacturing Process Development

The coretex process is a modified version of vacuum infusion. A closed mould is packed with a preform which consists of fibre fabric (in this case braids) and a low density foam. When a vacuum is applied to the closed mould this allows the foam inside the preform to expand and compress the braided fabric against the mould walls. A schematic of this process is shown in the following illustration.

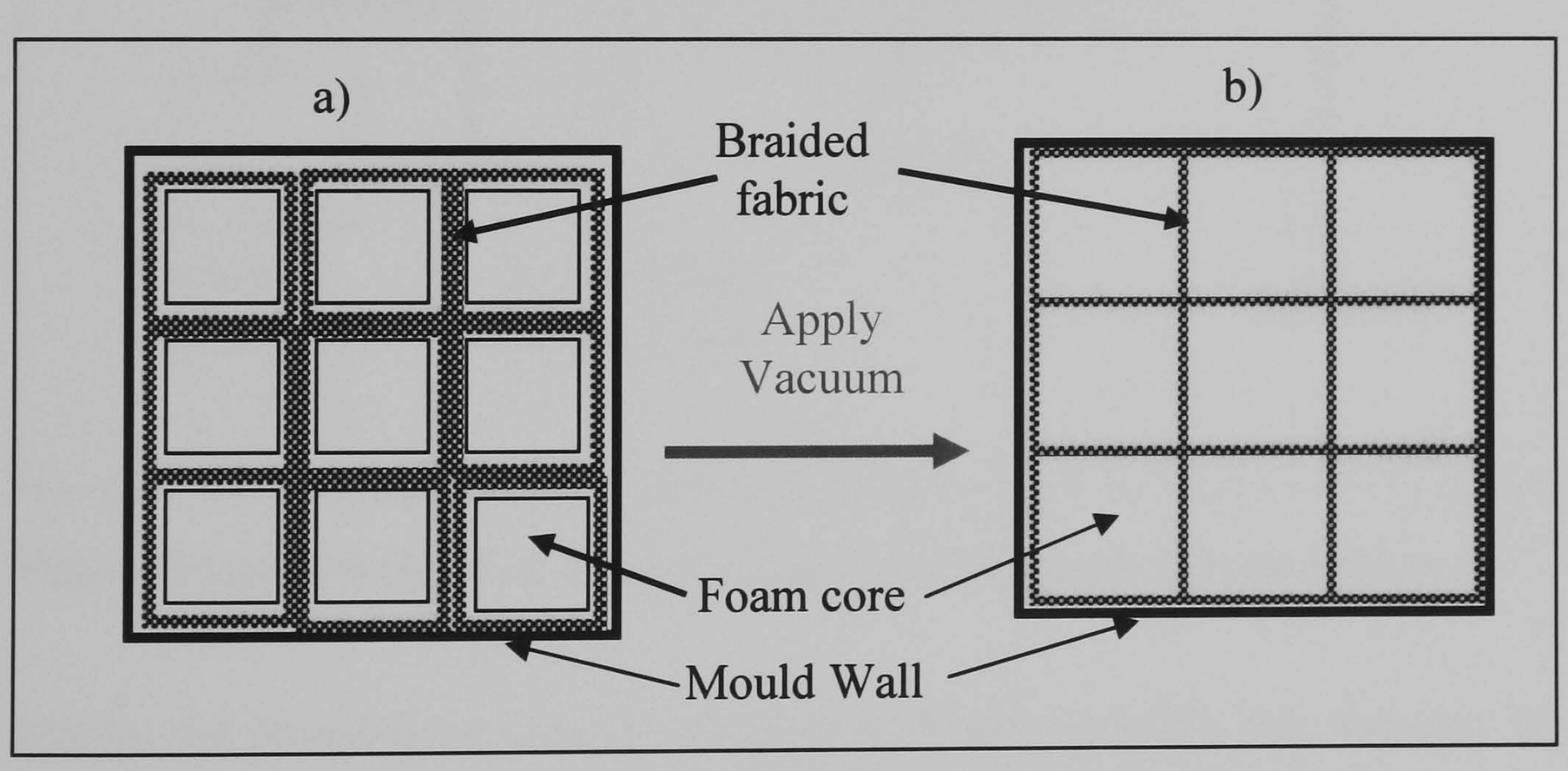


Figure 14 Schematic illustrating coretex preform before a) and during b) an applied vacuum.

The foam exerts a pressure inside the mould cavity and compresses the braided fabric. The vacuum in this process also has a second function; it is used to transfer the liquid resin from a resin pot to infuse the preform. Epoxy resins were used to infuse the coretex preform. The amount of resin used was determined by calculating the amount of carbon in the preform and then determining the mass of resin required to achieve a fibre volume fraction of around 50%. The two part epoxy resin was mixed at a temperature of around 30°C and then degassed for 10 minutes in a vacuum chamber.

The degassing allows any air trapped in the mixed resin to expand and be released from the liquid resin reducing the amount of bubbles in the resin. Nylon vacuum pipe is used as inlet and outlet pipe for the mould where the inlet pipe (which is clamped) is placed into the degassed pot of resin. When the operator is ready, the inlet pipe is unclamped and the resin flows into the mould, along the braided fabric 'wetting-out' the part as the flow front travels along the preform towards the outlet. Once the part is fully 'wet-out' this is cured in an oven or hot plate and then de-moulded. The following diagram shows a schematic of this set-up.

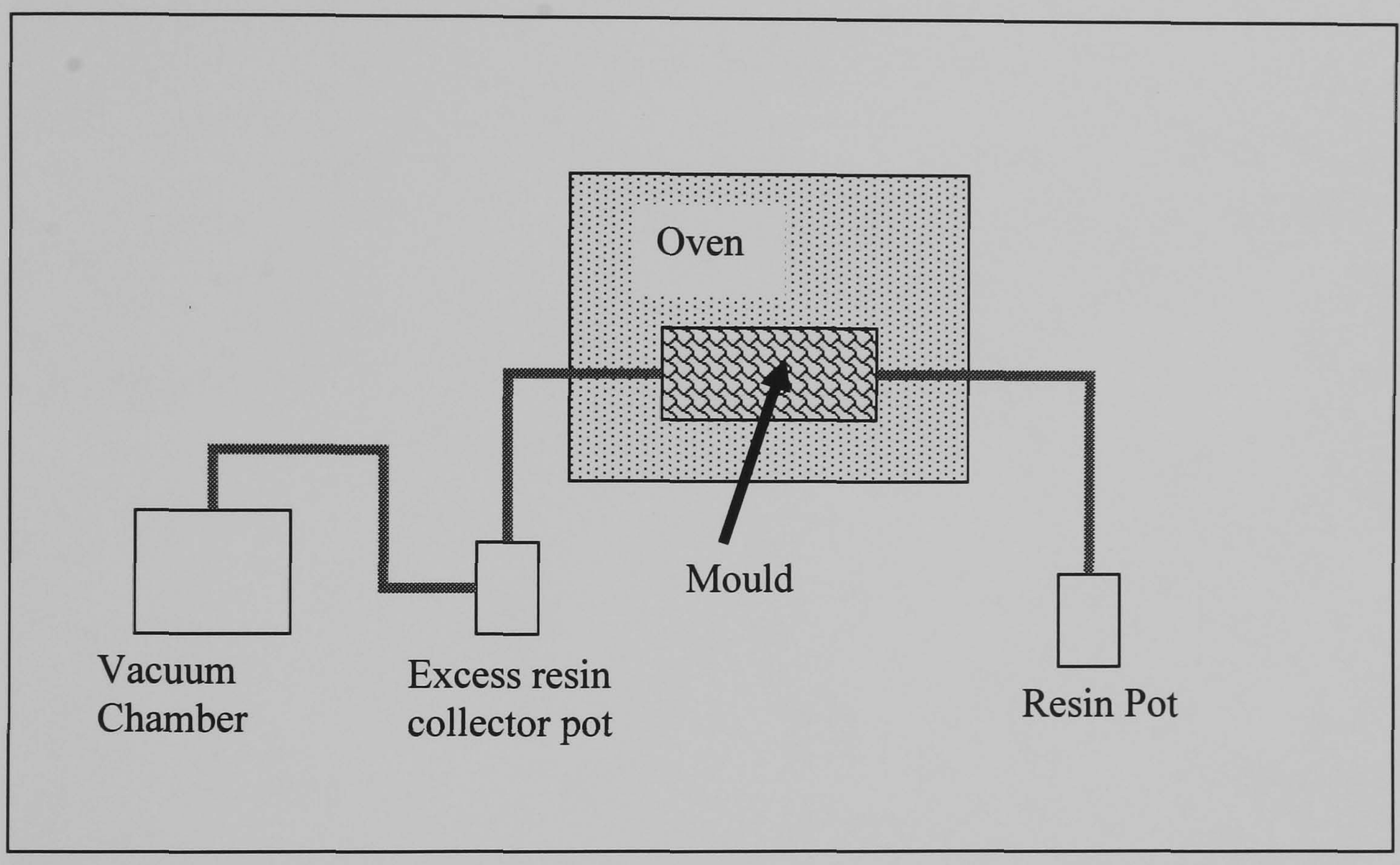


Figure 15 Schematic illustrating experimental set-up for coretex vacuum infusion

Ideally the de-moulded coretex component should be 100% full wet-out. The matrix should be free from any voids or gaps giving a smooth surface finish. Also the compaction of the braids should give a fibre volume fraction of around 50% minimising fibre waviness. The distribution of resin should be equal throughout the finished part. This would allow constant wall thickness and fibre volume fraction throughout the part.

Unfortunately ideal structures such as those described above have not been achieved in practice.

The following paragraphs illustrate the issues associated in producing coretex structures.

One of the first issues noticed was that in some areas of a coretex part there seemed to be resin rich areas within the component.

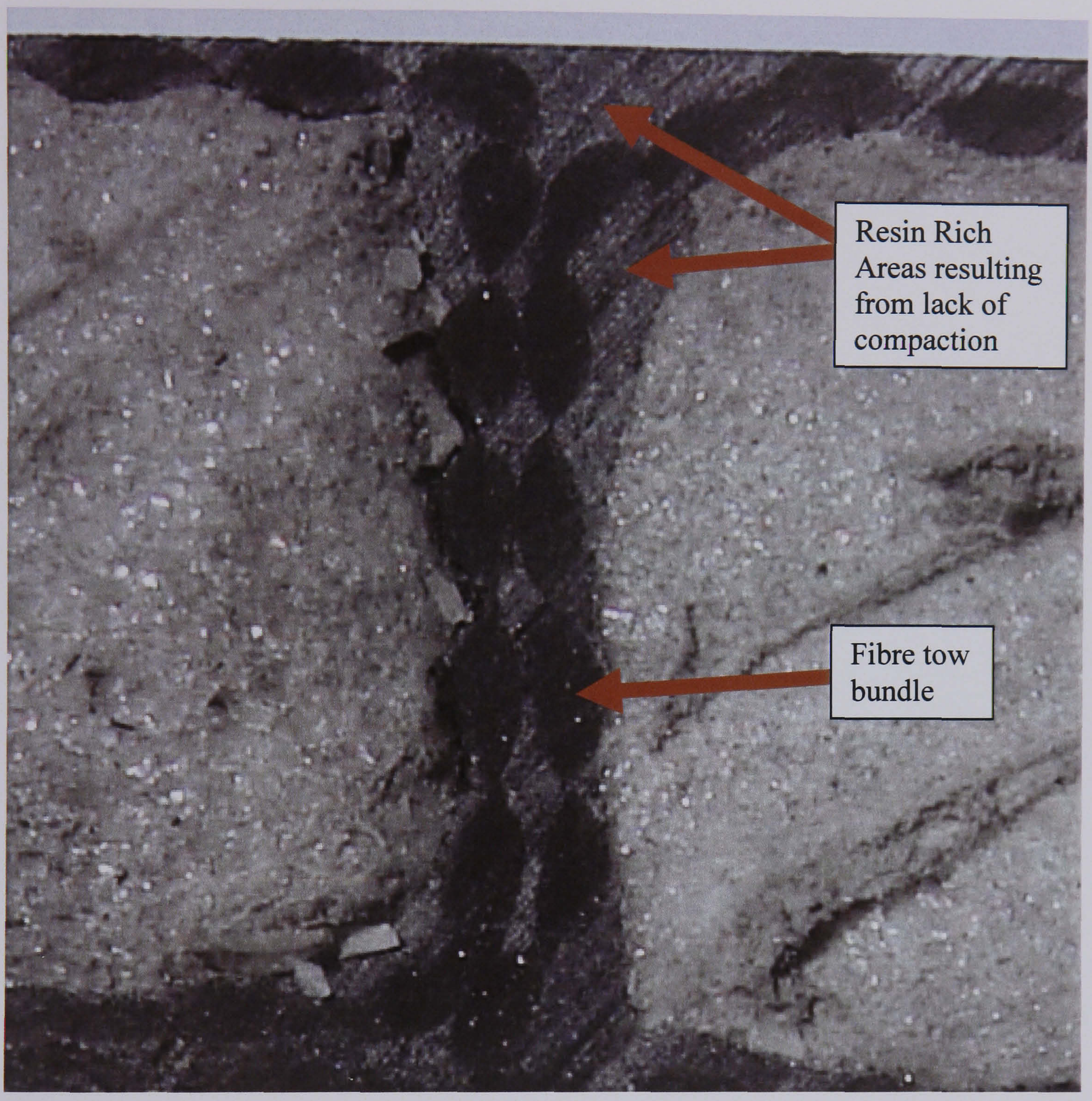


Figure 16 Photograph illustrating fibre and resin distribution on an inner wall of a 9 cell coretex beam

This was thought to be due to a lack of consolidation and so time was spent investigating the functional ability of the foam core. Experiments conducted in a vacuum oven showed that foam placed in the oven at 20°C increased in volume by less than 100% with an applied vacuum. When the foam was heated to 40°C the foam expanded in volume by about 400% under vacuum. At 80°C the foam expansion exceeded 400% but after a few minutes the foam collapsed. From this it was concluded that the foam could only function, that is sufficiently expand, in a certain temperature window, where the temperature range was between 40°C and 60°C

There were other processing problems with the foam such as the presence of voids and gaps in the cured structure.

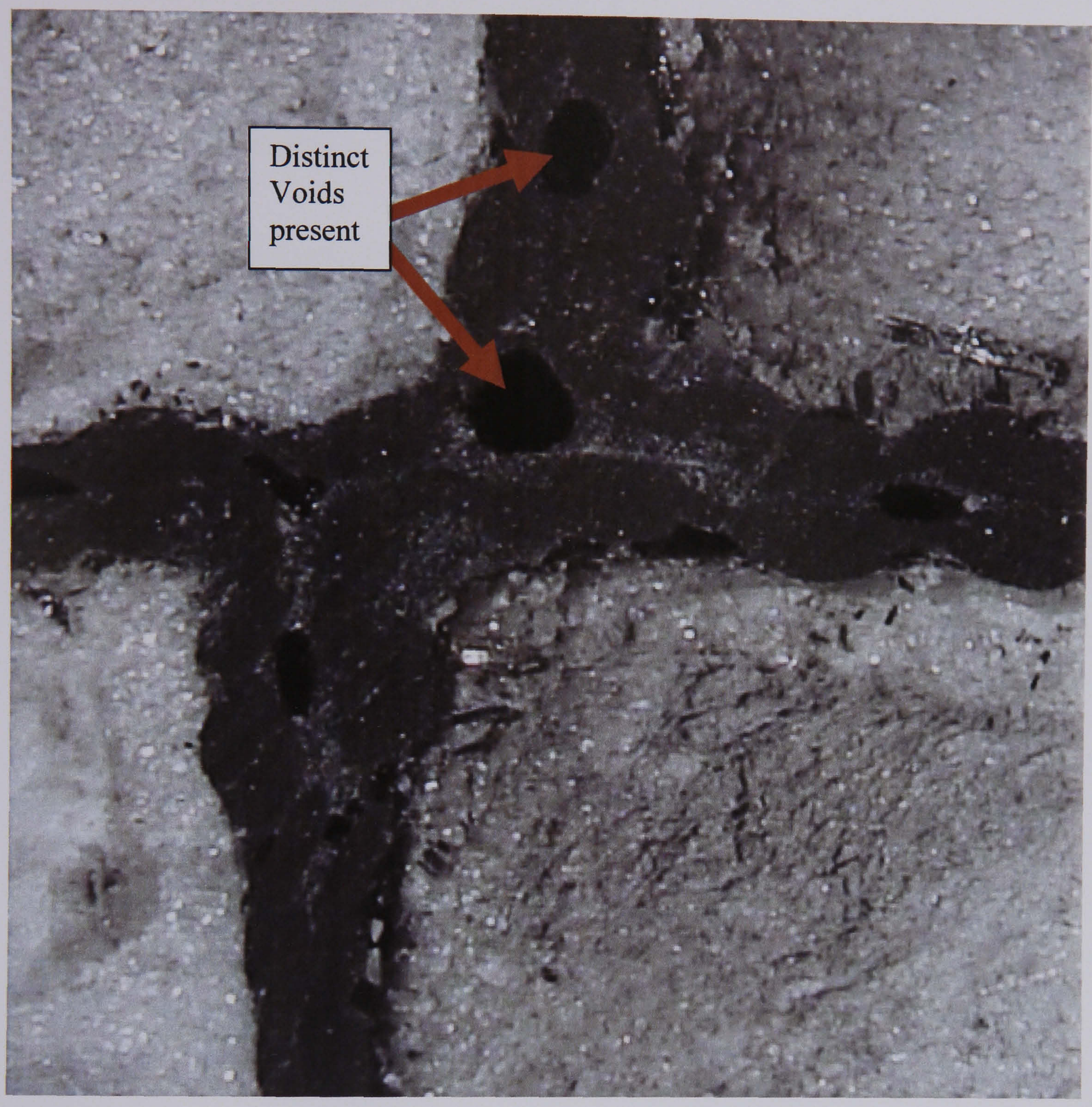


Figure 17 Photograph illustrating voids found between the inner walls in a 9 cell coretex beam

As the foam is a closed cell structure it was initially thought that any gas bubble or void found was either from the mould tool having a leak or small amounts of gas left in the resin even after degassing. This may well be the case but in addition to these factors, gas can diffuse through the foam cell walls and if any cells in the foam expand enough for the cell to burst then the gas will be released into the mould cavity.

When inspecting moulded coretex parts it was found, after sectioning the component that recorded mass values of parts cut from locations near the inlet were higher than

those found from mass readings near the outlet. As the foam and fibre mass is constant throughout the length of the structures this showed how the resin mass and therefore the resin distribution varied with distance from the inlet. One of the reasons this may have occurred is due to the foam losing its ability to compress the braided fabric as the flow front of the resin passes over the foam.

One of the important concepts to understand in coretex processing is that although the dimensions of the mould tool remain constant, the internal cavity volume surrounding the foam cores that is occupied by resin and fibre can vary with processing temperature and vacuum levels.

Initial development work sought to use low cost tooling methods for the coretex vacuum infusion process. A PVC extrusion was employed as a mould tool. The use of this tool is discussed in section 4.3.2 where the advantages and disadvantages of this type of tooling are noted. When a vacuum is applied and the tool is at temperatures above room temperature, the mould walls soften and deform from its original shape. As a result of the dimensional stability problem an alternative method of tooling was tried, namely a glass reinforced epoxy tool. Details of manufacture together with pros and cons of this type of tooling are shown in section 4.3.1. One of the major problems with this tooling was trying to minimise any vacuum leaks found in the tool. A number of sealing problems were encountered with this tool and so to overcome this problem, an aluminium tool with 'o-ring' vacuum seals was designed and manufactured. Details of this tooling are discussed in section 4.3.3.

4.2 Choice of Dimension

4.2.1 Cross sectional geometry

As discussed in the literature review (chapter 2.1.8) the most efficient cross sectional shape for axial energy absorption is circular. However, this shape was not chosen for two reasons. Firstly, in terms of handling the zote™ foam core, it was much cheaper and easier to cut square cross-section pieces of foam to fit into a square cross-sectioned beam. The alternative would be to use foam with a cross section similar to a

'slice of pie' so as to fit into a circular cross section. Secondly, many structural members in an automobile have a square or rectangular cross section. Some of the reasons for this are that it is generally simpler to accommodate attachments and fittings on to a flat surface. Also a beam structure with a square cross section often exhibits a superior bending stiffness when loaded in 3-point bend compared to a beam with a circular cross-section.

4.2.2 Corner radii

As a square cross section was decided upon, thought was given to the size of corner radii to be used, as the corners act as stress concentrations leading to the formation of splitting cracks and this tends to result in unstable collapse with low energy absorption. However, Price and Hull [43], illustrate for square sections, that the greater the corner radius, the higher the crushing energy absorption of the axially crushed column. That is, by increasing the corner radii of the square section a delocalisation of the load occurs, it being distributed more evenly over the whole cross section of the beam. A corner radius of 4.5mm was used for the manufactured beams. This was chosen as the extruded PVC that was used for tooling already bear this corner radius.

4.3 Mould Making

Various kinds of mould tools were designed and manufactured to form a cavity 60mm by 60mm square and 1 metre long. Various advantages and disadvantages of each type are discussed below.

4.3.1 Wet lay-up GRP mould

Manufacturing this mould tool is a fairly labour intensive process. Firstly a male master model has to be formed, usually from wood or aluminium. This master model is exactly the desired dimensions of the cavity required in the mould. This master model is then coated with 2 layers of gel coat. Layers of glass fibre chopped strand mat (CSM) are then impregnated (using a paint brush) with a room temperature

curing epoxy with added filler. Layer by layer the glass CSM is laid over the gel coat covered master model and dabbed in place to ensure a good surface contact and wetting of the gel coat. Designing how many parts the mould will have predetermines the positioning of the layers. Each part is then laid up one after another. As the layers build up, care is taken to ensure that any gaps between adjacent pieces of CSM are covered over in the next layer. Rollers are used to 'iron' out any air trapped between the layers and aid consolidation in the corners. Once the part is fully cured the male model is removed. Holes are drilled along the flanges of the mould tool so that nuts and bolts can be used to accurately locate each mould tool part with another and also aid in keeping the tool airtight, see Figure 18.

An advantage of wet lay-up moulds is that fairly complex shapes can be moulded with no extra cost. Also the mould materials - gel-coat, glass CSM, tooling resin are not expensive.

The disadvantages of this type of tool are that the quality of the mould depends on the skills and experience of the laminator. Furthermore, the hand lay-up process is a labour intensive process. Generally, composite moulds have a finite life and can only produce a relatively low number of parts. Repair and maintenance of the mould surfaces becomes a significant part of the whole production process of the parts.



Figure 18 GRP mould closed, sealed and ready for infusion

4.3.2 PVC mould

Extruded square cross section PVC tubes of dimensions 60mm by 60mm, usually used as 'downpipe' in domestic drainage systems, can be bought at a relatively low cost of around £2-3 per metre length which is the main advantage for using this system. As the pipe is extruded the quality of the mould's inside surface is good. This helps reduce time required for preparing the mould's surface for infusion. As the mould cavity in this instance is formed from a 1-piece tube plus 2 aluminium end plates, see Figure 19 and Figure 20, there are no split lines visible on the finished product and less areas for possible leakages to occur under a vacuum. However, as the pipe is made from PVC and the walls are less than 2mm thick, the operating temperature must be kept below 60°C. Above this temperature the plastic softens and

can deform, especially under a vacuum. Nevertheless, due to the PVC being relatively soft, the de-moulding process involves scoring the PVC with a knife and tearing the mould away from the final part. As the mould is destroyed in the de-moulding of the part, the mould is disposed of. As the mould is disposable there are no repair or maintenance issues. For an illustration of this process see Figure 23.



Figure 19 PVC mould showing coretex preform inside

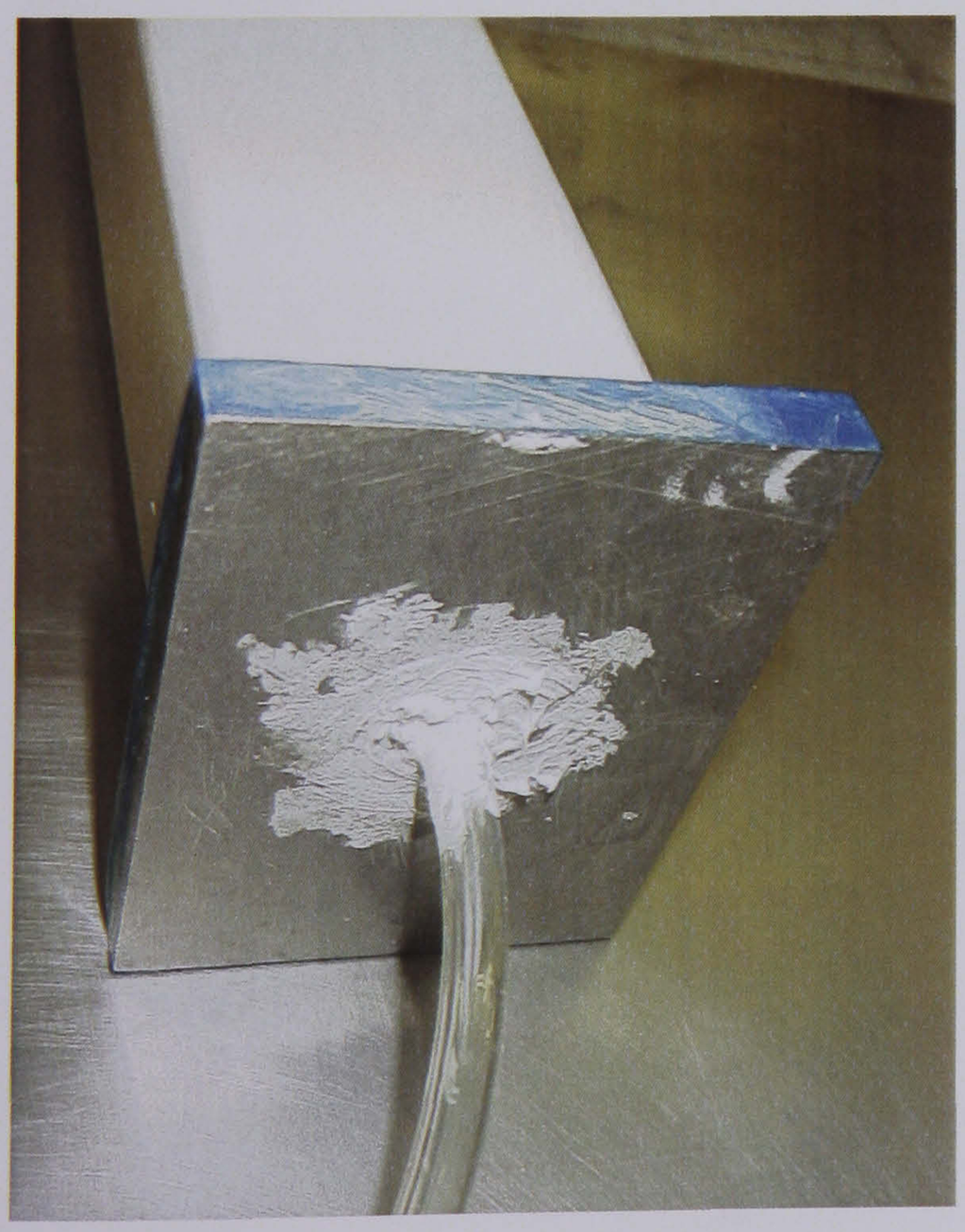


Figure 20 PVC mould with aluminium End Tabs

4.3.3 Aluminium Mould

To overcome the operating temperature limitations of the PVC mould an aluminium mould was produced. At a cost of around £1200 for an identical cross section found in the PVC tubes but only half a meter in length, this is not a cheap option. However, dimensional stability is obtained at high temperatures together with a good mould surface. Also, the operating life of a metal mould tool is significantly longer than a composite mould tool when maintained properly. Additionally, compression O-rings and grooves are used effectively to maintain a good level of vacuum, see Figure 21.



Figure 21 Aluminium mould with no lid

4.4 Processing

4.4.1 Preparation of mould tool

All mould tools were degreased and cleaned with acetone and coated with three layers of release agent. The GRP mould was also coated with a sealant to ensure a good surface before adding the release agent.

4.4.1.1 Formation of Preform

The foam was cut to shape; typically square cross sections of 19mm by 19mm with lengths of 1000mm. The braided carbon fibre is then sleeved over the lengths of foam to the coretex perform. These performs are then packed into the mould cavity one by one or pulled though in one bundle from one end to the other. Note that the mass of the foam and of the braid that constitute the preform is recorded.

4.4.1.2 Sealing Tool

Before closing the PVC and GRP moulds, a bead of silicone is placed along the closing mould surfaces to ensure an airtight seal. The tool is then left for 12 hours for the silicone to cure. In the aluminium mould tool, silicone is only used to help join o-rings where they have been cut.

4.4.1.3 Vacuum levels

To achieve the greatest expansion of the foam, ideally a level of vacuum below 20mbar is desired. However, this is not always seen in practice. The foam, when placed under a vacuum, increases close to its maximum volume when the vacuum level is less than 150mbar. When vacuum levels of around 30 to 60mbar are achieved the level of vacuum is low enough for infusion. Air leaks are checked by disconnecting the vacuum pump and assessing any drop off in vacuum level.

4.4.2 Infusion

Once the braided cores have been positioned into the mould and sealed, a vacuum infusion is used to transfer the resin into the part from one end of the beam to the other end.

As discussed in chapter 3.5, low viscosity, tough, two part epoxy resins are used for infusion. As the two parts of the epoxy resin are mixed, air is inadvertently introduced in to the resin. By placing the resin in a vacuum chamber the trapped air bubbles expand and depart from the mixed resin. This process, known as degassing, is important in keeping the porosity levels to a minimum in the finished structure, which in turn aids in forming a good surface finish. During infusion, the braids are gradually wet-out with the resin. It is also noted here that as the foam used in the preform is a closed cell structure the resin does not enter the foam core and so the foam cores act as 'expanding mandrels'.

4.4.2.1 Cure Cycle

Typically a cure cycle of 15hours at 50°C was used. This is a fairly low temperature cure cycle, as the foam cores in the structure tend to degrade at a temperature of 80°C. Also when using the PVC mould at temperatures above 60°C the PVC is prone to softening and as a result, can lose its structural integrity especially when a vacuum is applied allowing the atmospheric pressure outside the mould to 'push in' the walls of the mould, see Figure 22.

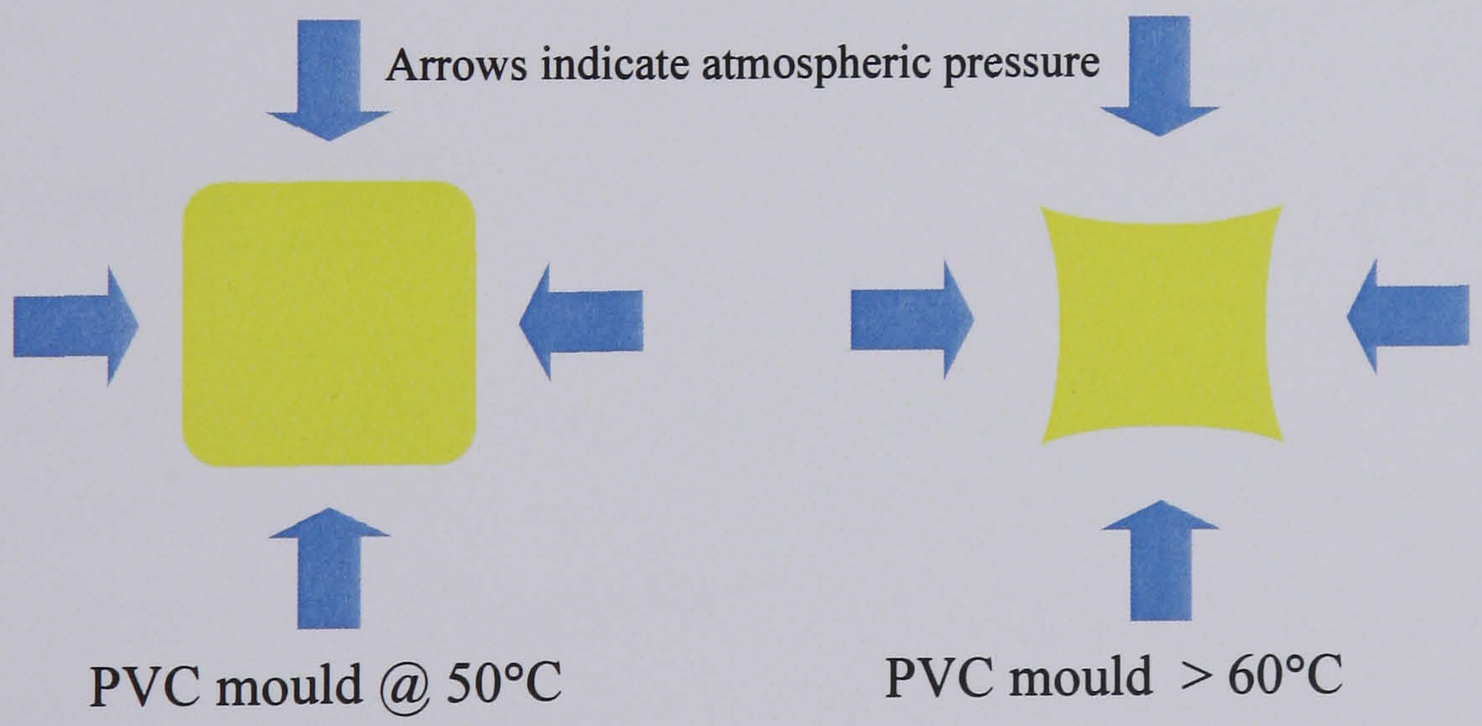


Figure 22 Schematic illustrating the effect of pressure on PVC mould walls at different temperatures when a vacuum is applied inside the mould.

4.4.3 De-moulding

In the case of the aluminium and GRP moulds, de-moulding is simply a case of unbolting and separating the mould parts. For the PVC mould, the mould wall is repeatedly scored with a blade. A wedge is placed between the mould and the finished part to tear away the PVC, see Figure 23.

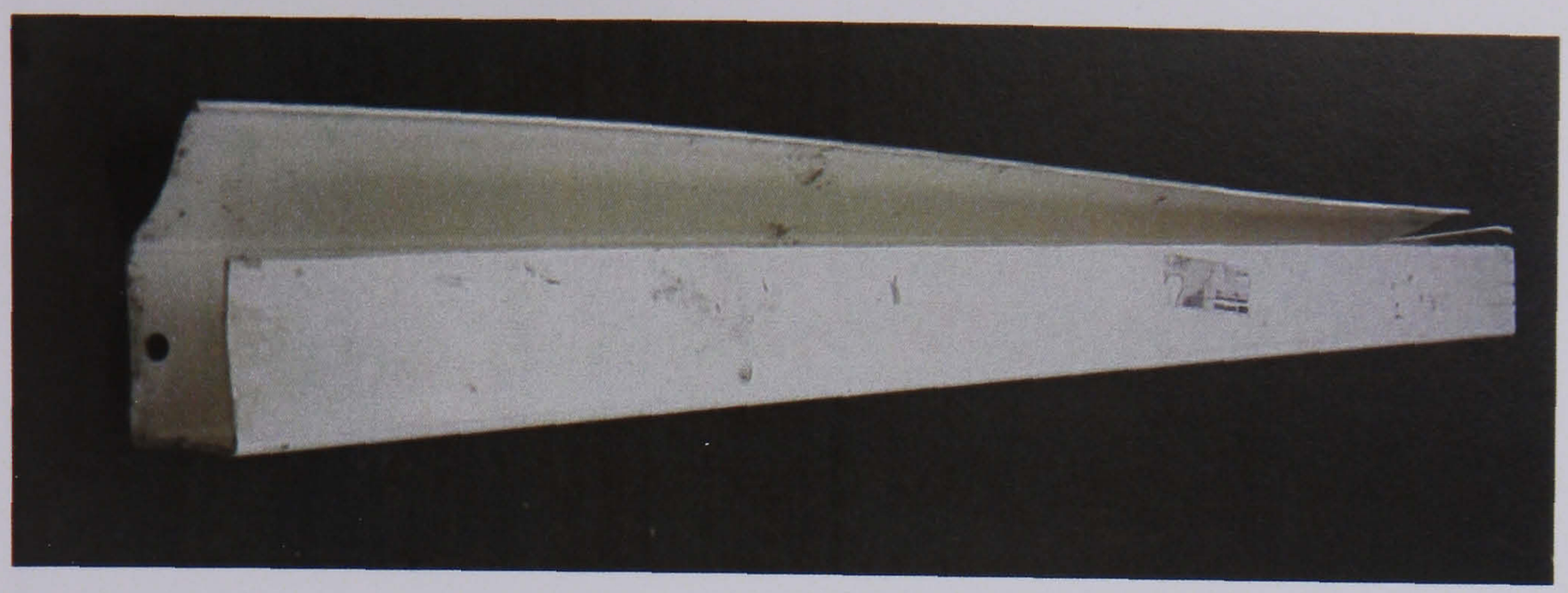


Figure 23 Photo illustrating PVC mould after demoulding

4.5 Specimens for testing

After demoulding, the coretex beam's mass is recorded. This information, together with the mass values of the braid and foam in the preform, allow an estimation of the overall fibre volume fraction of the part. See tabulated data of results in the appendix section B. Specimens of the beam are then cut into lengths. These specimens are then machined on a sanding wheel to ensure the ends of the specimen are flat and parallel. Their mass is recorded at this stage and is noted as the pre-triggered mass, see appendix B.

4.5.1 Chosen Trigger

There are various trigger designs discussed in the literature, see chapter 2.1.3.2, however, these designs are usually for circular tubes with no internal structure. For coretex structures, simply chamfering the outside of the beam may well result in a catastrophic failure as the internal composite structure has not been allowed to initiate a progressive crushing mode. However, an effective trigger design was used; see Figure 24, where the majority of walls in the tube are chamfered at 45 degrees.

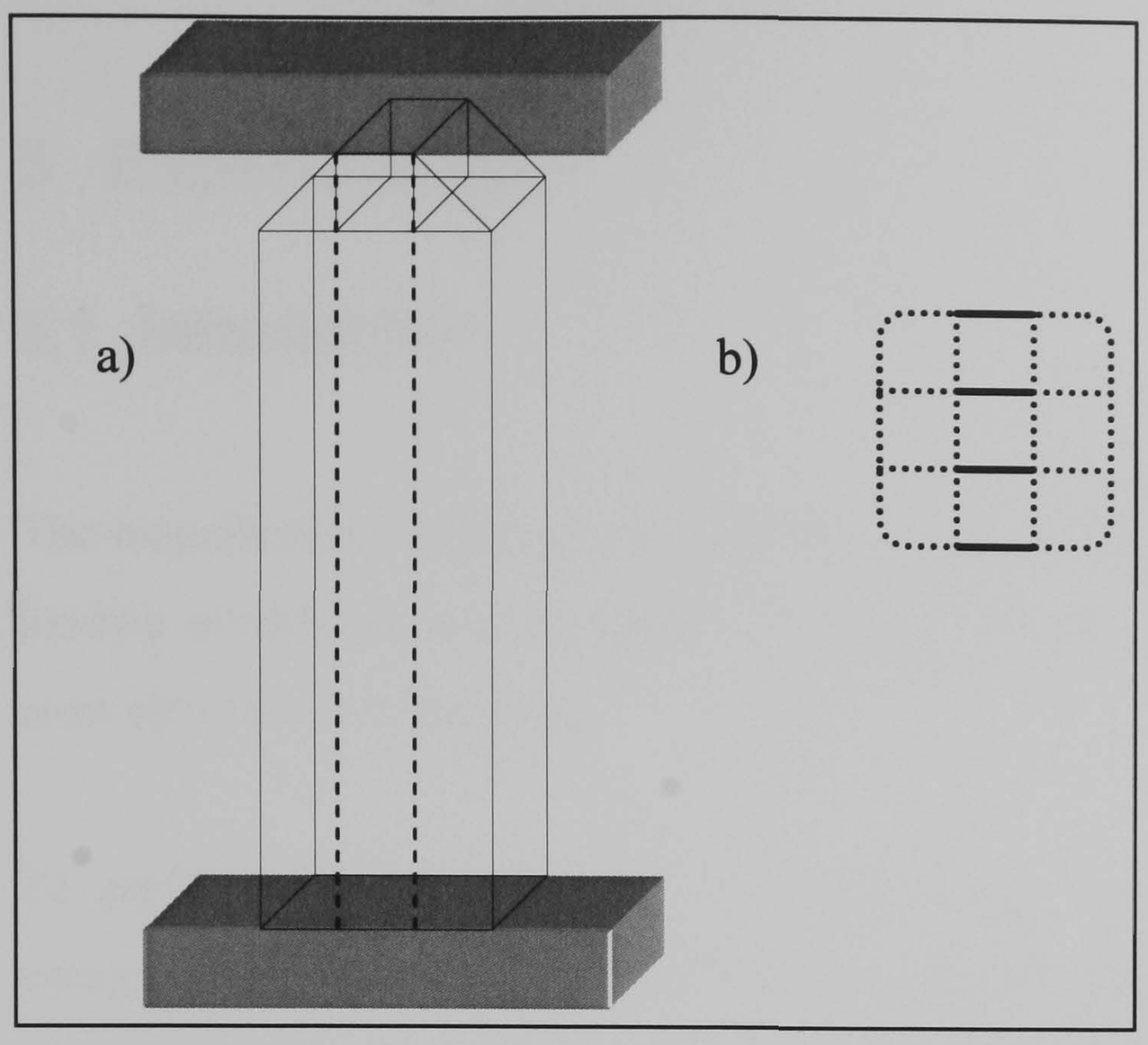


Figure 24 a) Schematic of triggered specimen between loading platens, b) Top view of triggered specimen where dotted lines indicate chamfered walls and solid lines indicate non chamfered walls.

Specimens tested with various trigger designs were carried out through trial and error, including designs where all the walls have been chamfered and where only some of the walls have been chamfered. If the trigger design allowed the specimen not to show a significant initial high load level and also initiate progressive crushing then that particular trigger was deemed adequate. Figure 24 is an example of an adequate trigger that was used for the multi-celled coretex structures.

4.5.2 Length

Specimens were usually cut at 200 to 250mm in length. This allowed ample length for the triggers to be machined, which are 25 to 30mm in depth, and still have enough crushing length to collect data from.

5 Experimental

5.1 Introduction

The manufactured coretex beam specimens were tested for evaluation in a number of loading conditions, namely quasi-static crush testing and axial impact testing. Beams were also tested in bending.

To gain a better understanding of how the coretex structures perform in absorbing energy in crush and impact conditions, a range of material and structural parameters was varied. The following chart (Figure 25) details the various configurations that have been investigated for the reinforcement, matrix, core and beam structure.

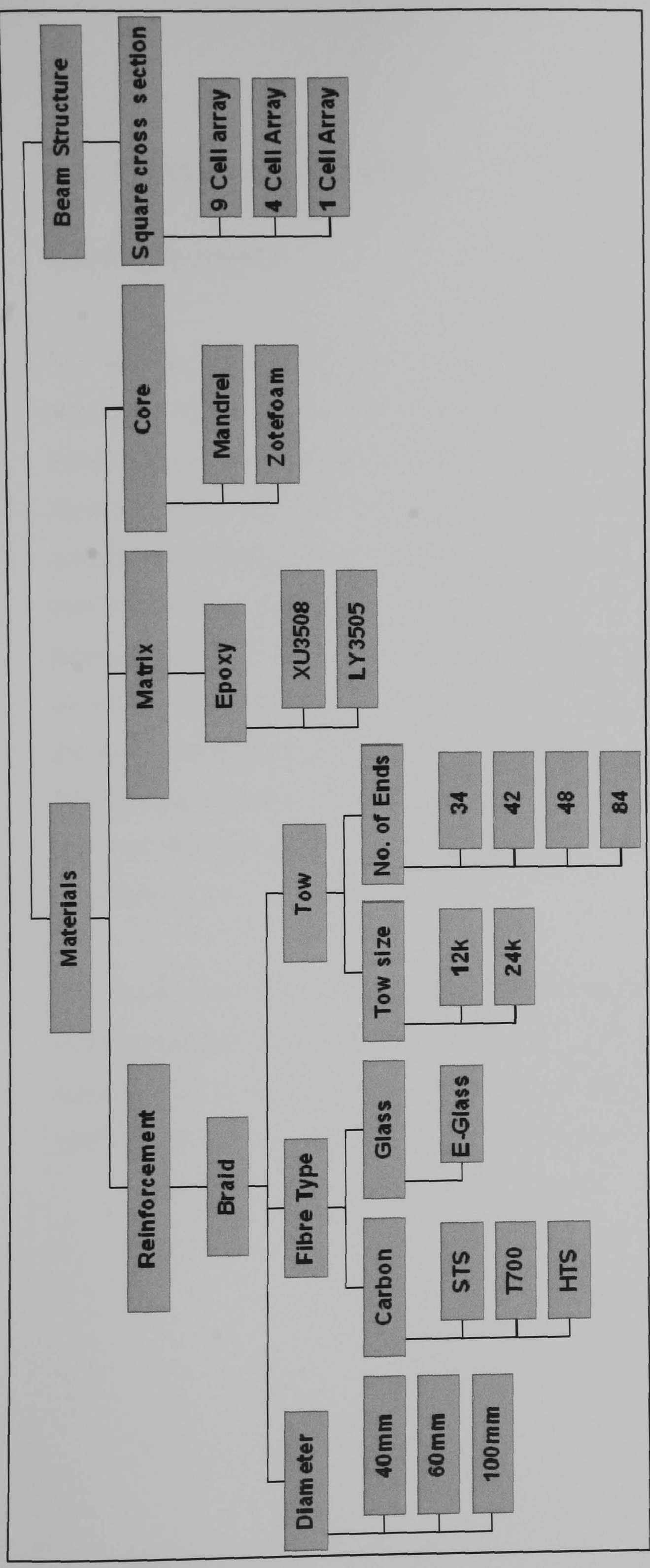


Figure 25 Chart illustrating breakdown of investigated coretex parameters

5.2 Quasi-static Testing

5.2.1 Procedure

For constant speed crush testing, a screw driven displacement controlled Instron 8500 was used with a load cell capable of 100kN load. Some larger beam structures were tested on a hydraulic driven Instron, see Figure 26, with a load cell capable of 250kN load. The observed load was recorded during each test. The Instron is controlled via crosshead displacement and so a constant crosshead velocity of 10mm per minute is employed during the test on the basis that this is equivalent to nominal quasi-static testing speed. Mild steel flat plates typically more than 5mm in thickness were placed on the top and bottom of the test specimen. These plates were not fixed or bonded to the specimen in any way. During the test, load and displacement data were recorded at 0.03125mm intervals with a typical test crushing the specimen by 100mm in length. The test arrangement is shown in Figure 27 A four-cell coretex beam undergoing quasi-static crush loading.

The energy absorbed during the test was calculated by employing a modified version of the trapezium rule to give the area of each interval, see Figure 28. These areas were accumulated to give the total area underneath the load displacement curve and therefore the total energy, see Equation 5 on page 66.

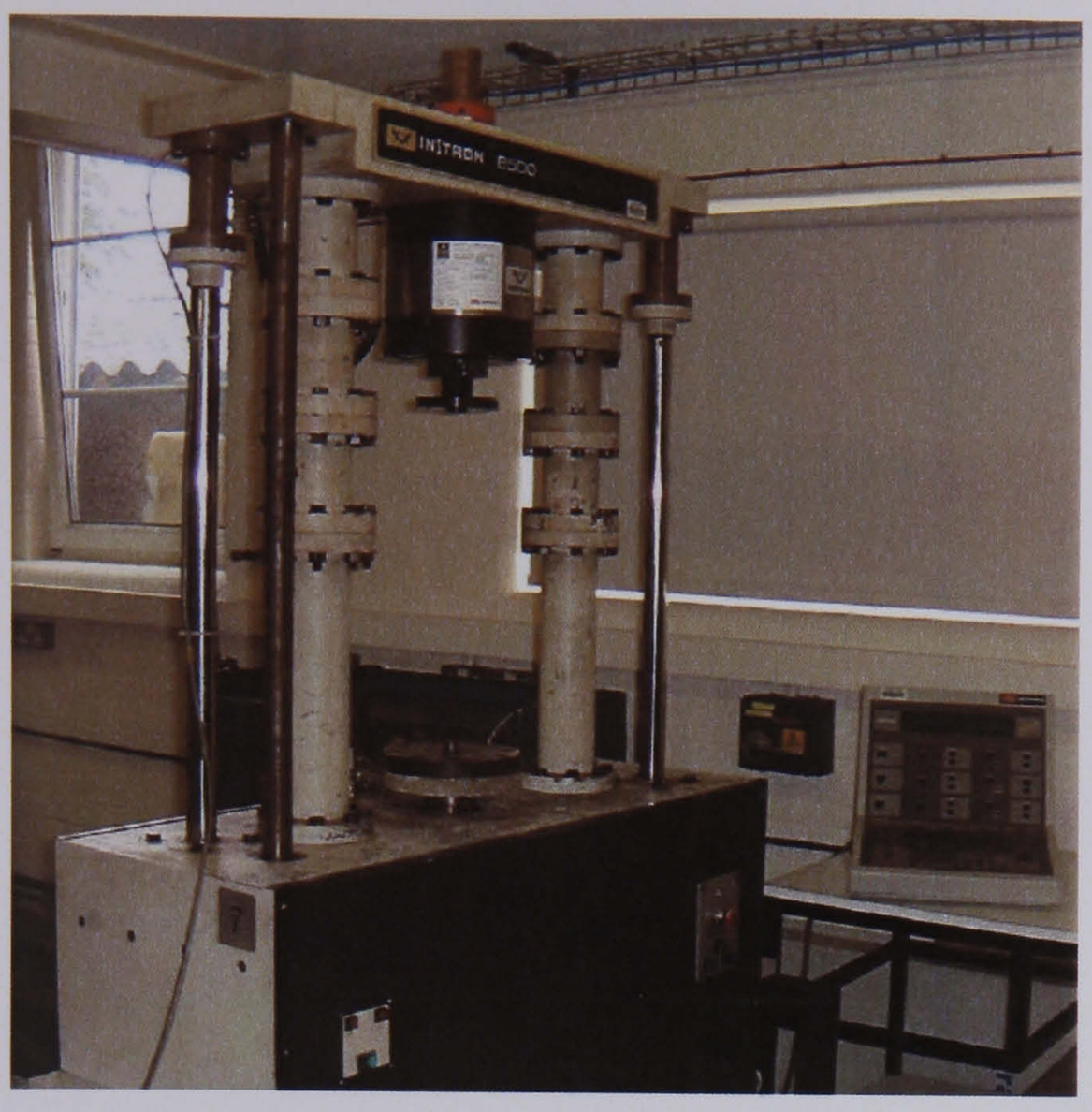


Figure 26 Hydraulic Instron test machine with 250kN load cell.



Figure 27 A four-cell coretex beam undergoing quasi-static crush loading

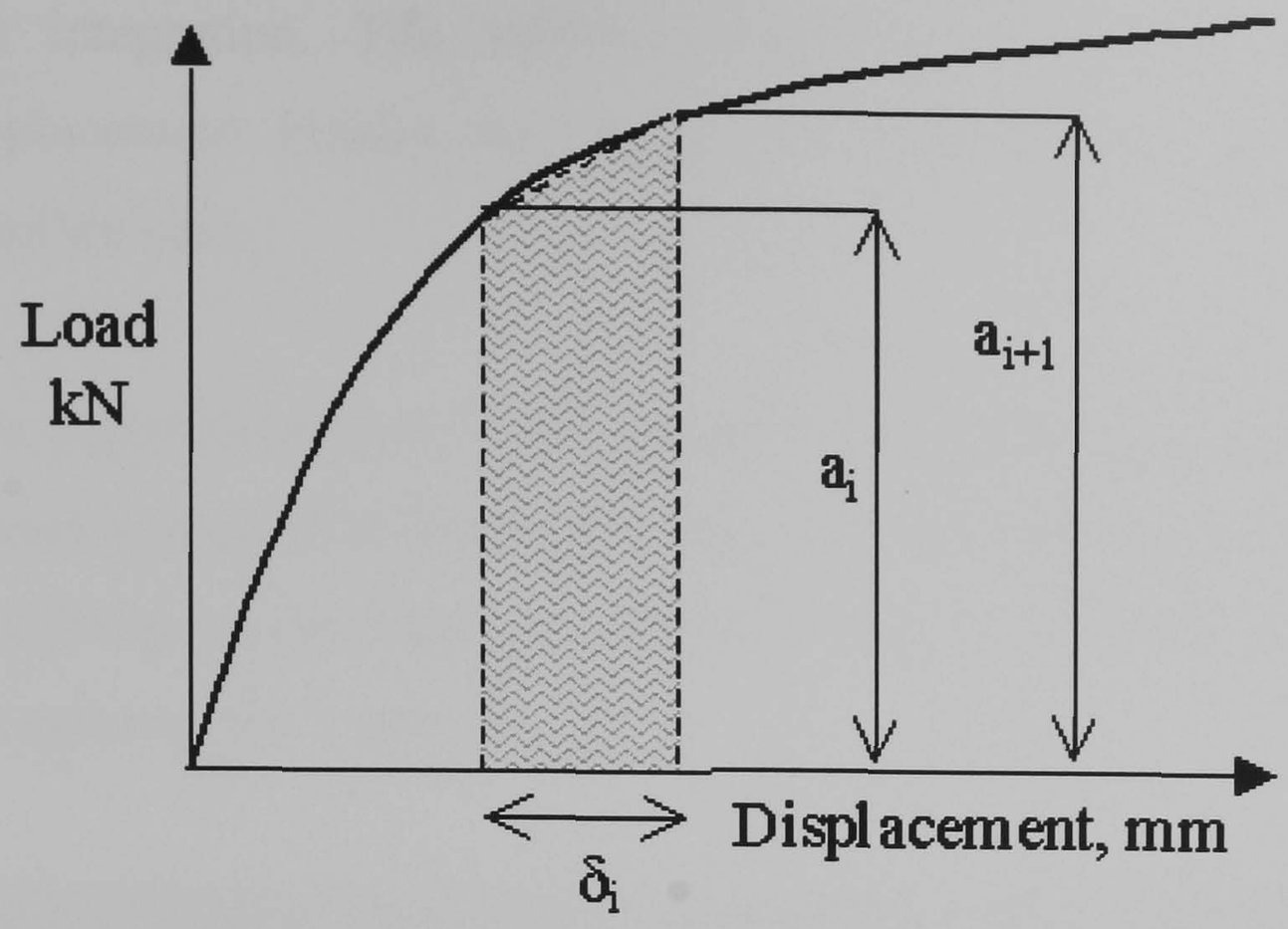


Figure 28 Schematic of load displacement curve showing calculation of area

$$TotalEnergy = \sum_{i=0}^{n-1} \frac{(a_i + a_{i+1})\delta_i}{2}$$

Equation 5 Equation for the total energy under load displacement graph

5.3 Impact Testing

5.3.1 Procedure

Impact tests were carried out on an upgraded and modified Rosand 'Instrumented Falling Weight Impact Tester' – IFWIT. See Figure 29. The capacity of the machine permitted impact tests at up to 8 m/s with an increased load carriage of up to 100kg. This provided impact energies of around 3kJ. A Kistler force transducer with a capacity limit of 120kN was used to measure the forces during an impact.

During a test, the load carriage was raised to the desired height. When the load was allowed to fall freely, an optical sensor was used to measure the velocity of the striker just prior to impact. As time was continuously measured, the forces recorded during the impact event were captured at a constant sample rate. Using the equation 'Force = Mass x Acceleration' the acceleration was derived. The acceleration data, together with the initial impact velocity (recorded optically), was used to derive the velocity

via integration. The velocity data were integrated once more to derive the displacement. Finally, the energy was calculated by integrating force with respect to displacement.

The striker head used in this system has a total area of a circle 80mm in diameter. To ensure a good distribution of load on to the whole cross section of a square shaped 60x60mm coretex beam, a mild steel plate was placed between the striker head and the coretex, see Figure 30.

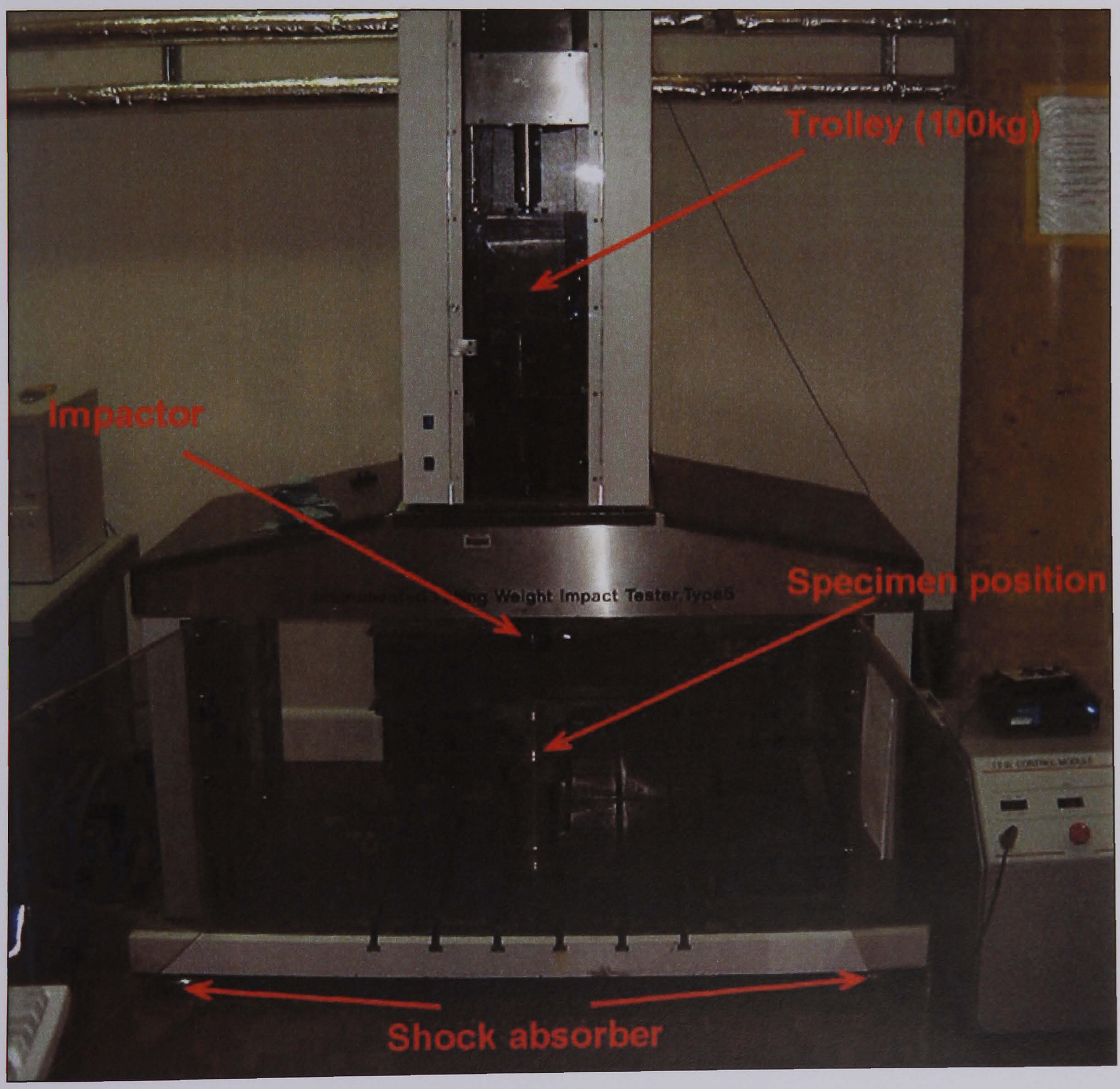


Figure 29 Photograph of drop tower impact machine

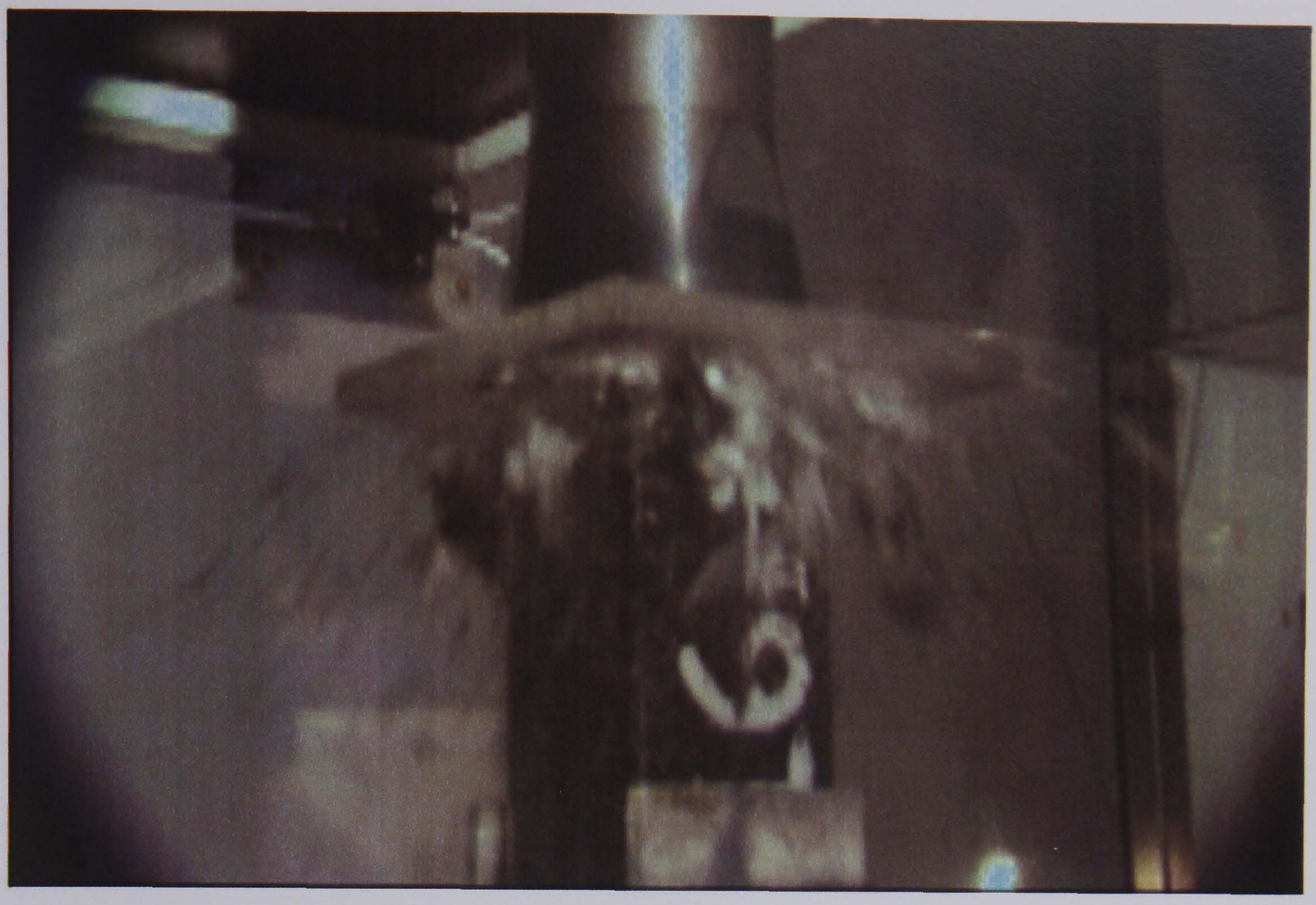


Figure 30 Coretex beam undergoing impact crush loading

After each impact, a force displacement curve was plotted. See Figure 31 below

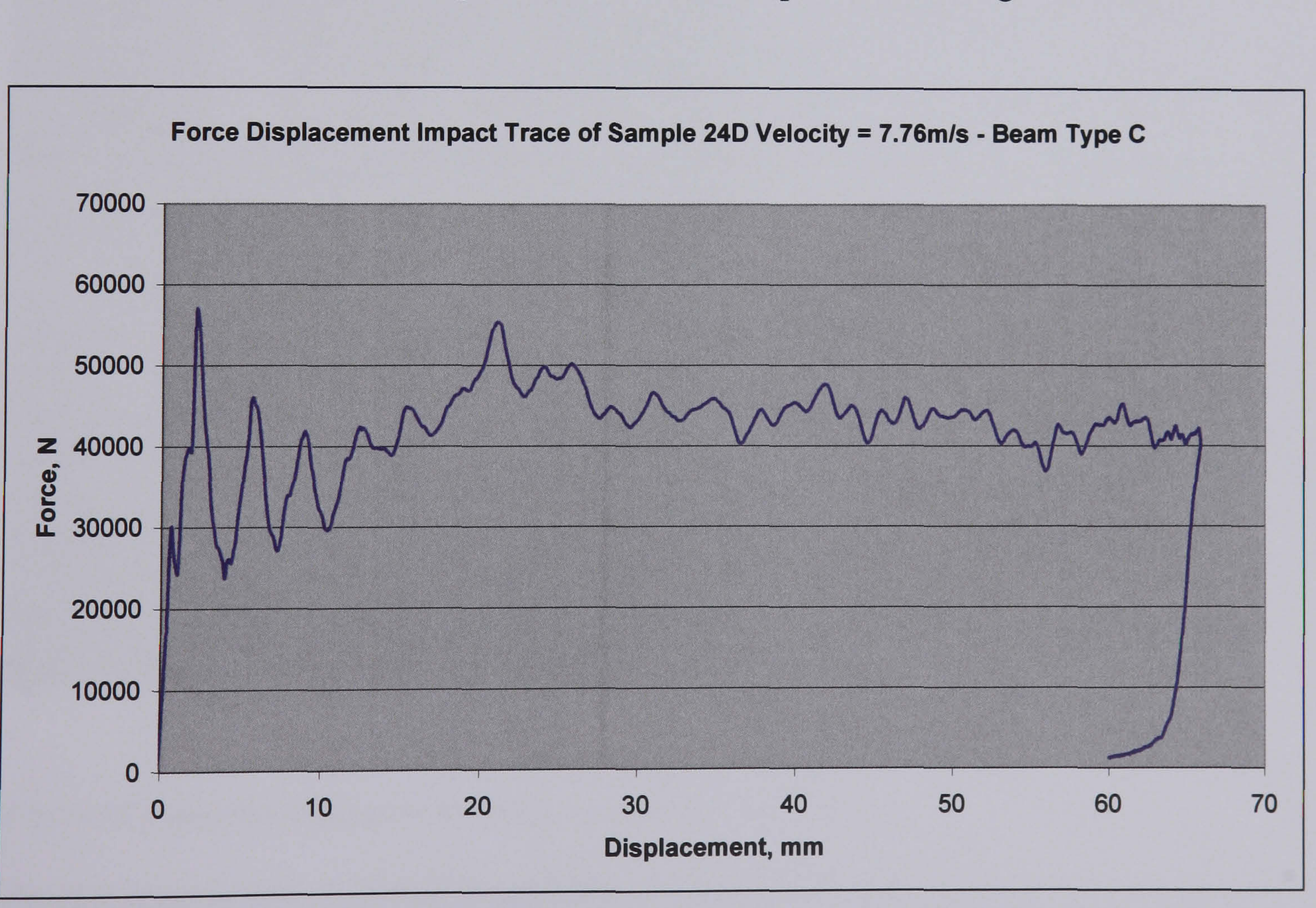


Figure 31 Chart illustrating a typical example of an impact trace

5.4 Bend Testing

Beams were tested in bending according to the quasi-static door crush test described in the 'Federation of Motor Vehicle Safety Standard' - FMVSS214. The test rig illustrated in Figure 32 consists of an 'Instron 8500' test machine with a 300 mm diameter aluminium half-cylinder impact header. The composite beam specimens were supported on 2 cylindrical rollers with a diameter of 38mm. A jig with a span length of 485mm supports the two rollers.

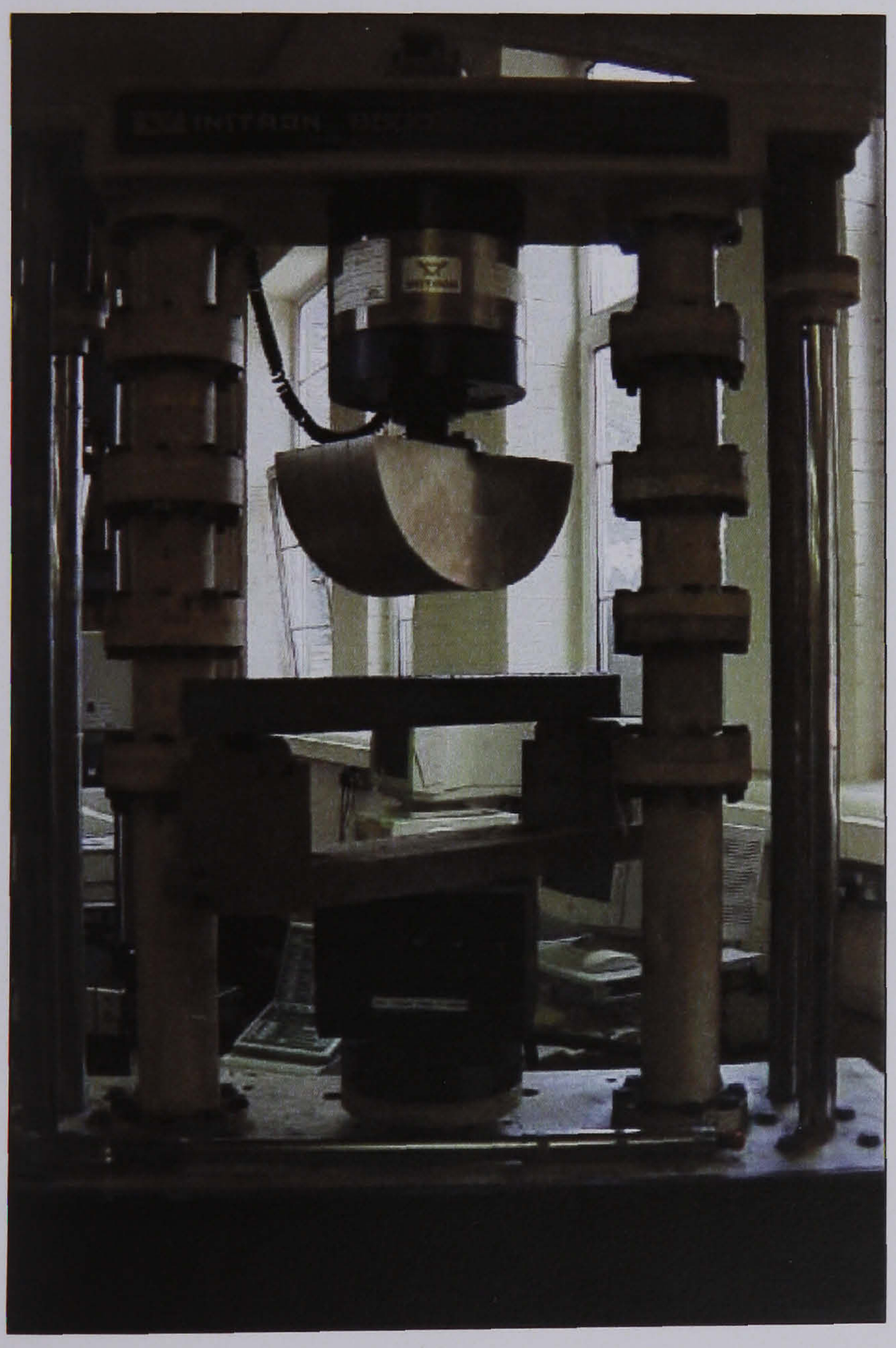


Figure 32 Photo illustrating set-up of the 3-point bend test used

Beams were tested at 10mm per minute and load deflection data were recorded. The results and discussion of these tests can be found in chapter **8.7**.

6 Test Programme

6.1 Introduction

As mentioned in chapter 3.3.1, by varying the original diameter of the braid, the final braid angle in the beam can be varied. Therefore, if a different braid angle is required, changing the initial diameter of the braid in question does this. To vary the thickness of the braid, independently of braid diameter, varying the number of tow ends will directly vary the braid's average thickness. Increasing the size of a tow will also result in an increase in average thickness for the braid and increase the waviness and coarseness of the braid.

6.2 Test Matrix

A beam manufacture test programme was constructed and this is detailed in the following table, see Table 4.

TowSize	Fibre Type	Diameter	Fibre Angle	No. of Tow Ends	No. of braids	Array structure	Type	Number
24k	STS	40	±32	34	4	2x2	a	12
				42			b	2
			±21		9	3x3	c	11
			±32	48	4	2x2	d	8
			±21		9	3x3	e	6
		60	±21	34	4	2x2	f	7
			±15		9	3x3	g	4
			±21	42	4	2x2	h	3
			±15		9	3x3	I	4
			±21	48	4	2x2	j	6
			±15		9	3x3	k	1
			±55	48	2	1 cell foam core	m	2
	T700	100	±30	84			n	6
					3	1 cell mandrel	o	2
12k	HTA	40	±21	48	9	3x3	p	1
					18		q	1

Table 4 Table illustrating combination of various parameters for test matrix

Table 4 enables certain parameters to be evaluated by comparing the experimental results of particular beams. For example, comparing beam type 'a' with beam type 'b' is used to examine the effect of changing the number of ends, as all other parameters in the test matrix have not been changed between the two types.

The following effects may be examined as a result of this test matrix.

The effect of changing the: -

i. Tow size –

Beam type e with p

ii. Original braid diameter (braid angle) –

Beam type a with f, b with h, c with i, d with j and e with k

iii. Number of tow ends –

Beam type a with b with d, c with e, f with h with j, g with and i with k

iv. Internal structure from 4 cells to 9 cells with a change in braid angle (by using the same original braid diameter) –

Beam type b with c, d with e, f with g, h with i and j with k

v. Internal structure from 4 cells to 9 cells with no change in braid angle (by using different original braid diameters) –

Beam type c with h and e with j

vi. Internal structure from 1 cell to a 4 cell with no change in fibre angle.

Beam types n and 0, compared with a, b and d.

7 Results

7.1 Introduction

From each of the specimens crushed, load-displacement data were recorded and plotted. A typical load – displacement curve is illustrated in Figure 33. Using these data an average load value is obtained for the total crush displacement of each specimen. The energy absorbed during the crush is determined by adding up the area under the load-displacement curve.

7.2 Quality assessment of samples

After infusing, curing and post curing the coretex beams, the specimens were assessed before testing.

Upon cutting the test specimens both the internal and external walls of the samples were revealed. A typical cross section of each beam type is illustrated in appendix D. Firstly the internal structure was not always regular. A vivid example of this feature is noted in beam sample '25B' in beam type C, found on page 118. This shows noticeable irregularities where certain cells are larger than others. This may be due to small differences in the original size of the foam used in manufacture. An example of a cross section of a beam with a more regular cell size would be '20B' in beam type J on page 125. It may be that the regularity of the cells depended on how accurately the foam was cut. Further work on foam cutting tolerances measurements would allow this to be specified.

The internal and external wall thicknesses for each beam type were measured as this was initially thought to be the most suitable way to characterise the beams structure. However, due to the nature of the braids having areas of fibre overlapping and areas in the braid where there are fibre gaps, there is fibre waviness in the structure walls which result in variations in the wall thickness. A typical example of this is shown in beam '40C' in beam type G where the internal wall thickness varies from 1.6 to 2.2mm thick. As a result of this inconsistency it is difficult to use wall thickness as a quantitative measure in comparing different beams. This variation in wall thickness was also observed in external cell walls of single cell beams, for example sample 35A

in beam type N on page 128 where in some areas the wall thickness has nearly doubled. Therefore a way of averaging out these local variations was to assess the manufactured test specimens in terms of global density as a quantitative measure of the quality of the specimens. This allowed processed specimens with the same initial material and geometry parameters (that is, the same beam type) to be easily compared with one another in terms of density and fibre volume fraction. A table that includes the details of all the specimens tested is presented in the appendix D where values such as global density and fibre volume fraction are illustrated. Also in this appendix is a section illustrating the equations used to calculate the processed data.

When comparing specimens of the same beam type, that is the same fibre architecture for all specimens, the variation of wall thickness was found to be directly related to the variation found in resin mass. This variation has been correlated to beam energy absorption performance and is described and commented upon in section 8.5 on page 91.

Conventionally, in fibre reinforced composite materials where the fibre density is greater than the matrix density, an increase in fibre volume fraction would also correspond to an increase in the overall or 'global' density of a composite with a fixed volume. However, in coretex structures where the effective volume or cavity may not be constant due to the volume change of the foam, the fibre volume fraction of the overall structure decreases with an increase in overall (or global) density. This trend has been observed when a set of beams have been manufactured with the same braid and foam mass used as the preform but variations in the final mass of the part are found. This is due to the variation in volume found in the expanded foam when under vacuum. If the expanded foam volume is less than expected, the infusing resin will substitute its space resulting in a beam with resin rich areas. As the outside dimensions have remained constant the mass and global densities have increased with a corresponding drop in fibre volume fraction.

7.3 Effect of tow size

The 9 cell geometrical structure was chosen to show the effect of tow size over the 4 cell and single structures for braid supplier convenience. By comparing beam type 'e' with beam type 'p', see Table 4, the effect of tow size can be examined. The difference in fibre tow size was investigated in the axial quasi-static crush of 3x3 array coretex beams, made from HTS 12K fibre, and 24K STS fibre.

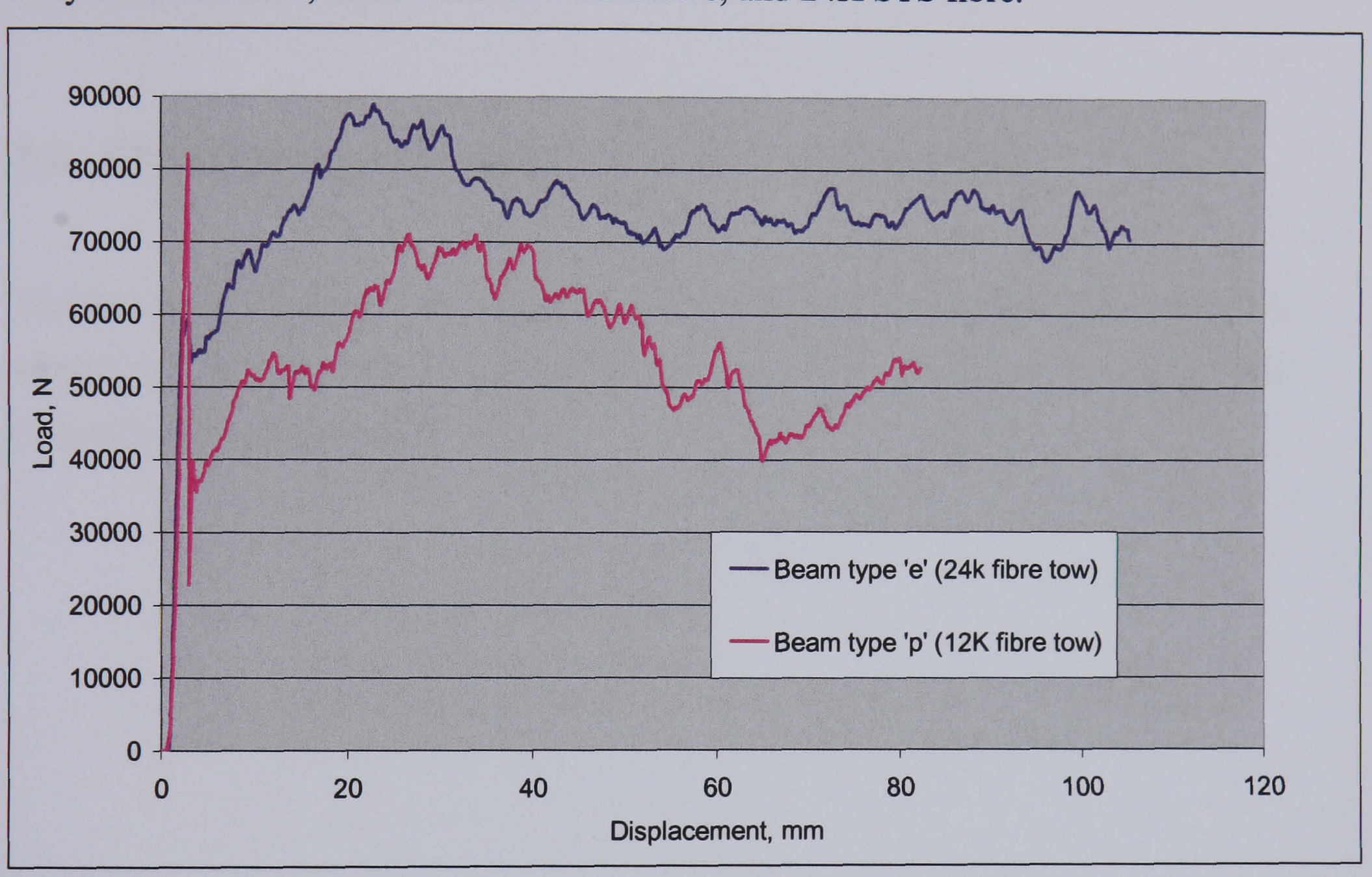


Figure 1 Load versus displacement chart illustrating effect of tow size

Specific energy absorption, SEA, was found to be higher in the 12K fibre beams than the 24K fibre beams. Even though the 12K beam exhibits a lower average load than the 24K beam; the global density in the 12K tow beam is significantly lower than that of the 24K tow beam, see Table 5. Consequently, this results in a more efficient crush for the 12K beam in terms of specific energy absorption.

Fibre Type	Density, g/cm^3	Ave. Load, kN	SEA, J/g
12K HTS (48E, 40mm)	0.241	57.2	69.1
24K STS (48E, 40mm)	0.347	73.2	60.1

Table 5 Typical data for beam type 'e'- 24K STS (48E, 40mm) and beam type 'p' - 12K HTS (48E, 40mm)

7.4 Effect of original braid diameter (braid angle)

The following bar chart, see Figure 34, illustrates how the original braid diameter affects the specific energy absorption of coretex tubes crushed at quasi static (10mm/min) loading conditions.

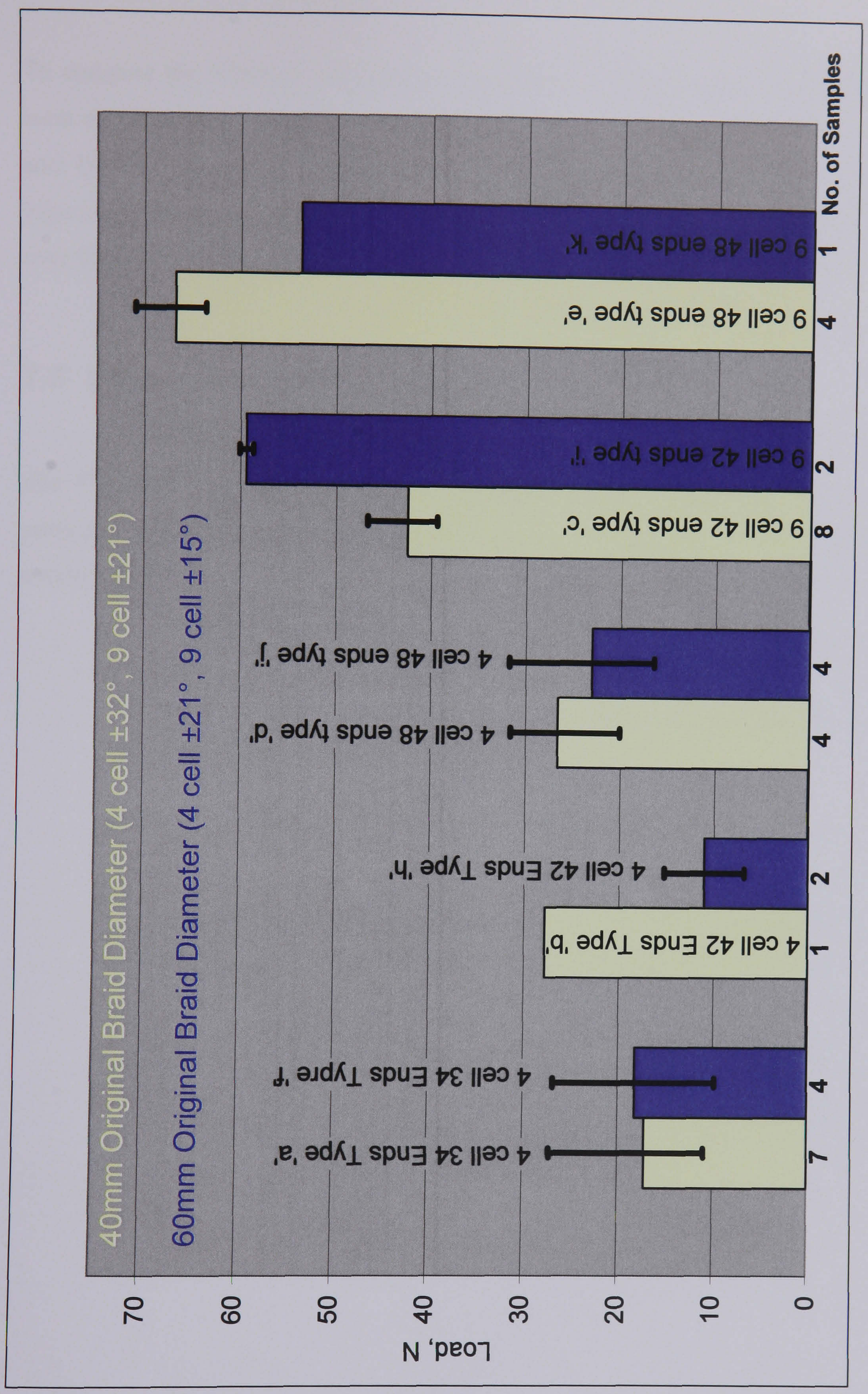


Figure 34 Bar chart illustrating the effect of varying the original braid diameter and therefore braid angle for coretex beams tested at 10mm/min crush. Each bar shows the mean value with the error bars indicating the maximum and minimum values.

To compare the effect of original braid diameter, ten different beam configurations were manufactured. '4-cell' beams with three types of 'number of fibre ends' – 34, 42 and 48 ends and '9-cell' beams with 42 and 48 fibre ends were used. In general, Figure 34 indicates that there is no obvious advantage of using one braid diameter over the other. See chapter 8.2 on page 86 for discussion.

7.5 Effect of number of tow ends

The following bar chart, Figure 35, illustrates how the number of tow ends for particular beam types varies with specific energy absorption under quasi-static crush conditions.

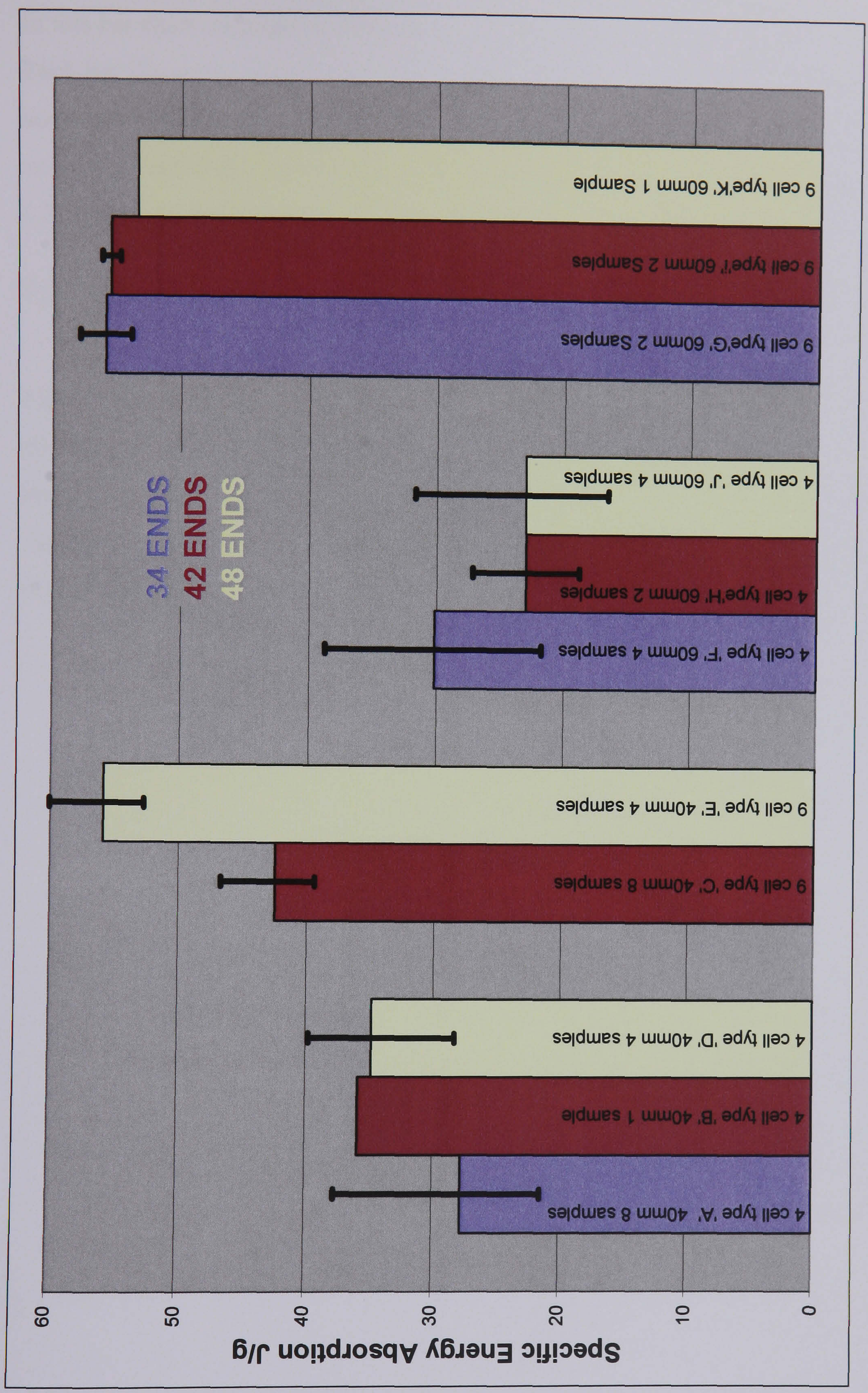


Figure 35 Bar chart illustrating the effect of varying the number of tow ends in a braid on specific energy absorption when tested in crush at 10mm/min. Each bar shows the mean value with the error bars indicating the maximum and minimum values.

In this bar chart each bar is labelled with the beam type and number of samples tested. Each bar illustrates the average value obtained from the samples. The maximum and minimum values observed are shown using the range (error) bars. There seems to be no general correlation of fibre tow ends with specific energy absorption. See chapter 8.3 on page 87 for discussion.

7.6 Effect of internal structure

Figure 36 is a bar chart showing the effect of internal geometry with specific energy absorption. More specifically it illustrates the effect of changing the number of braided tubes in the structure from 4 tubes to 9 tubes, as shown in Figure 37. The 'scatter bars' on the chart show the range of results from maximum to minimum, and the number of samples is recorded on the chart for each beam type.

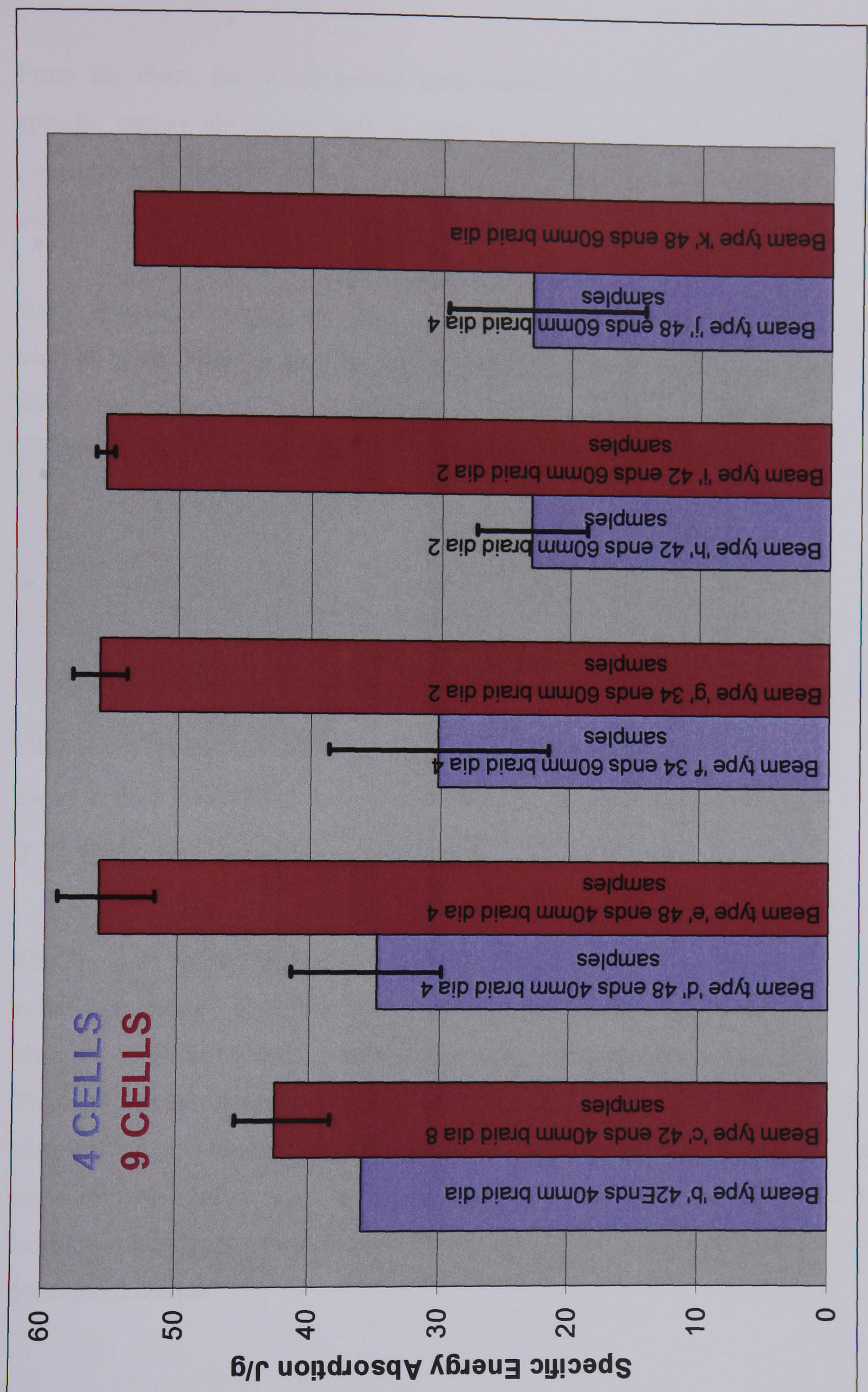


Figure 36 Bar chart illustrating the effect of varying the internal structure from 4 cells to 9 cells on specific energy absorption when tested in crush at 10mm/min. Each bar shows the mean value with the error bars indicating the maximum and minimum values.

From the chart, the 9-cell beams have consistently resulted in higher values for specific energy absorption and so there is a general correlation between internal geometry and specific energy absorption. See chapter 8.4 on page 87 for further discussion.

Beam structures bearing the same braid angle but with differing internal geometry, such as beam types 'c' with 'h' and 'e' with 'k', also display higher specific energy absorption values with the 9-cell beams as illustrated in Figure 36 above.

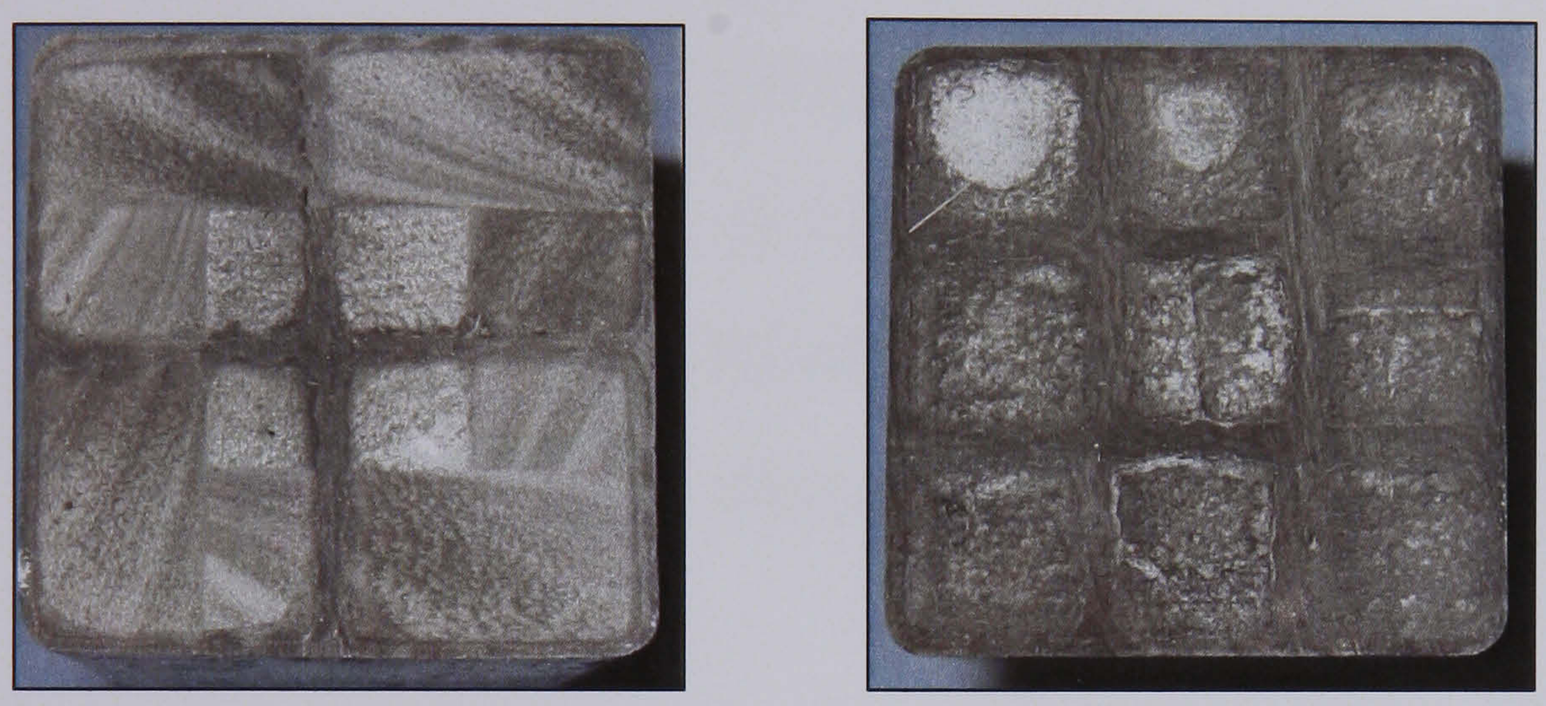


Figure 37 Photographs illustrating the cross section of a four-cell and nine-cell beam

7.7 Effect of loading condition

The bar chart below, Figure 38, highlights the effect of test loading condition on the coretex structures. Each pair of columns in the bar chart shows the specific energy absorption value of a beam that has been crushed and a beam that has been impacted. These beams have not only been paired together because of the beam type being identical but also because their global density and fibre volume fraction are either the same or very similar. This is an attempt to give the fairest comparisons between loading rate effects when every sample manufactured for this research could be considered unique.

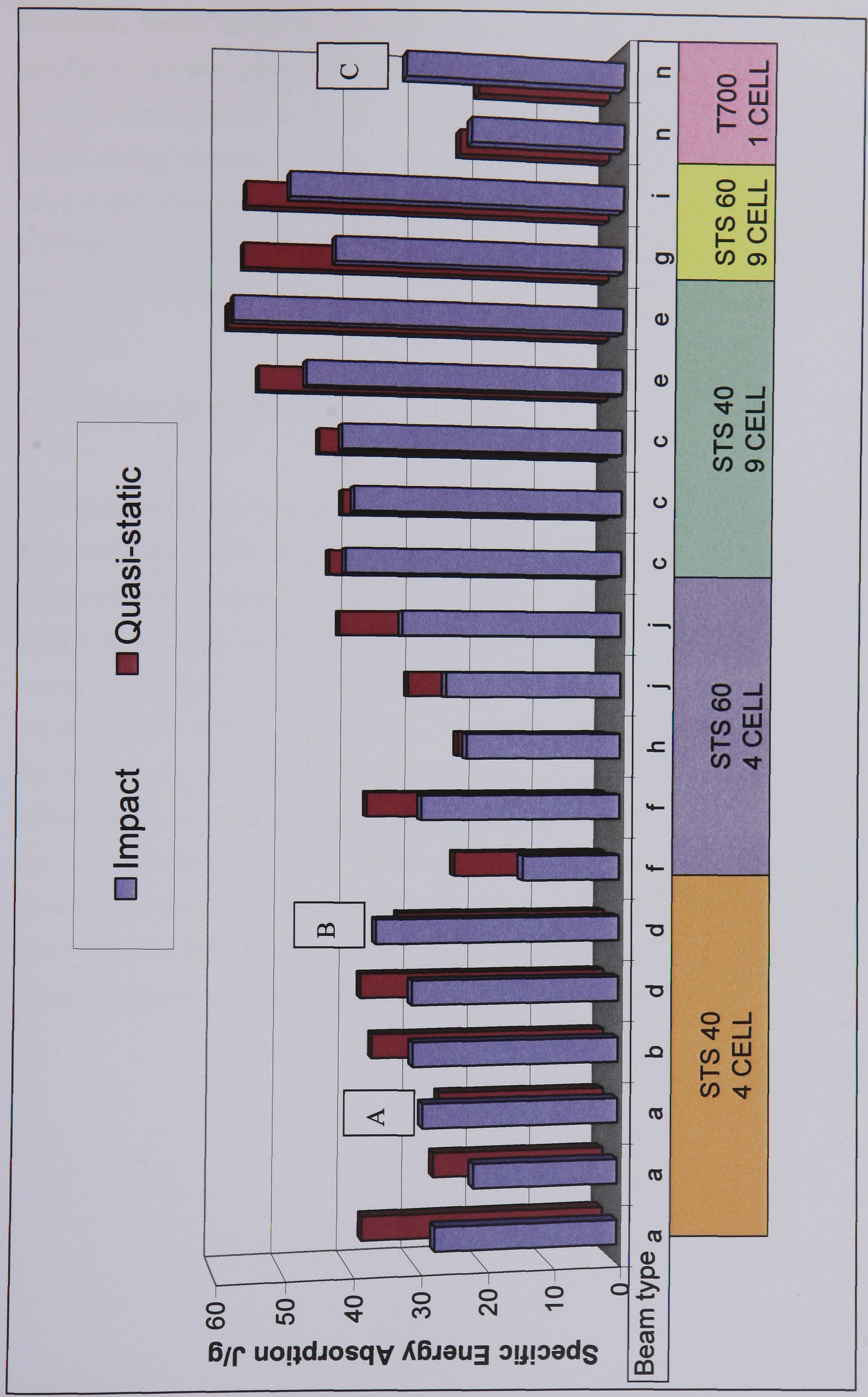


Figure 38 '3-D' column bar chart illustrating the effect of varying the loading condition from quasi-static to impact on the specific energy absorption.

Generally, beams tested in quasi-static 'crush' loading present higher values of specific energy absorption than those beams tested under impact. However, it is noted that in 3 cases, labelled A, B and C on the bar chart, beams crushed in impact show higher energy absorption values than those crushed quasi-statically. The first two cases A and B have been manufactured using a toughened resin, XU3508 instead of LY3505. The case labelled C showed a change due to buckling. For further discussion see chapter 8.6 on page 93. Details of all the beam types are presented in the appendix.

7.8 Effect of Resin Type

The initial test matrix programme was designed to compare the effect of different braid parameters and beam structures. However, the resin (matrix) part of the composite plays a significant role in the crush performance of the structure. Farley et al. [15] showed that using a matrix with a high strain to failure increases the specific energy absorption of graphite composite tubes and so two epoxy resins, namely LY3505 and XU3508, exhibiting high strains to failure were chosen, see chapter 3.5 for resin property data. Ramakrishna et al. [26] identified that the fracture energy, G_{IC}, of the epoxy is a key parameter in determining its performance under crush situations. As a result these 2 resins were chosen for their similar mechanical properties apart from the fact that XU3508 resin has a G_{IC} value 5 times more than that of the base line resin, LY3505. The following bar chart, Figure 39, shows how the specific energy absorption of beam type 'a' varies with the 2 resin systems.

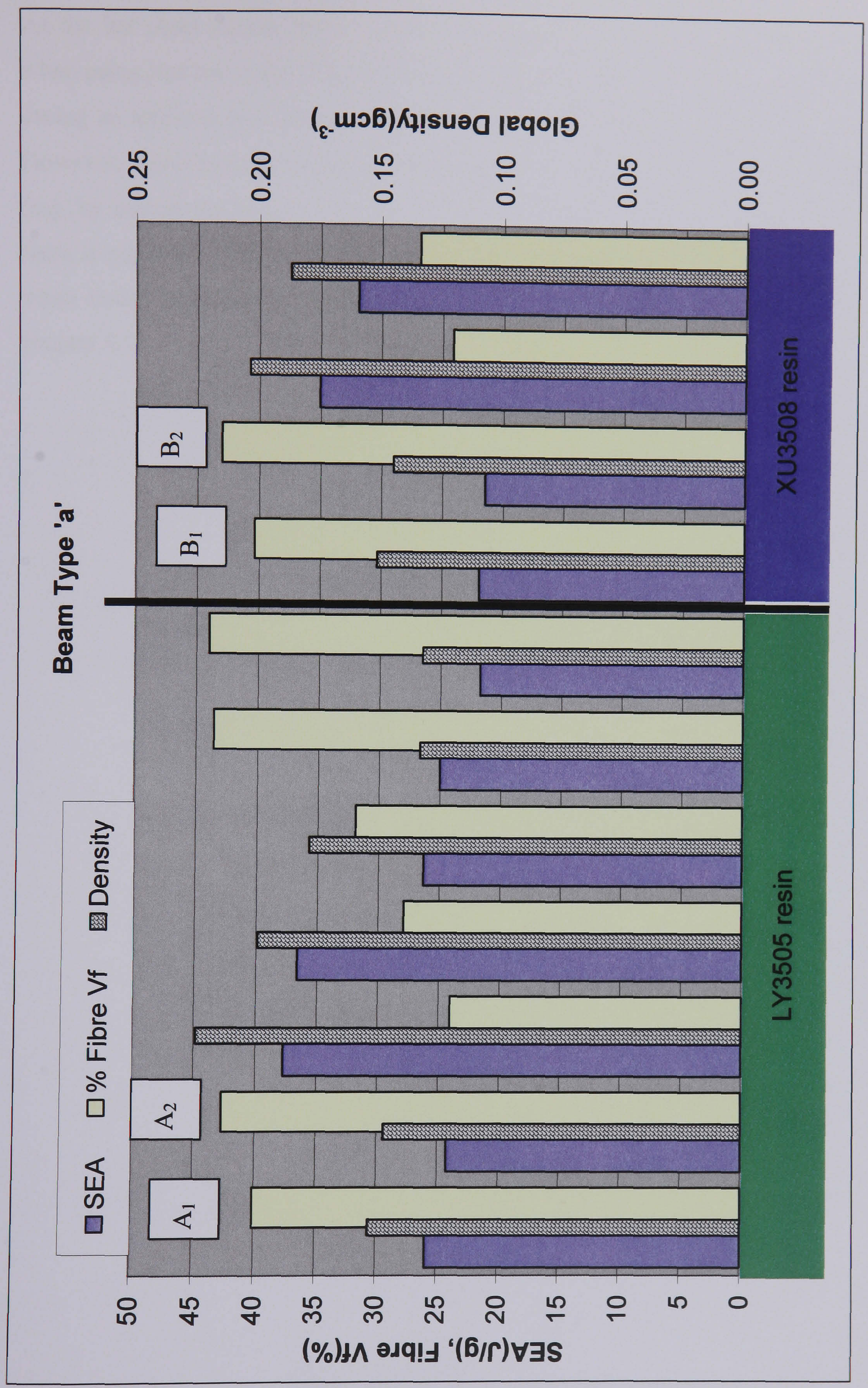


Figure 39 Bar chart illustrating the effect of resin type on beam type 'a' with specific energy absorption under both loading conditions.

As the bar chart shows, there is a variation in the performance of the beams even when using just one resin. This is attributed to the variation in amount of resin take-up during an infusion thus altering the beams' fibre volume fraction and global density. However, when beams of similar global density but of a different resin are compared, (e.g. by comparing beams labelled A_1 with B_1 and A_2 with B_2 on the above chart) there is relatively little difference observed in their specific energy absorption values when tested in quasi-static crush. This variation in results is discussed further in chapter 8.5.

8 Discussion

The results presented in chapter 7 are discussed in the following paragraphs.

8.1 Tow size effects

The 15% increase in specific energy absorption attributed to the 12k fibre beam, type 'p' when compared to beam type 'e' is a significant one. (Results presented in Figure 33 are analysed in Table 5 on page 74.) The 24K fibre beam (type 'e') has thicker walls and double the mass of fibre in comparison to the 12K fibre beam. This increases the average load observed when the beam is crushed. However, with a relatively high fibre mass content, this gives the beam a mass penalty. Consequently when using the specific energy absorption parameter in evaluating the beam's performance in crushing, this mass penalty becomes the dominating factor. Effectively, the increase in average load observed does not balance out the added mass and therefore the energy absorbed per unit mass is lower.

Similar observations of the effect of tow size have been found by Schultz et al [43] where carbon – epoxy composite tubes with fibre tows of size 50k were compared to tubes with 12k size fibre tows in quasi-static crush conditions. An increase in specific energy absorption of over 20% was found with the smaller 12K tow fibre tube. Furthermore, studies in Cranfield have shown that an increase of 7 to 17% in specific energy absorption was observed when decreasing the braided HTS carbon fibre tow size from 12k to 6k [6].

In spite of this, larger tow size carbon fibres are attractive in terms of their cost per unit mass. A kilogram of HTS 12k fibre costs approximately 20 Euros [44], 33% more than the same unit mass of STS 24k fibre (15 Euros) and so initially a large tow size is preferred for economic reasons.

However, when buying the 12K fibre in braid form compared to the 24K braided fibre, the difference in cost per kg for the 12K braid is less than 20% more expensive. As a result, when comparing cost per energy absorbed of a composite beam, the 12K

braid is only 75% of the cost of the 24K braid. Therefore the 12K tow size is more favourable in terms of energy absorbed per unit mass and energy absorbed per unit cost

It is thought that the decrease in specific performance of the 24k fibre is due to the increased waviness and coarseness observed when compared to the 12k fibre tows. This allows larger areas in between the tows where resin-rich cavities are observed. This is undesirable as this results in a less homogenous composite structure and therefore more significant differences in modulus between the two phases (that is the fibre composite phase and the resin-rich matrix phase) leading to a modulus mismatch and an area prone to stress cracking.

Additionally, the heavier, 24k tows have a smaller proportion of the fibres in the 'in-plane' direction, due to the increased waviness. This may produce a decrease in the ultimate axial compression strength of the composite, which has been proved to be a good indicator of crush performance in other thermosetting composite material systems, see [25].

8.2 Braid angle (diameter) effects

As mentioned in chapter 3.3.1, braid angles of ±32° and ±21° were used to produce beams constructed of a four cell structure, namely the beam types a, b, d, f, h and j, see Table 4 and Figure 34. It may be expected that the beams with lower angle braids, that is ±21°, would give higher specific energy absorption values. A possible reason for this is that fibre angles that are closer to the direction of loading, that is towards zero degrees become more efficient in sustaining the applied compression loads. This would concur with investigations conducted by Chiu et al. [45] where a carbon epoxy triaxially braided tube with a braid fibre angle of ±20° gave the best performance in crush compared to higher fibre angled tubes. However, this is not found to be the case in four cell coretex beams of which specific energy absorption values are shown in Figure 34 on page 75.

Similar findings have been found with varying the braid angle from ±21° to ±15° on the 9 cell coretex beams. Again it is not obvious which fibre angle performs best in absorbing energy under quasi-static crush conditions.

8.3 Effects of number of tow bundles in braid

Apart from varying the fibre angle, another way to alter the properties of a braid is to vary the number of tow ends or tow bundles that form the braided fabric. In the 4 and 9-cell multi-cellular coretex beams, braids with three different amounts of tow ends were used, namely braids with 34, 42 and 48 tow ends. This obviously changes the mass per metre of the braids in question, see chapter 3.3.2, but also affects the average wall thickness of the braid, as well as other parameters such as surface coverage. In reviewing the literature, changing wall thickness and especially changing the diameter to wall thickness ratio can affect the specific energy absorption of a crush structure as discussed in chapter 2.1.8.

However, in comparing the amount of tow ends in 4 cell coretex structures with their corresponding specific energy absorption values (as shown in Figure 35) there does not seem to be a correlation. In terms of specific energy absorption, it is quite possible that any increase in average crush load (and therefore energy absorbed) by braids with a high number of tow ends is effectively balanced out by the increase in braid mass found in the structure.

8.4 Effect of internal structure

As illustrated in chapter 7.6, 9-cell coretex beams gave significantly higher specific energy absorption values than coretex beams constructed from 4 cells. Initially this phenomenon was thought to be partially due to the increased stability that the internal structure gave to the outer walls. However, it was also noted that the global density of a nine-cell coretex structure was on average significantly higher than that of a four-cell structure with the same external dimensions. For this reason, steps were made to

determine whether the increase in specific energy absorption shown for the nine-cell coretex beams was primarily a geometrical factor or a mass factor.

In doing this, specific energy absorption values for each specimen tested in quasi-static crush or impact loading were plotted against global density and shown in the following Figure 40.

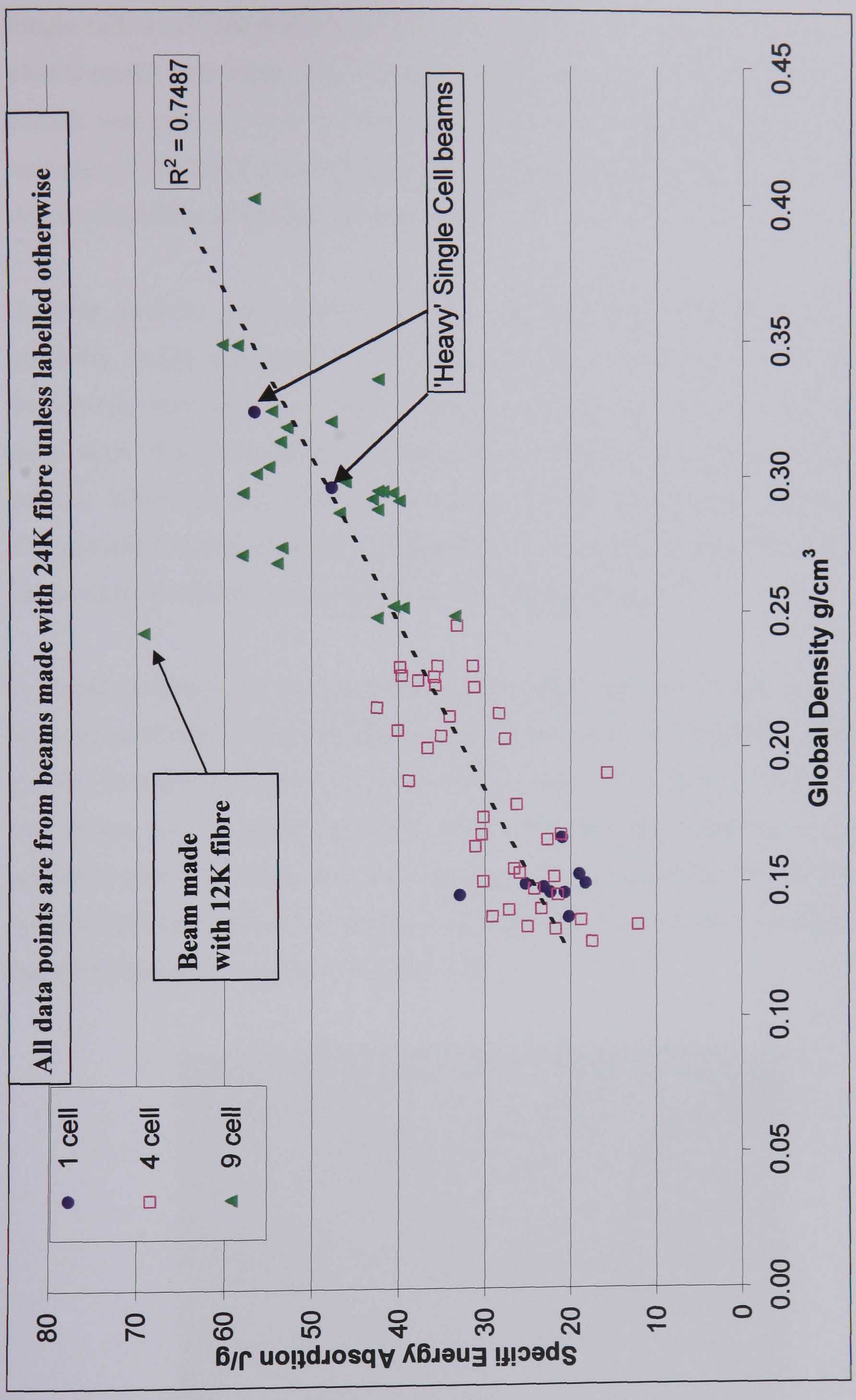


Figure 40 Scatter chart plotting specific energy absorption values against global density for all coretex test specimens

Single cell, 4-cell and 9-cell coretex beams with a range of global densities were all plotted on the same chart. The relation between specific energy absorption and global density was assessed with a linear correlation. An 'r-squared' value of $r^2 = 0.7487$ indicates a reasonably good correlation between specific energy absorption and global density regardless of the internal geometry.

To help confirm the independence of specific energy absorption from internal geometry, single cell beams - namely beam type 'o' (see Table 4 on page 70 for description) were produced. These beams were designed so that they would have the same mass of a typical nine-cell coretex beam without any of the internal structure present. When tested in quasi-static crush, it was found that these single cell beams also absorbed similar amounts of energy when compared to energy absorption values achieved by 9-cell beams. These results are shown in Figure 40.

It should be noted that the relatively high-density single cell beams, beam type 'o', manufactured with 3 layers of braid to give a substantial wall thickness, progressively crushed in a similar manner to multi-cellular beams, see Figure 41. However, single cell beams such as beam type 'n', with a smaller wall thickness, crushed in an accordion-type buckling mode. See Figure 42. This suggests that the thickness of the walls in the beam and not the internal structure of the beam is the controlling factor in determining specific energy absorption values.



Figure 41 Beam type 'o' undergoing quasi-static crush showing a progressive crush failure mode

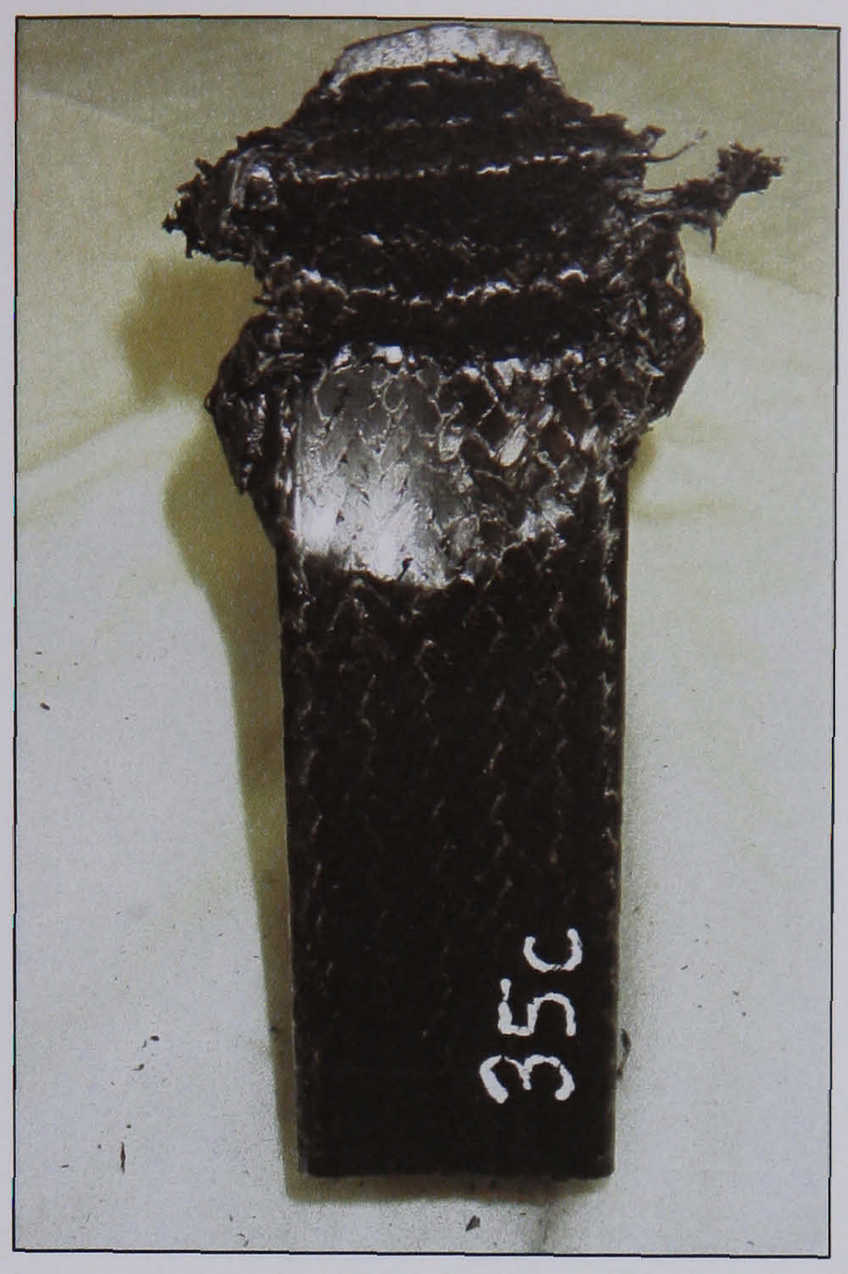


Figure 42 Beam type 'n' after a quasi-static crush showing accordion-type buckling failure mode

In section D of the appendix, photographs of cross sections of each beam type are illustrated. These photographs, together with maximum and minimum values of wall thickness measured from the arbitrary cross sections, indicated that the extent of variation on a local scale is considerable. However, scatter in the results of the axial crush tests is significantly lower. In order to give an overall view of the work, it was decided that the effect of local variation would be assessed.

It was therefore decided that global properties would be used to assess the basic crush behaviour of the beams. It is recognised that there is considerable scope for further analysis in the production of these beams.

8.5 Resin effects

As illustrated in the results in chapter 7.8, the effect of using a toughened resin did not significantly improve the specific energy absorption values seen by the test specimens. However, a significant degree of variation in these values was found. The following bar chart, see Figure 43 helps illustrate the cause of this variability. The bar chart below shows that specimens with identical braid mass, architecture, angle and structure can still exhibit relatively large variation in specific energy absorption values simply due to the amount of resin mass infused in to the specimens.

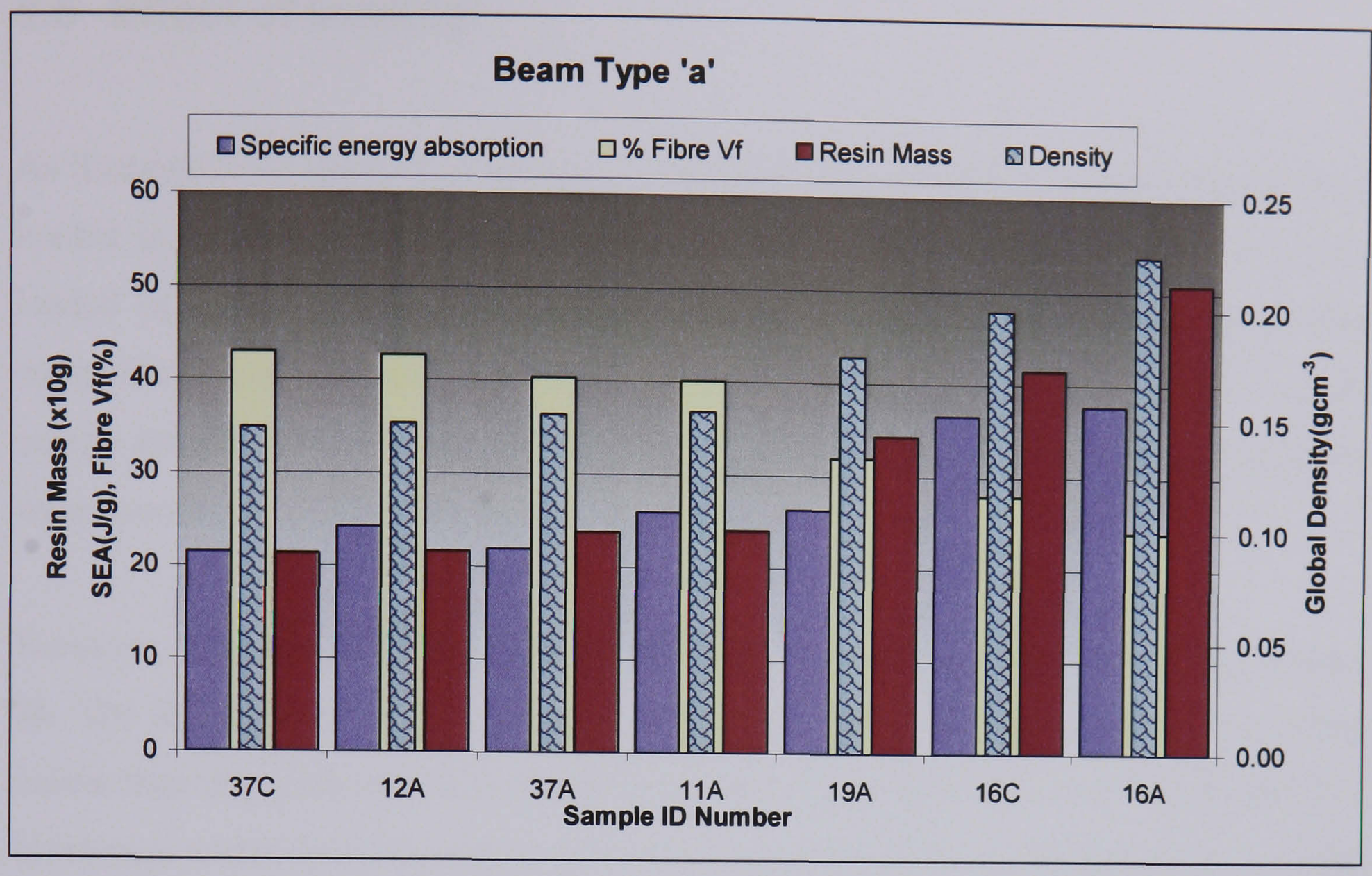


Figure 43 Bar chart illustrating the effect of variation in resin mass on the density, volume fraction and specific energy absorption in beam type 'a' specimens.

As the fibre and foam mass are constant in all specimens, the variation in global density seen from beam sample to beam sample is attributed to a variation in the amount of resin infused into the different beams. Beams with relatively high global densities will have relatively low fibre volume fractions. Also, beams showing relatively high global densities will also show high specific energy absorption values. This trend is also seen in Figure 40.

The observation of specific energy absorption increasing, as the effective fibre volume fraction of the composite is decreasing is not a usual one [29]. This is possibly explained due to the differences in the manufacturing process of coretex structures. Resin infused tubes manufactured using hard surface tooling for both the internal and external surfaces of the tube allow a constant volume (minus the fibre preform volume) to be filled. However, in coretex structures, the foam used to form the internal surface of the tube walls is soft and may allow for variations in wall thickness that effectively may allow for variations in the amount of overall resin mass found in a beam.

8.6 Effect of loading

As illustrated in Figure 38 on page 81, specific energy absorption values of specimens loaded in crush are on average 8% higher than values calculated from specimens loaded in impact. This trend was also found in other recent studies of braided composites where the same fibre and matrix system was used and increases in specific energy absorption values of 15% [46] from impact to quasi-static loading conditions were found.

However, the opposite of this trend is found for the beams labelled A and B in Figure 36. The difference in resin type may explain why the impacted beams show higher values than the quasi-statically crushed beams as the toughened resin will present less brittleness under dynamic testing and will support the fibres for longer period of time thus sustaining load levels for longer. The case labelled C on the graph has not been manufactured with the toughened resin but a change in failure mode, namely local buckling, possibly due to a different fibre type and/or structural geometry being used may be attributed to explain this result.

There are a number of theories trying to explain this phenomenon. A possible reason for the reduced amount of energy absorbed under impact conditions is due to the possible difference in frictional forces acting in the crush zone and crush interface. At higher strain rates, the coefficients of friction may change. As a significant amount of the energy transformed in crushing is taken up as friction, this becomes an important parameter.

Under impact, the energy is absorbed in just a few milliseconds. The numerous fractures and new surfaces that are created increase the temperature seen at the crush zone interface. This increase in temperature, albeit for a short time, may increase the temperature of the matrix resin closer to its glass transition temperature and 'soften' the resin reducing its mechanical properties. As this happens it may be possible that longer crack lengths occur at the crush zone interface. This effectively increases the length of the crush zone and allows fractures to occur at lower crush loads.

8.7 3-Point Bend Tests

As mentioned in the experimental chapter 5.4. A bending test, set-up to replicate the FMVSS 214 quasi-static door crush test was employed to evaluate the performance of these multi-cellular braided structures with respect to the application of potential use as side impact beams in car door frames. The following chart, Figure 44 illustrates the load displacement curve of the best performing coretex braided beam from a sample of four coretex beams tested in bending.

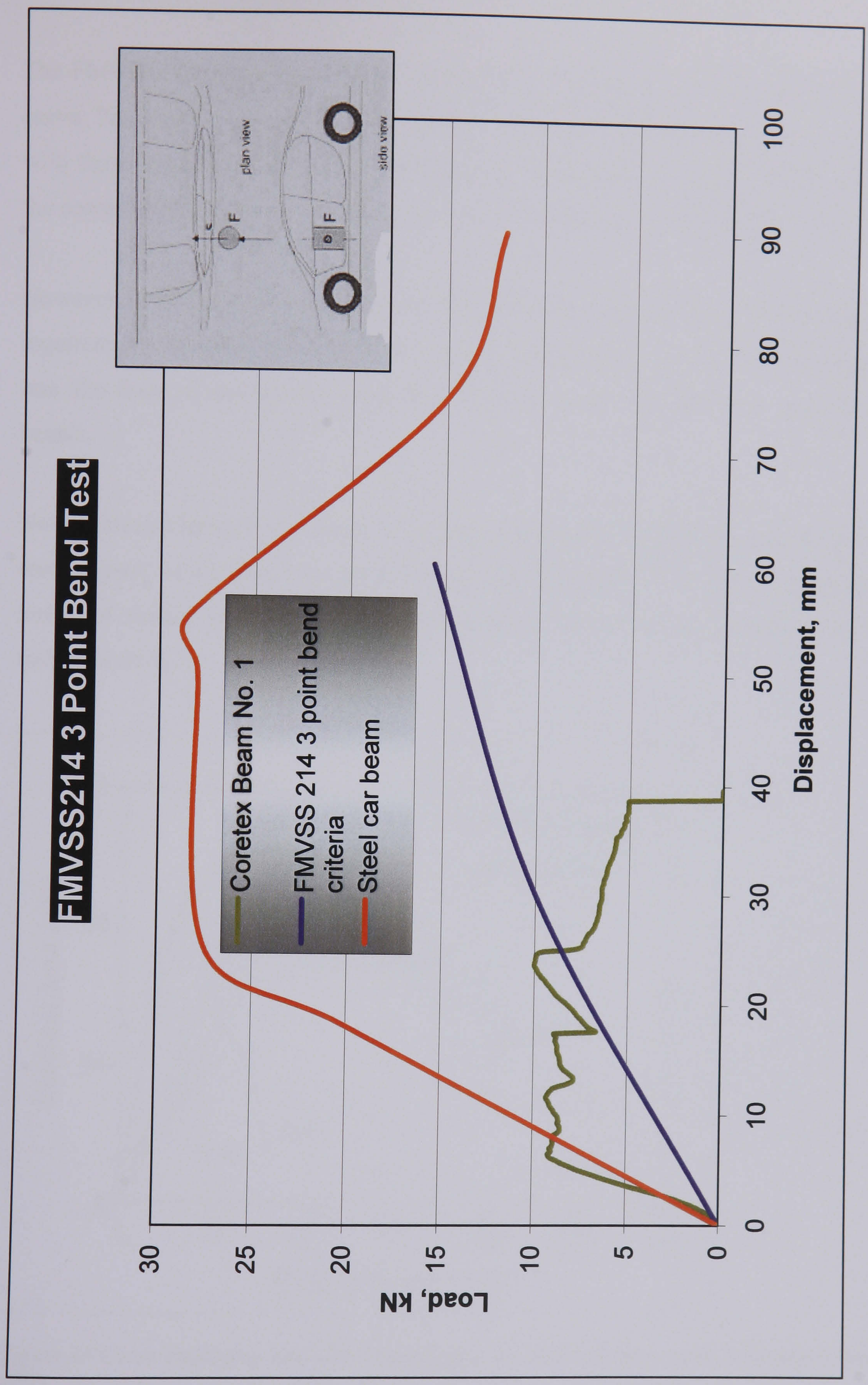


Figure 44 Chart illustrating load deflection data of FMVSS 214 3-point bend test including the plan and side view of FMVSS 214 door crush test with force deflection criteria displayed graphically.

The FMVSS214 door crush test criterion is also represented in Figure 42 as the blue curve. The figure graphically illustrates how the loads sustained by the beam compare with those loads required by the test criterion. Where, after a displacement of 25mm the coretex beam load levels are too low thus not satisfying the FMVSS214 criterion.

However, it should be noted that FMVSS214 only provide performance standard requirements for the door as one part, which includes any side protection integrated into the door. Consequently there are no performance standards for just the side beams.

Nevertheless, research by Cheon et al. [47] conducted FMVSS214 tests on just the steel impact beam found in existing cars and compared it to various glass/epoxy beams of similar geometry. The following graph illustrates the differences between these materials.

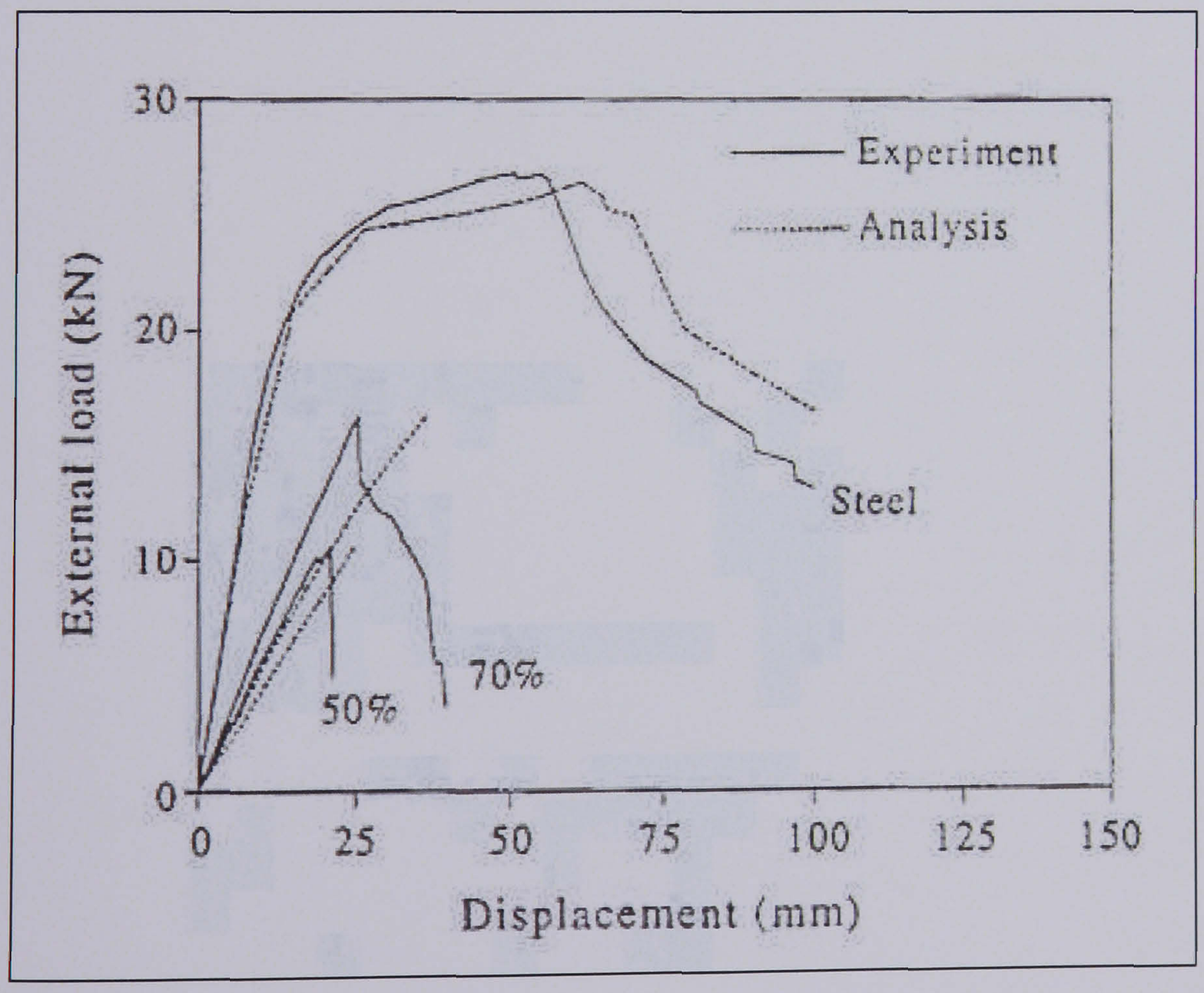


Figure 45 Chart displaying load displacement data for steel and glass-epoxy side impact beams [47]

The curves labelled 50% and 70% are the glass/epoxy beams with the percentages defining the weight compared to the steel beam. From the graph it is clear to see that

the load displacement data obtained from the steel side impact structure varies greatly from the FMVSS 214 standard curve shown in Figure 44 for the whole door.

Yet, the load displacement curve for the steel side impact beam (shown as the red curve in figure 42) is a good guideline for the performance requirement of a side beam alone. When this curve is compared to the curve found for the braided carbon beam (Figure 44) it is clear that this composite beam under performs in this type of loading. The ductile failure of the steel beam, which is not observed with the composite beams, allows the beam to absorb energy at large displacements.

Due to these results found towards the beginning of the experimental period, it was decided to concentrate experimental work in axial crush rather than transverse loading.

8.8 Mould Tooling

A significant part of this experimental programme was concerned with designing suitable moulds for manufacturing the various composite beams. It was found that the aluminium mould tools produced the best quality beams. This was achieved using nitrile o-ring cord sealing technology resulting in low vacuum leak rates. The less expensive PVC mould tooling was prone to producing composite beams with a significantly low level of dimensional tolerance. This was due to the lack of stiffness of the PVC mould tool walls which softened at temperatures above room temperature. Increasing the PVC mould tool's wall thickness would increase the stiffness and the overall dimensional stability of the moulded part. However, the increase in thickness would also make demoulding more difficult due to the increase in stiffness of the mould tool walls thus increasing time to demould the part. Thickening the PVC mould tool would also increase the cost of the mould which may become a significant factor as the moulds would be used as disposable tools. As the PVC will soften at much lower temperatures than aluminium, using a resin system with a higher curing temperature for infusion would also render the PVC mould tools unsuitable.

Increased dimensional stability would be found using GRP mould tools as opposed to PVC moulds and with the automotive industry in mind, the choice of tooling depends greatly on the number of parts per year desired. For low volume / niche production volumes, GRP mould tools may be a feasible option. As the capital costs for GRP tooling is generally less than that of steel or aluminium tooling. However for larger production volumes metal mould tools such as aluminium may be the most feasible as they tend to last longer than GRP tools and typically, tooling repair and maintenance is costs are lower. Although the coefficient of thermal expansion of aluminium is relatively high the difference between the maximum and minimum temperatures observed during a typical curing cycle are not larger than about 60 degrees Celsius. This difference in temperatures does not significantly affect the final external dimensions of the cured structure. An advantage of the of the high thermal conductivity shown by aluminium is that cycle times for pre heating the mould and cooling the mould after curing are less than that observed for GRP mould tools thus reducing the overall cycle time for manufacture.

8.9 Summary

Upon discussion of the experimental results it is found that beam type 'p' - a multi-cellular beam of 9 cells produced from 12k tow carbon fibre with a braid angle of ±20° and a fibre volume fraction of 35% exhibited the highest value of specific energy absorption of just under 70 J/g in axial loading. This value of specific energy absorption performance is over double that observed in aluminium crash structures used in existing cars [46].

However, as cost is a dominant factor in the automotive industry, the cheaper, 24k tow STS carbon fibre may be used for the braid. A reduction in performance in terms of specific energy absorption of 10 to 15J/g would be observed in using this braid but the fibre material costs could be reduced by a third thus making beam type 'e' the most attractive option.

9 Conclusions

The performance of carbon-fibre epoxy multi-cellular braided composite structures in terms of their specific energy absorption values obtained under crush and impact loading has been investigated. Within this investigation a number of material and testing parameter effects were observed.

It can be concluded that

- Initial development work has shown that it is necessary to use a temperature between 40 and 70 degrees Celsius in order to give adequate expansion of the foam to produce the required consolidation while maintaining resin flow. Under these conditions it was established that aluminium was superior to PVC and GRP for the production of mould tools.
- Structures with the same fibre angle and cross sectional geometry show lower specific energy absorption values with 24k size fibre tows than the more expensive and smaller 12k size fibre tows.
- Generally, specimens tested in impact loading conditions exhibited lower specific energy absorption values than specimens tested in quasi-static loading conditions.
- With the two epoxy resins systems used, it was found that the amount of resin, and therefore the volume fraction of the composite was a more significant factor in affecting the specific energy absorption values observed than the difference in fracture toughness, G_{IC}, values of these resins.
- From the two fibre braid angles compared, there was no distinct advantage of using one fibre angle over another in terms of specific energy absorption values observed.
- In general the specific energy absorption values observed increased with increased global density of the specimens.
- No correlation has been observed between the number of tow ends in the braid and specific energy absorption values observed in the four-cell composite structures tested.

- Although nine-cell structures exhibit higher specific energy absorption values than four-cell structures this is attributed to the higher global density observed in nine cell structures and not the difference in internal geometry.

Traditionally, metallic tubes are used for energy absorption in cars. As a preliminary survey, the specific energy absorption of some metallic tubes was compared with the best performing coretex beams from this work. These coretex structures gave values at least twice those obtained from the metallic tubes. As a result coretex structures have the potential to be viable alternatives to traditional crash structures in reducing mass and increasing energy absorbing performance in automotive vehicles.

10 FUTURE WORK

Much development work of the processing of coretex structures has been carried out in this research to achieve a higher level of understanding of the unique vacuum infusion process used to manufacture coretex parts. Even so, further investigations into the behaviour of the foam during processing would be desirable to help reduce variability of wall thickness and fibre volume fraction found between infused coretex beams. This should achieve greater consistency and repeatability in producing components, increasing confidence levels in predicting the behaviour in energy absorbing conditions.

In this work only braided composites have been examined, but due to the nature of braided fabric, it is inevitable that some of the in-plane properties are lower compared with layers of stitched carbon fabrics where there is no crimping of the fibres. It would be sensible to compare the energy absorption performance of braided coretex structures with the more conventional fabric materials. This would highlight any potential benefits or drawbacks in the manufacturing and final energy absorbing performance of preforms such as NCFs (non crimp fabrics).

Coretex beams constructed from biaxial braided fibres were investigated in this research, but it is suggested that the use of triaxial braided reinforcement may further increase performance in specific energy absorption. However, there may be consolidation problems arising due to using a triaxial braid.

Modelling the crush behaviour of the coretex beams would be a valuable tool in tailoring their design to optimise performance for specific scenarios and allow detailed improvements to meet design and manufacturing requirements.

11 REFERENCES

1. Johnson, W. and A.G. Mamalis, *Crashworthiness of Vehicles*. 1978, London, UK: Mechanical Engineering Publications.
2. Mamalis, A., et al., *Crashworthiness of Composite Thin-Walled Structural Components*. 1998: Technomic Publishing Co., Inc.
3. Mills, A., A. Castanos, and M. Frost. *Development of a Carbon Fiber Composite Ultra- Lightweight Vehicle Structure for the Aero-Stable Carbon Car-Fastframes*. in *SAE 2002 World Congress & Exhibition*. 2002. Detroit, MI, USA: SAE Technical Papers 2002-01-1121.
4. Mills, A., A. Castanos, and M. Frost. *Development of a carbon fibre composite ultra lightweight vehicle structure*. in *23rd International SAMPE Europe Conference*. 2002. Paris, France.
5. Ramakrishna, S., *Microstructural design of composite materials for crashworthy structural application.* Materials and Design (UK), 1997. **18**(3): p. 167-173.
6. Defays, P., *Low cost materials and process technologies for side impact crash structures, MSc*, in *The School of industrial and manufacturing science*. 2004, Cranfield University.
7. Jacob, G.C., et al., *Energy Absorption in Polymer Composites for Automotive Crashworthiness.* J. Compos. Mater., 2002. **36**(7): p. 813-849.
8. Jimenez, M.A., et al., *Effect of trigger geometry on energy absorption in composite profiles.* Composite Structures (UK), 2000. **48**(1-3): p. 107-111.
9. Farley, G.L. and R.M. Jones, *Crushing Characteristics of Continuous Fiber-Reinforced Composite Tubes.* Journal of Composite Materials (USA), 1992. **26**(1): p. 37-50.
10. Thornton, P.H., *Energy Absorption in Composite Structures.* J. Compos. Mater., 1979. **13**: p. 247-262.
11. Fairfull, A.H. and D. Hull. *Effects of specimen dimensions on the specific energy absorption of fibre composite tubes*. in *Proceedings of the sixth International Conference on Composite Materials combined with the second European*

Conference on Composite Materials. 1987. Imperial College of Science and Technology, London,UK.

12. Schmueser, D.W. and L.E. Wickliffe, *Impact energy absorption of continuous fibre composite tubes.* J. Eng. Mat. Trans. ASME, 1987. **109**: p. 72-77.
13. Farley, G.L., *Effect of Specimen Geometry on the Energy Absorption Capability of Composite Materials.* J. Compos. Mater., 1986. **20**(4): p. 390-400.
14. Farley, G.L., *Energy Absorption of Composite Materials.* J. Compos. Mater., 1983. **17**(3): p. 267-279.
15. Farley, G.L., *Effect of Fiber and Matrix Maximum Strain on the Energy Absorption of Composite Materials.* J. Compos. Mater., 1986. **20**(4): p. 322-334.
16. Farley, G.L. *Energy Absorption in Composite Materials for Crashworthy Structures*. in *Proceedings of the sixth International Conference on Composite Materials combined with the second European Conference on Composite Materials*. 1987. Imperial College of Science and Technology, London,UK.
17. Thornton, P.H. and P.J. Edwards, *Energy Absorption in Composite Tubes.* J. Compos. Mater., 1982. **16**: p. 521-544.
18. Hull, D., *A unified approach to progressive crushing of fibre-reinforced composite tubes.* Composite Science and Technology, 1991. **40**: p. 377-421.
19. Hamada, H., et al., *Energy Absorption Behavior of Hybrid Composite Tubes.* ASM International (USA), 1994: p. 511-522.
20. Ramakrishna, S. and H. Hamada, *Energy absorption characteristics of crash worthy structural composite materials.* Key Engineering Materials (Switzerland), 1998. **141-143**(2): p. 585-619.
21. Chiu, C.H., C.K. Lu, and C.M. Wu, *Crushing characteristics of 3-D braided composite square tubes.* Journal of Composite Materials (USA), 1997. **31**(22): p. 2309-2327.
22. Tao, W., R. Robertson, and P.H. Thornton, *Effects of material properties and crush conditions on the crush energy absorption of fiber composite rods.* Composite Science and Technology, 1993. **47**: p. 405-418.

23. Thornton, P.H. and R.A. Jeryan, *Crash energy management in composite automotive structures.* International Journal of Impact Engineering (UK), 1988. **7**((2)): p. 167-180.
24. Ramakrishna, S., et al., *Energy absorption behaviour of carbon-fibre-reinforced thermoplastic composite tubes.* Journal of Thermoplastic Composite Materials, 1995. **8**: p. 323-344.
25. Warrior, N.A., et al., *Effect of resin properties and processing parameters on crash energy absorbing composite structures made by RTM.* Composites: Part A, 2003. **34**: p. 1-8.
26. Ramakrishna, S., H. Hamada, and H. Sato, *Effect of Fiber Orientation the Energy Absorption Capability of Carbon Fiber/PEEK Composite Tubes.* J. Compos. Mater., 1996. **30**(8): p. 947-963.
27. Hamada, H. and S. Ramakrishna, *Scaling effects in the energy absorption of carbon-fiber/PEEK composite tubes.* Composites Science and Technology (UK), 1995. **55**(3): p. 211-221.
28. Mamalis, A.G., et al., *The static and dynamic axial crumbling of thin-walled fiberglass composite square tubes.* Composites Part B: Engineering (UK), 1997. **28B**(4): p. 439-451.
29. Ramakrishna, S. and D. Hull, *Energy absorption Capability of epoxy composite tubes with knitted carbon fibre fabric reinforcement.* Composite Science and Technology, 1993. **49**: p. 349-356.
30. Farley, G.L., *The Effects of Crushing Speed on the Energy-Absorption Capability of Composite Tubes.* Journal of Composite Materials (USA), 1991. **25**(10): p. 1314-1329.
31. Mamalis, A., et al., *Energy absorption capability of fibreglass composite square frusta subjected to static and dynamic axial collapse.* Thin-Walled Structures (UK), 1996. **25**(4): p. 269-295.
32. Thornton, P.H., *The Crush Behaviour of Pultruded Tubes at High Strain Rates.* J. Compos. Mater., 1990. **24**(6): p. 594-615.
33. Verpoest, I., *Composite Preforming Techniques*, in *Comprehensive Composite Materials*. 2000, Elsevier Science Ltd. p. 623-669.

34. Campbell, F.C., *Manufacturing Processes for Advanced Composites*. 2004: Elsevier Ltd.

35. Ko, F.K., *'Braiding'*. Engineered Materials Handbook. Vol. 1. 1987: ASM International. pp.519-528.

36. Byun, J.H. and T.-W. Chou, *Mechanics of Textile Composites*, in *Comprehensive Composite Materials*. 2000, Elsevier. p. 719-761.

37. Chou, T.-W., *Microstructural Design of Fiber Composites*. 1992, New York: Cambridge University Press.

38. Falzon, P.J. and I. Herszberg, *Mechanical performance of 2-D braided carbon/epoxy composites.* Composite Science and Technology, 1998. **58**: p. 253-265.

39. Karbhari, V.M., P.J. Falzon, and I. Herzberg, *Energy absorption characteristics of hybrid braided composite tubes.* Journal of Composite Materials (USA), 1997. **31**(12): p. 1164-1186.

40. Chang, F.-K. and S. Beard. *Design of Braided Composite Tubes for Energy Absorption*. in *42nd AIAA/ASME/ASCE/AHS/ASC Structures, Structural Dynamics, and Materials Conference and Exhibit*. 2001. Seattle, WA.

41. Castanos, A. and A. Mills. *Analysis of Multicell Braided Composite Joints*. in *Future Car Congress*. 2002. Hyatt Crystal City, VA, USA: SAE Technical Papers 2002-01-1951.

42. Eurocarbon, *Eurcarbon carbon fibre braid manufactures Braid mass equations*. 2002.

43. Schultz, M.R. and W. Hyer, *Static Energy Absorption Capacity of Graphite-Epoxy Tubes.* Journal of Composite Materials (USA), 2001. **35**(19): p. 1747-1761.

44. *Telephone Communication with Tenax Fibres*. 2004: Wuppertal.

45. Chiu, C.H., K.-H. Tsai, and W.J. Huang, *Effects of Braiding Parameters on Energy Absorption Capability of Triaxially Braided Compoaites Tubes.* Journal of Composite Materials (USA), 1998. **32**(21): p. 1964-1983.

46. Pickett, A.K., S.D. Lazarus, and A. Lamb, *Static and dynamic testing of braided composite tubes under axial and oblique impact : Report for VW AG, Wolfsburg*. 2004, August, Cranfield University.

47. Cheon, S.S., D.G. Lee, and K.S. Jeong, *Composite side-door impact beams for passenger cars.* Composite Structures (UK), 1997. **38**(1-4): p. 229-239.

48. Farley, G.L. and R.M. Jones, *Crushing characteristics of composite tubes with 'near elliptical' cross sections.* Journal of Composite Materials (USA), 1992. **26**: p. 1252.

49. Hamada, H., et al., *Comparison of energy absorption of carbon-epoxy and carbon-PEEK composite tubes.* Composites, 1992. **23**(4): p. 245-252.

50. Hamada, H., et al., *The crushing performance of a braided I-beam.* Composites Science and Technology (UK), 1999. **59**(12): p. 1881-1890.

51. Hamada, H., *Effective braided preforms for crush elements in car.* Society for the Advancement of Material and Process Engineering, Evolving and Revolutionary Technologies for the New Millenium (USA), 1999. **44**(2): p. 2268-2276.

52. Pickett, A.K., S.D. Lazarus, and A. Lamb, *Static and dynamic testing of braided composite tubes under axial and oblique impact : Report for VW AG, Wolfsburg.* August 2004, Cranfield University.

12 APPENDICES

Appendix A: Specific Energy Absorption Table

Material	Type	Lay-up	SEA	t/D	Reference	Notes
Carbon - Epoxy	Laminate					
		[0/±15]	99	0.033	[14]	
		[0/±15]	75	0.045	[15]	
		[0/±45]	46	0.032	[14]	
		[0/±45]	55	0.051	[15]	
		[0/±45]	65	0.020	[30]	
		[±45]	58	0.048	[15]	
		[±45]	55	0.036	[13]	
		[±45]	60	0.031	[48]	
		[±45]	55	0.062	[17]	
		[±45]	53		[49]	
		[0]	53		[49]	G_{IC}= 0.21-0.26 kJ/m^2
		[0/90]	80		[10]	
		[0/90]	65		[10]	At 100°C temp.
		[±75]	63		[30]	At 10m/s crush speed
			110		[49]	Ratio of hoop to axial fibres is 1:3
			70	0.035	[10]	
	Knitted		85		[29]	Vf =22.5% fibre. Weft tested
			25		[29]	Vf = 15.75 fibre. Warp tested
Carbon-PEEK	Laminate	[0]	180	0.050	[49]	G_{IC}= 1.56-2.4 kJ/m^2
		[±30]	127	0.050	[49]	

Material	Type	Lay-up	SEA	t/D	Reference	Notes
Kevlar-Epoxy	Laminate	[0/±15]	31	0.036	[14]	
		[0/±15]	9	0.020	[30]	
		[0/±45]	30	0.033	[14]	
		[0/±45]	21	0.022	[30]	
		[±45]	31	0.042	[17]	
		[±45]	23	0.022	[30]	
		[±45]	22	0.030	[48]	
		[±45]	60	0.066	[10]	
		[0/90]	50	0.033	[14]	
		[±75]	38		[30]	At 10m/s crush speed
Hybrid -Epoxy	Laminate	$[0_{GR}\pm45_{GL}]$	44		[14]	Graphite/Glass – Epoxy
		$[0_{GR}\pm45_{K}]$	51		[14]	Graphite/Kevlar – Epoxy
		$[0_{K}\pm45_{GR}]$	35		[14]	Kevlar/Graphite- Epoxy
Glass - Epoxy	Laminate	[0/±15]	30	0.060	[14]	
		[0/±45]	31	0.059	[14]	
		[0/±75]	53	0.070	[14]	
		[0/90]	60		[10]	
	Knitted		60		[29]	
	Braided		70		[50]	I cross section with Vf=60%
Glass - Vinyl ester	Pultruded		58		[32]	Bevel trigger
			68		[32]	Tulip trigger

Material	**Type**	**Lay-up**	**SEA**	**t/D**	**Reference**	**Notes**
Glass- Polyester	Pultruded		41		[32]	Bevel trigger
			39		[32]	Tulip trigger
			25		[10]	Tested at 100°C
	Filament Wound		50		[18]	Winding angle= 65°
Aluminium			90	0.057	[14]	6061 grade
			72	0.060	[10]	
			50		[51]	
			31	0.02	[52]	At 10mm/min crush and 4m/s impact
Mild Steel			33		[10]	

Table 6 Shows specific energy absorption values of a selection of polymer composite and metallic materials found in the literature

Appendix B: Table of Manufacturing and Testing Results Data for all Test Samples

Beam Type	Fibre type and Diameter mm	No. of ends	Array	Sample Number		Type of Loading	Density g/cm3	Resin Type	Mass per metre, g	Est. Fibre Mass, g	Real Fibre Mass, g	Foam Mass g	Est. Resin Mass, g	Real Resin Mass, g	Est. Vf %	Real Vf %	Overall SEA J/g	Average Load kN
a	STS 40	34	2x2	11	A	Q-S	0.153	LY3505	570.1	256	308.2	73.7	240.4	188.2	40.1	50.7	25.9	13.5
	STS 40	34	2x2	12	A	Q-S	0.147	LY3505	548.0	256	311.9	75.9	216.1	160.2	42.7	55.0	24.2	12.0
	STS 40	34	2x2	16	A	Q-S	0.224	LY3505	834.4	256	310.1	70.1	508.3	454.2	24.0	30.0	37.7	27.5
	STS 40	34	2x2	16	C	Q-S	0.199	LY3505	741.8	256	310.1	70.1	415.7	361.6	27.9	35.0	36.6	24.4
	STS 40	34	2x2	16	D	IMP	0.203	LY3505	754.5	256	310.1	70.1	428.4	374.3	27.3	34.2	27.7	20.2
	STS 40	34	2x2	19	A	Q-S	0.179	LY3505	664.3	256	305.9	65	343.3	293.4	31.9	39.6	26.3	16.2
	STS 40	34	2x2	19	B	IMP	0.168	LY3505	623.4	256	305.9	65	302.4	252.5	34.7	43.2	21.1	12.8
	STS 40	34	2x2	19	D	IMP	0.166	LY3505	616.0	256	305.9	65	295.0	245.1	35.3	44.0	22.7	14.1
	STS 40	34	2x2	37	A	Q-S	0.152	XU3508	564.8	256	313.6	71	237.8	180.2	40.4	52.2	21.9	13.8
	STS 40	34	2x2	37	B	IMP	0.150	XU3508	558.2	256	313.6	71	231.2	173.6	41.0	53.2	30.2	16.4
	STS 40	34	2x2	37	C	Q-S	0.145	XU3508	540.2	256	313.6	71	213.2	155.6	43.0	55.9	21.5	12.9
	STS 40	34	2x2	37	D	IMP	0.137	XU3508	509.8	256	313.6	71	182.8	125.2	46.8	61.2	29.1	14.7
b	STS 40	42	2x2	18	A	Q-S	0.226	LY3505	839.3	316	375.9	70.1	453.2	393.3	30.5	37.5	35.9	27.8
	STS 40	42	2x2	18	D	IMP	0.222	LY3505	825.4	316	375.9	70.1	439.3	379.4	31.1	38.4	31.2	24.8
c	STS 40	42	3x3	8	C	Q-S	0.291	LY3505	1083.0	648	762	85.7	349.3	235.3	53.8	67.1	42.9	45.4
	STS 40	42	3x3	8	D	IMP	0.294	LY3505	1093.3	648	762	85.7	359.6	245.6	53.1	66.1	41.7	39.7
	STS 40	42	3x3	10	A	Q-S	0.251	LY3505	934.0	576	636.7	80.1	277.9	217.2	56.6	64.8	39.4	36.4
	STS 40	42	3x3	10	C	Q-S	0.247	LY3505	920.2	576	636.7	80.1	264.1	203.4	57.8	66.3	42.4	36.6
	STS 40	42	3x3	10	D	IMP	0.252	LY3505	935.9	648	636.7	80.1	207.8	219.1	66.2	64.6	40.5	38.8
	STS 40	42	3x3	24	A	Q-S	0.335	XU3508	1246.5	648	710	77	521.5	459.5	43.9	49.3	42.2	46.1
	STS 40	42	3x3	24	C	Q-S	0.286	XU3508	1063.5	648	710	77	338.5	276.5	54.6	61.7	46.7	44.8
	STS 40	42	3x3	24	D	IMP	0.287	XU3508	1068.4	648	710	77	343.4	281.4	54.3	61.3	42.3	43.9
	STS 40	42	3x3	25	A	Q-S	0.293	XU3508	1091.4	648	688.3	77	366.4	326.1	52.6	57.0	40.6	40.9
	STS 40	42	3x3	25	C	Q-S	0.290	XU3508	1080.3	648	688.3	77	355.3	315.0	53.4	57.9	39.8	41.1
	STS 40	42	3x3	M48	A	Q-S	0.297	LY3505	1106.5	648	654	71.8	386.7	380.7	51.3	51.9	46.0	46.7

Beam Type	Fibre type and Diameter mm	No. of ends	Array	Sample Number		Type of Loading	Density g/cm3	Resin Type	Mass per metre, g	Est. Fibre Mass, g	Real Fibre Mass, g	Foam Mass g	Est. Resin Mass, g	Real Resin Mass, g	Est. Vf %	Real Vf %	Overall SEA J/g	Average Load kN
d	STS 40	48	2x2	17	A	Q-S	0.230	LY3505	854.5	360	436.1	67	427.5	351.4	34.6	43.8	35.5	26.5
	STS 40	48	2x2	17	C	Q-S	0.229	LY3505	852.5	360	436.1	67	425.5	349.4	34.7	44.0	39.8	30.4
	STS 40	48	2x2	17	D	IMP	0.230	LY3505	854.9	360	436.1	67	427.9	351.8	34.6	43.8	31.4	21.4
	STS 40	48	2x2	39	A	Q-S	0.222	XU3508	827.9	360	434.4	71.3	396.6	322.2	36.3	45.9	35.7	28.3
	STS 40	48	2x2	39	B	IMP	0.211	XU3508	785.1	360	434.4	71.3	353.8	279.4	39.0	49.4	34.1	27.2
	STS 40	48	2x2	39	C	Q-S	0.212	XU3508	789.3	360	434.4	71.3	358.0	283.6	38.7	49.0	28.3	21.3
	STS 40	48	2x2	39	D	IMP	0.226	XU3508	840.9	350	434.4	71.3	419.6	335.2	34.4	44.9	39.6	32.7
e	STS 40	48	3x3	9	A	Q-S	0.323	LY3505	1202.5	747	846.5	77.5	378.0	278.5	55.4	65.6	54.4	63.0
	STS 40	48	3x3	9	C	Q-S	0.317	LY3505	1180.4	747	846.5	77.5	355.9	256.4	56.9	67.5	52.7	60.9
	STS 40	48	3x3	9	D	IMP	0.319	LY3505	1188.4	747	846.5	77.5	363.9	264.4	56.3	66.8	47.6	54.1
	STS 40	48	3x3	32	A	Q-S	0.347	XU3508	1293.0	747	928.7	76.7	469.3	287.6	50.0	67.0	60.1	73.2
	STS 40	48	3x3	32	C	Q-S	0.401	XU3508	1492.1	747	928.7	76.7	668.4	486.7	41.3	54.5	56.3	70
	STS 40	48	3x3	32	D	IMP	0.347	XU3508	1292.2	747	928.7	76.7	468.5	286.8	50.1	67.1	58.3	69.3
f	STS 60	34	2x2	23	A	IMP	0.128	LY3505	475.4	232	263.2	74.8	168.6	137.4	46.4	54.6	17.5	7.8
	STS 60	34	2x2	23	B	Q-S	0.133	LY3505	495.9	232	263.2	74.8	189.1	157.9	43.5	51.2	25.0	11.3
	STS 60	34	2x2	23	C	Q-S	0.132	LY3505	492.6	232	263.2	74.8	185.8	154.6	44.0	51.7	21.8	12.2
	STS 60	34	2x2	23	D	IMP	0.134	LY3505	498.8	232	263.2	74.8	192.0	160.8	43.2	50.7	12.1	12.1
	STS 60	34	2x2	30	A	Q-S	0.204	XU3508	758.2	232	270.1	67.7	458.5	420.4	24.1	28.8	35.1	23.8
	STS 60	34	2x2	30	C	Q-S	0.187	XU3508	696.7	232	270.1	67.7	397.0	358.9	26.9	32.1	38.8	25.4
	STS 60	34	2x2	30	D	IMP	0.174	XU3508	646.7	232	270.1	67.7	347.0	308.9	29.6	35.5	30.2	22.5

Beam Type	Fibre type and Diameter mm	No. of ends	Array	Sample Number		Type of Loading	Density g/cm3	Resin Type	Mass per metre, g	Est. Fibre Mass, g	Real Fibre Mass, g	Foam Mass g	Est. Resin Mass, g	Real Resin Mass, g	Est. Vf %	Real Vf %	Overall SEA J/g	Average Load kN
g	STS 60	34	3x3	40	A	Q-S	0.270	LY3505	1004.9	504	569.7	74.8	426.1	360.4	42.6	49.8	57.9	55.4
	STS 60	34	3x3	40	B	IMP	0.273	LY3505	1015.8	504	569.7	74.8	437.0	371.3	42.0	49.1	53.3	49.0
	STS 60	34	3x3	40	C	Q-S	0.267	LY3505	994.3	504	569.7	74.8	415.5	349.8	43.3	50.6	53.9	51.2
	STS 60	34	3x3	40	D	IMP	0.248	LY3505	922.8	504	569.7	74.8	344.0	278.3	47.9	56.3	33.4	30.2
h	STS 60	42	2x2	22	A	Q-S	0.136	LY3505	505.3	288	327.5	77	140.3	100.8	56.3	67.1	18.8	8.5
	STS 60	42	2x2	22	B	Q-S	0.140	LY3505	519.3	288	327.5	77	154.3	114.8	54.0	64.2	27.2	13.5
	STS 60	42	2x2	22	D	IMP	0.140	LY3505	520.8	288	327.5	77	155.8	116.3	53.7	63.9	23.4	10.5
i	STS 60	42	3x3	42	A	Q-S	0.303	LY3505	1126.2	621	688.2	75.2	430.0	362.8	47.6	54.4	54.8	58.5
	STS 60	42	3x3	42	B	IMP	0.293	LY3505	1090.3	621	688.2	75.2	394.1	326.9	49.8	57.0	57.7	54.0
	STS 60	42	3x3	42	C	Q-S	0.300	LY3505	1116.8	621	688.2	75.2	420.6	353.4	48.1	55.0	56.2	60.2
	STS 60	42	3x3	42	D	IMP	0.294	LY3505	1094.0	621	688.2	75.2	397.8	330.6	49.5	56.7	42.3	42.4
j	STS 60	48	2x2	20	A	Q-S	0.167	LY3505	623.0	332	378.4	76.2	214.8	168.4	49.3	58.6	30.4	16.5
	STS 60	48	2x2	20	C	Q-S	0.163	LY3505	606.5	332	378.4	76.2	198.3	151.9	51.3	61.0	31.1	16.9
	STS 60	48	2x2	20	D	IMP	0.155	LY3505	575.8	332	378.4	76.2	167.6	121.2	55.5	66.2	26.6	13.5
	STS 60	48	2x2	26	A	Q-S	0.206	XU3508	765.6	332	375.9	67.4	366.2	322.3	36.3	42.3	40.1	27.0
	STS 60	48	2x2	26	C	Q-S	0.214	XU3508	797.1	332	375.9	67.4	397.7	353.8	34.4	40.0	42.5	31.7
	STS 60	48	2x2	26	D	IMP	0.245	XU3508	909.8	332	375.9	67.4	510.4	466.5	29.0	33.6	33.2	26.9
k	STS 60	48	3x3	M51	A	Q-S	0.312	LY3505	1161.0	711	700.6	75	375.0	385.4	54.4	53.3	53.4	53.7

Beam Type	Fibre type and Diameter mm	No. of ends	Array	Sample Number		Type of Loading	Density g/cm3	Resin Type	Mass per metre, g	Est. Fibre Mass, g	Real Fibre Mass, g	Foam Mass g	Est. Resin Mass, g	Real Resin Mass, g	Est. Vf %	Real Vf %	Overall SEA J/g	Average Load kN
m	STS 60	48	1(x2)	31	A	Q-S	0.146	LY3505	543.0	266	291.2	69.6	207.4	182.2	44.6	50.1	20.7	9.5
				31	C	Q-S	0.137	LY3505	509.4	266	291.2	69.6	173.8	148.6	49.0	55.2	20.2	9.1
n	T700 100	84	1(x2)	34	A	Q-S	0.166	XU3508	618.9	308	356.7	84.3	226.6	177.9	46.1	55.8	21.0	12.0
				34	B	IMP	0.148	XU3508	550.7	309	356.7	85.3	156.4	108.7	55.4	67.3	23.2	15.3
				34	C	Q-S	0.149	XU3508	554.9	308	356.7	84.3	162.6	113.9	54.3	66.3	25.2	12.9
				35	A	Q-S	0.149	LY3505	555.7	308	357.1	87.3	160.4	111.3	54.7	66.8	18.2	9.1
				35	B	IMP	0.145	LY3505	539.5	309	357.1	88.3	142.2	94.1	57.7	70.5	32.9	14.1
				35	C	Q-S	0.146	LY3505	543.4	308	357.1	87.3	148.1	99.0	56.7	69.4	22.4	11.3
				M46	A	Q-S	0.153	LY3505	568.6	308	328.4	87	173.6	153.2	52.7	57.4	19.0	10.1
o	T700 100	84	1(x3)	M47	A	Q-S	0.295	LY3505	1098.8	462	466.2	-	636.8	632.6	31.3	31.7	47.6	47.3
				M52	A	Q-S	0.323	LY3505	1201.9	462		-	739.9	1201.9	28.2	0.0	56.4	58.5
p	HTA 40	48	3x3	M49	A	Q-S	0.241	LY3505	897.9	369	382.2	71.8	457.1	443.9	33.7	35.1	69.1	57.2

Key for Manufacturing and Results Data Table

Density (g/cm^3) = mass of sample / (cross sectional area X length)

Mass per metre = Mass value experimentally measured from whole beam

Estimated fibre mass g/m = Wusedia X (number of braids in structure)

Real fibre Mass = Mass value of braid inserted into beam experimentally measured

Foam mass = Mass value of foam inserted into beam experimentally measured

Estimated Resin Mass = (Mass per metre) – [(Foam mass) + (Estimated fibre mass)]

Real Resin Mass = (Mass per metre) – [(Foam mass) + (Real fibre mass)]

Estimated Fibre V_f = [(Estimated fibre mass) / 1.75] / [(Estimated resin mass) / 1.15]

Real Fibre V_f = [(Real fibre mass) / 1.75] / [(Real resin mass) / 1.15]

Overall SEA = experimentally measured Energy / Mass of sample length crushed

Average Load = Average value of all load data recorded during test for each sample

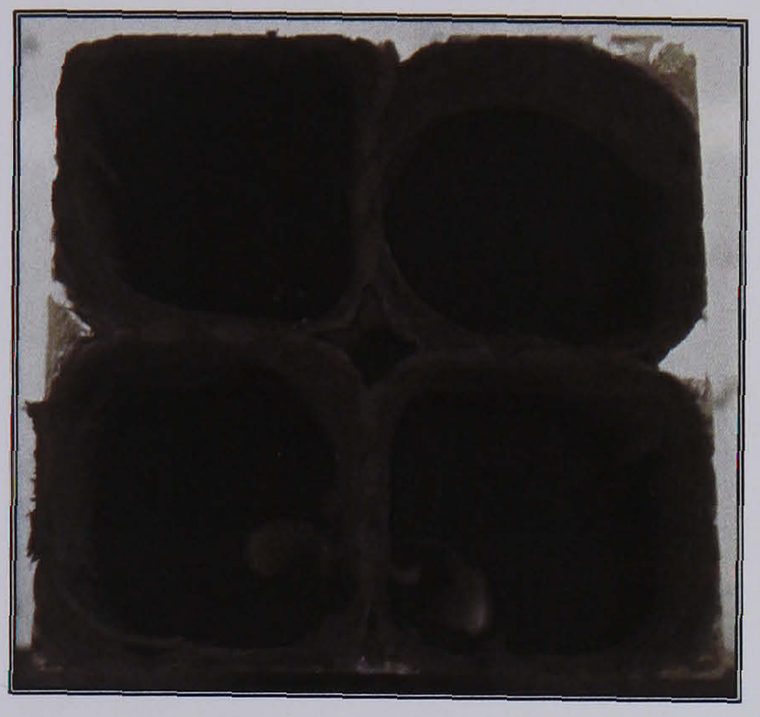
Appendix C: Tabulated data for each braid type showing braid mass per metre

Braid diameter *do, mm*	Number of ends *n*	Tex number *tex*	Mass per metre *Wb, g/m*	Mass per metre^2 *Wa, g/m^2*	Change in Diameter *mm*	Change in Diameter *%*	Change in Length *%*	W_{usedia} *g/m*	Braid Angle *degrees*
40	48	1600	109	864	40→ 30	75	20	**91**	32
40	48	1600	109	864	40 → 20	50	32	**82**	21
40	48	800	54	432	40 → 20	50	32	**41**	21
40	42	1600	95	756	40→ 30	75	20	**79**	32
40	42	1600	95	756	40 → 20	50	32	**72**	21
40	34	1600	77	612	40→ 30	75	20	**64**	32
40	34	1600	77	612	40 → 20	50	32	**58**	21
60	48	1600	109	576	60→ 30	50	32	**82**	21
60	48	1600	109	576	60→ 20	33	37	**79**	15
60	42	1600	95	504	60→ 30	50	32	**72**	21
60	42	1600	95	504	60→ 20	33	37	**69**	15
60	34	1600	77	408	60→ 30	50	32	**58**	21
60	34	1600	77	408	60→ 20	33	37	**56**	15
60	48	1600	109	576	60 → 68	113	-18	**132**	54
60	42	1600	95	504	60 → 68	113	-18	**116**	54
60	34	1600	77	408	60 → 68	113	-18	**94**	54
100	84	1600	190	605	100 → 68	68	23	**155**	30

Appendix D: Wall Thickness Data

BEAM TYPE A

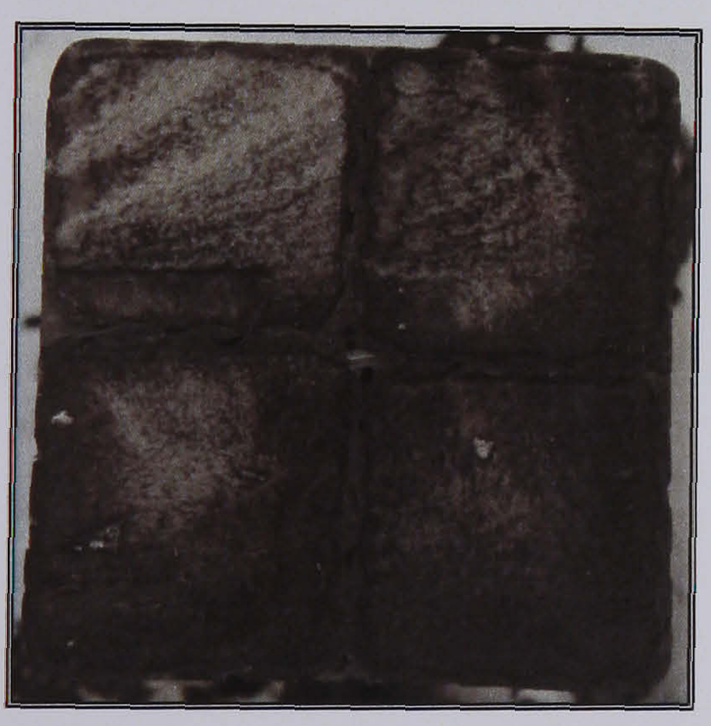
11 C



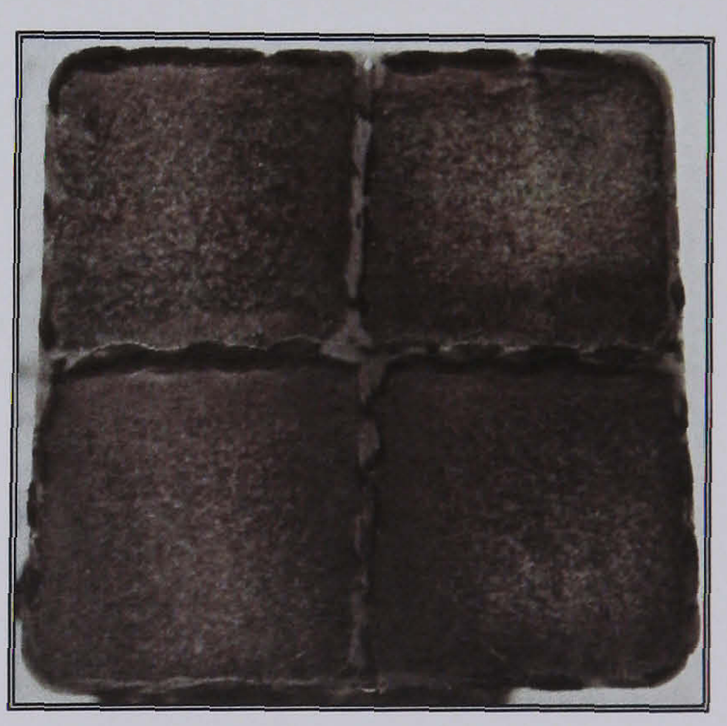
16 B



19 D

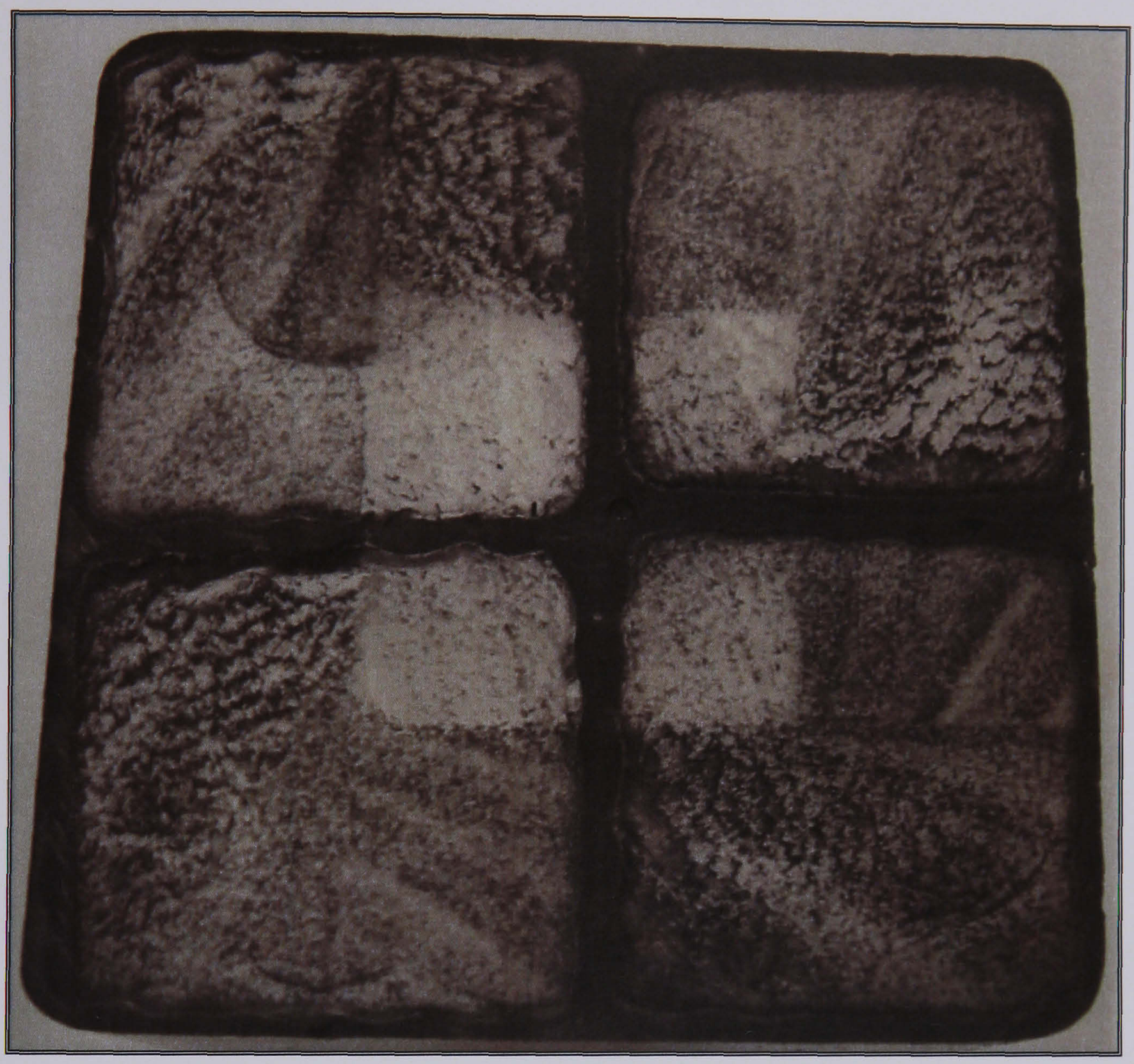


37 A



Sample Number	Measured Internal Wall thickness Range (Min-Max) mm	Measured External Wall Thickness Range (Min-Max) mm
11 C	1.9 – 2.5	0.8 – 1.4
16 B	2.0 – 2.3	0.9 – 1.4
19 D	1.8 – 2.2	1.0 – 1.4
37 A	1.7 – 1.9	0.8 – 1.2

BEAM TYPE B



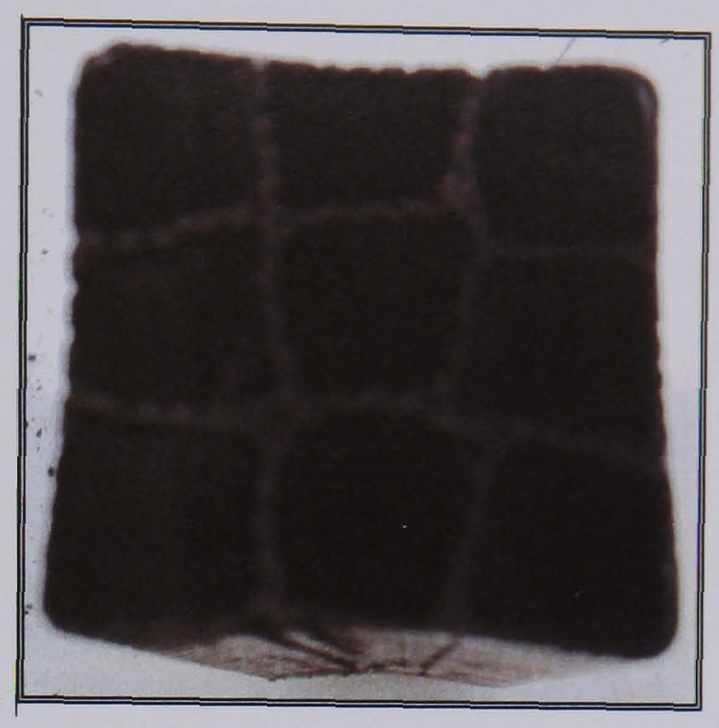
18 C

Sample Number	Measured Internal Wall thickness Range (Min-Max) mm	Measured External Wall Thickness Range (Min-Max) mm
18 C	2.0 – 2.7	1.1 – 2.1

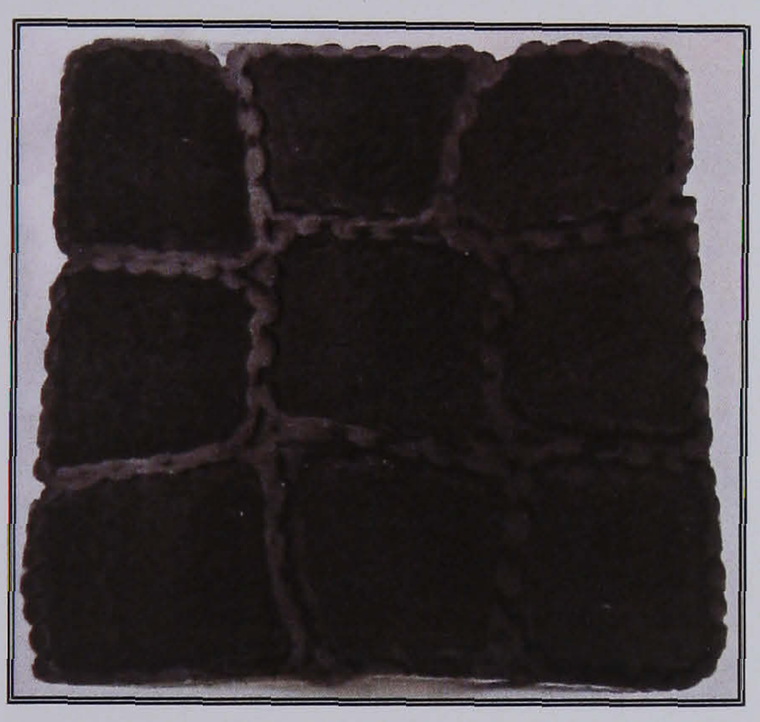
BEAM TYPE C



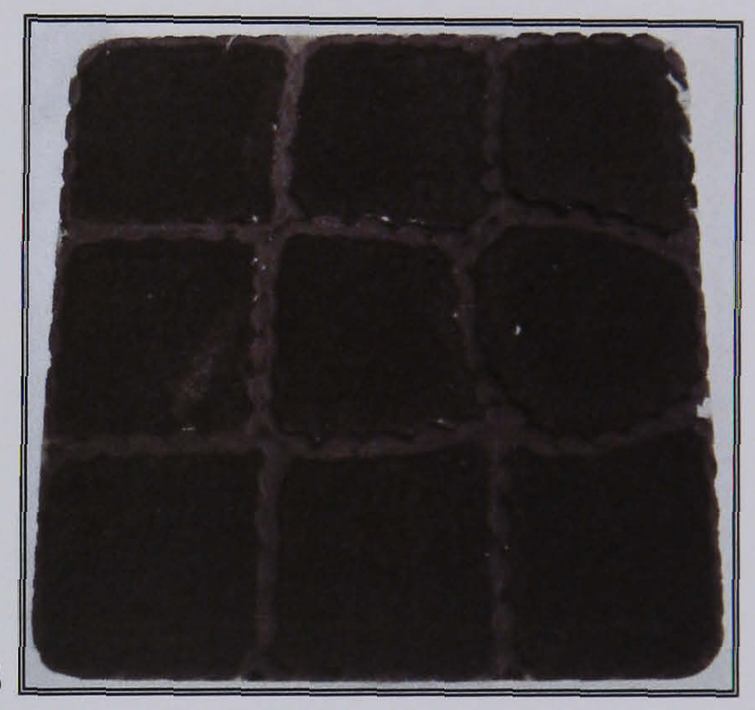
8 B



24 B



25 B



M48B

Sample Number	Measured Internal Wall thickness Range (Min-Max) mm	Measured External Wall Thickness Range (Min-Max) mm
8 B	1.8 – 4.0	0.9 – 1.6
24 B	2.1 – 2.7	0.9 – 1.6
25 B	2.2 – 2.6	1.1 – 1.7
M48B	2.0 – 2.4	0.9 – 1.3

BEAM TYPE D



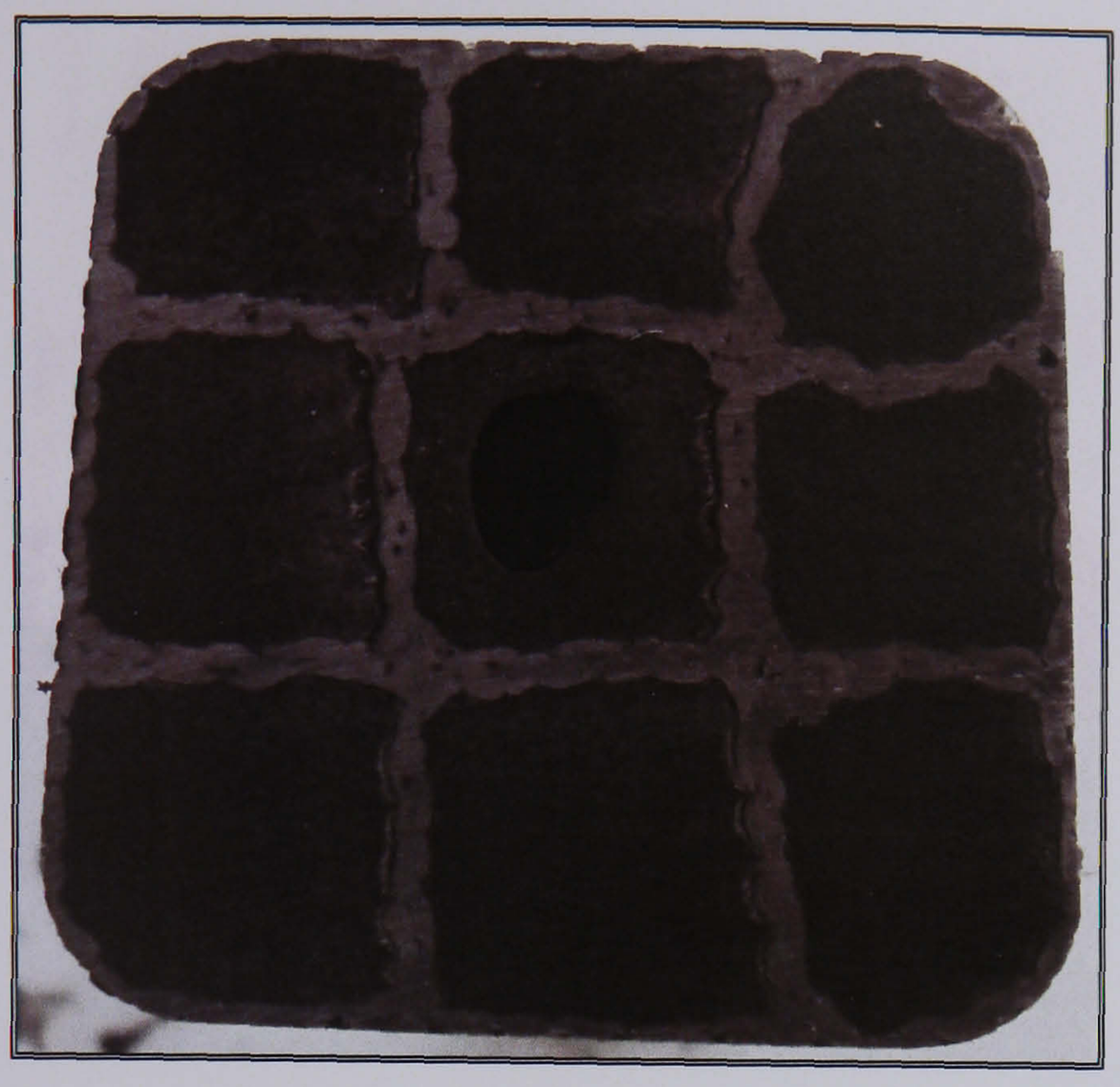
17 D



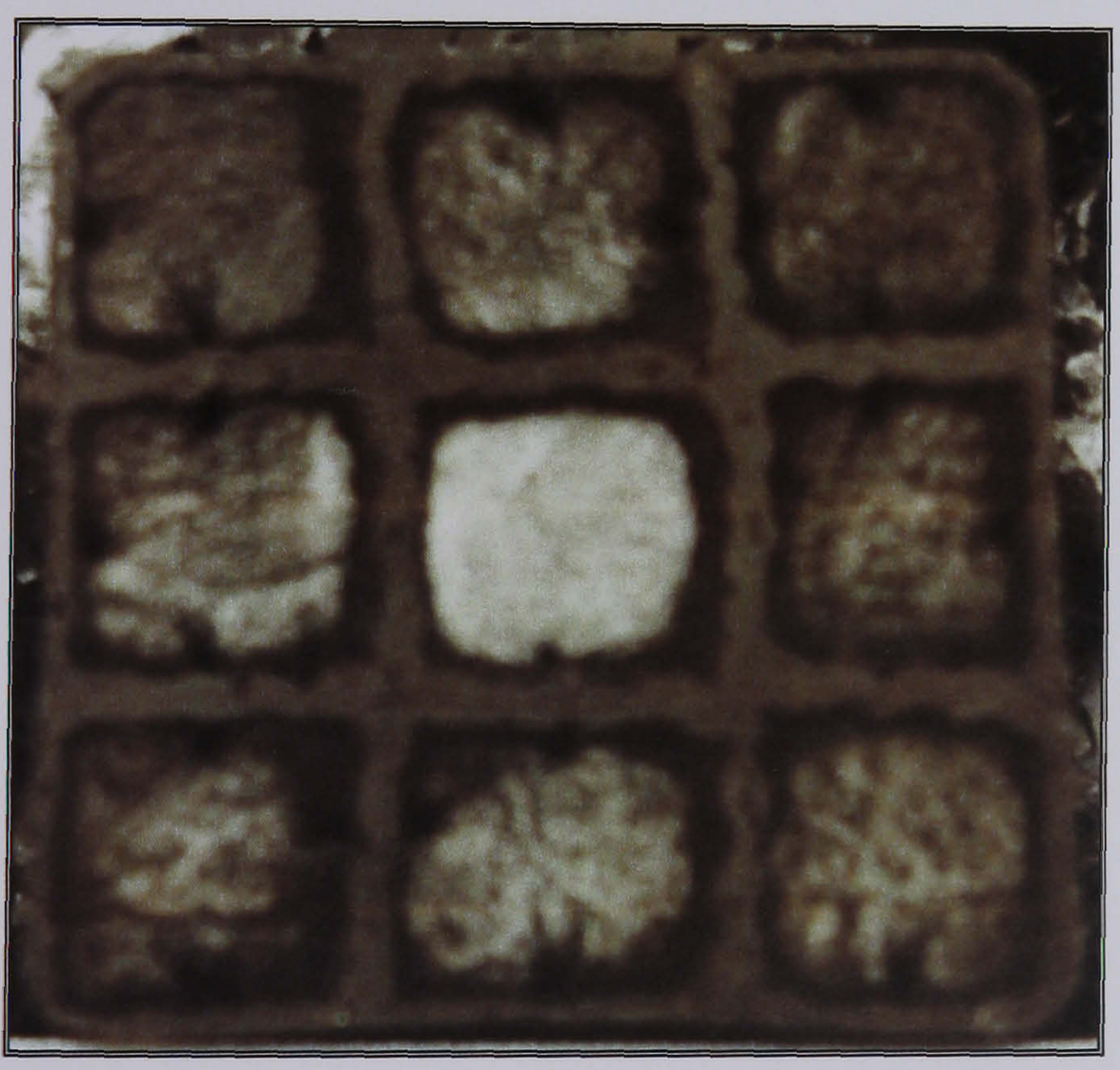
37 A

Sample Number	Measured Internal Wall thickness Range (Min-Max) mm	Measured External Wall Thickness Range (Min-Max) mm
17 D	2.6 – 3.0	1.2 – 1.6
39 A	2.4 – 2.8	1.3 – 1.6

BEAM TYPE E



9 B



32 C

Sample Number	Measured Internal Wall thickness Range (Min-Max) mm	Measured External Wall Thickness Range (Min-Max) mm
9 B	2.3 – 3.0	1.1 – 1.5
32 C	2.8 – 3.3	1.3 – 1.8

BEAM TYPE F



23 B



30 B

Sample Number	Measured Internal Wall thickness Range (Min-Max) mm	Measured External Wall Thickness Range (Min-Max) mm
23 B	1.5 – 2.0	0.6 – 1.0
30 B	1.8 – 2.4	0.8 – 2.4

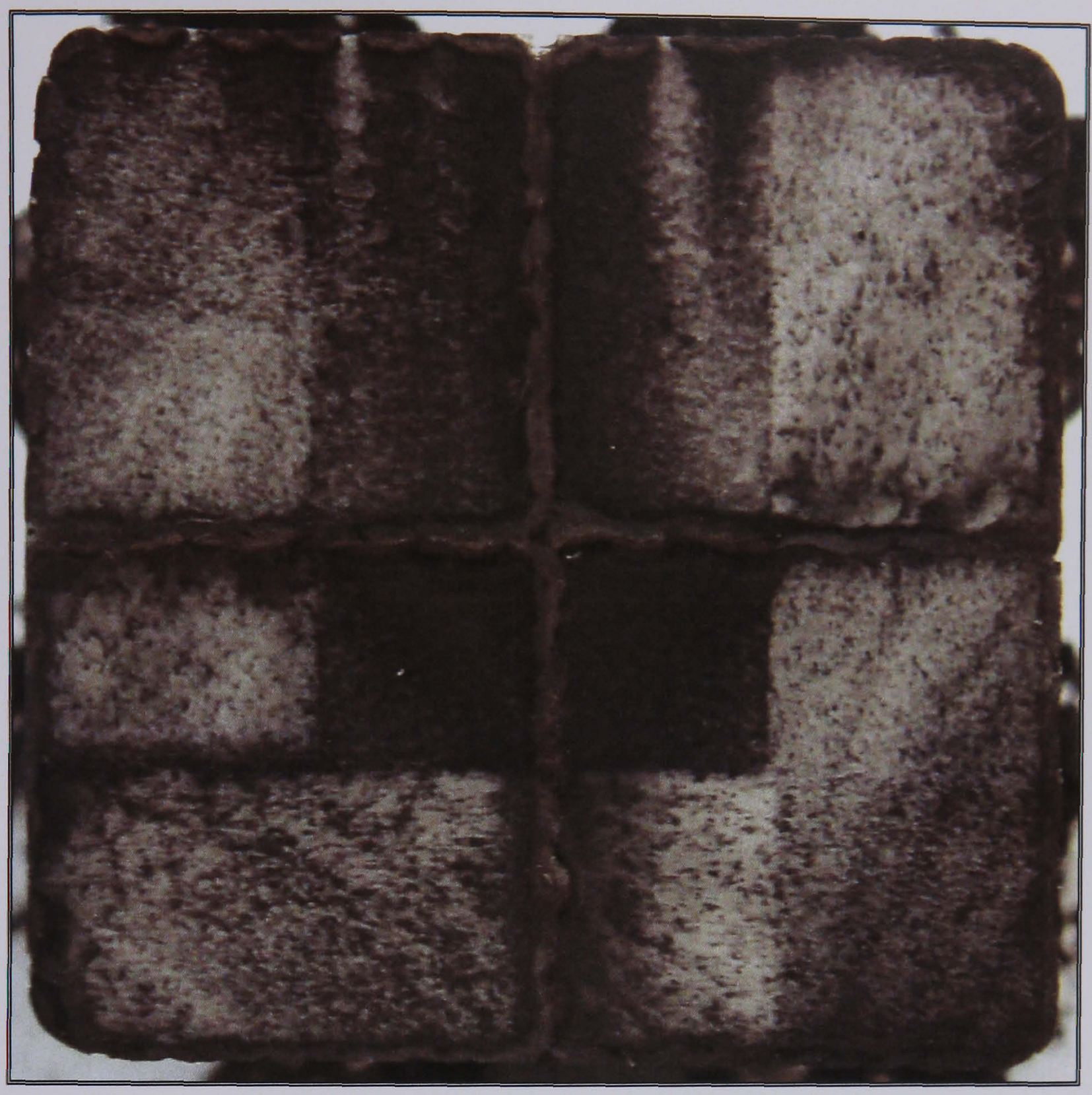
BEAM TYPE G



40 C

Sample Number	Measured Internal Wall thickness Range (Min-Max) mm	Measured External Wall Thickness Range (Min-Max) mm
40 C	1.6 – 2.2	0.8 – 1.1

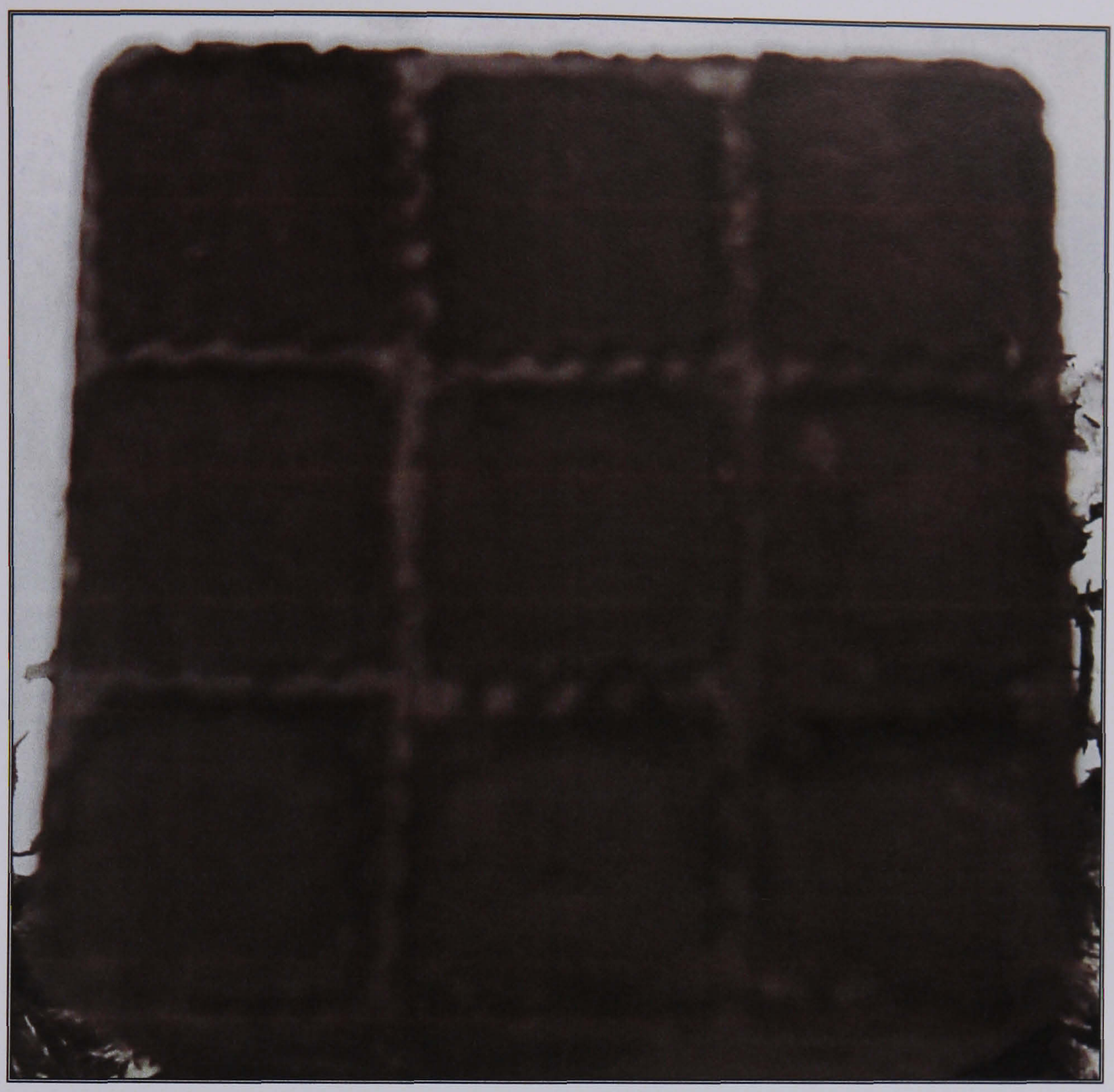
BEAM TYPE H



22 B

Sample Number	Measured Internal Wall thickness Range (Min-Max) mm	Measured External Wall Thickness Range (Min-Max) mm
22 B	1.5 – 1.8	0.7 – 1.0

BEAM TYPE I



42 A

Sample Number	Measured Internal Wall thickness Range (Min-Max) mm	Measured External Wall Thickness Range (Min-Max) mm
42 A	2.2 – 2.7	0.8 – 1.8

BEAM TYPE J



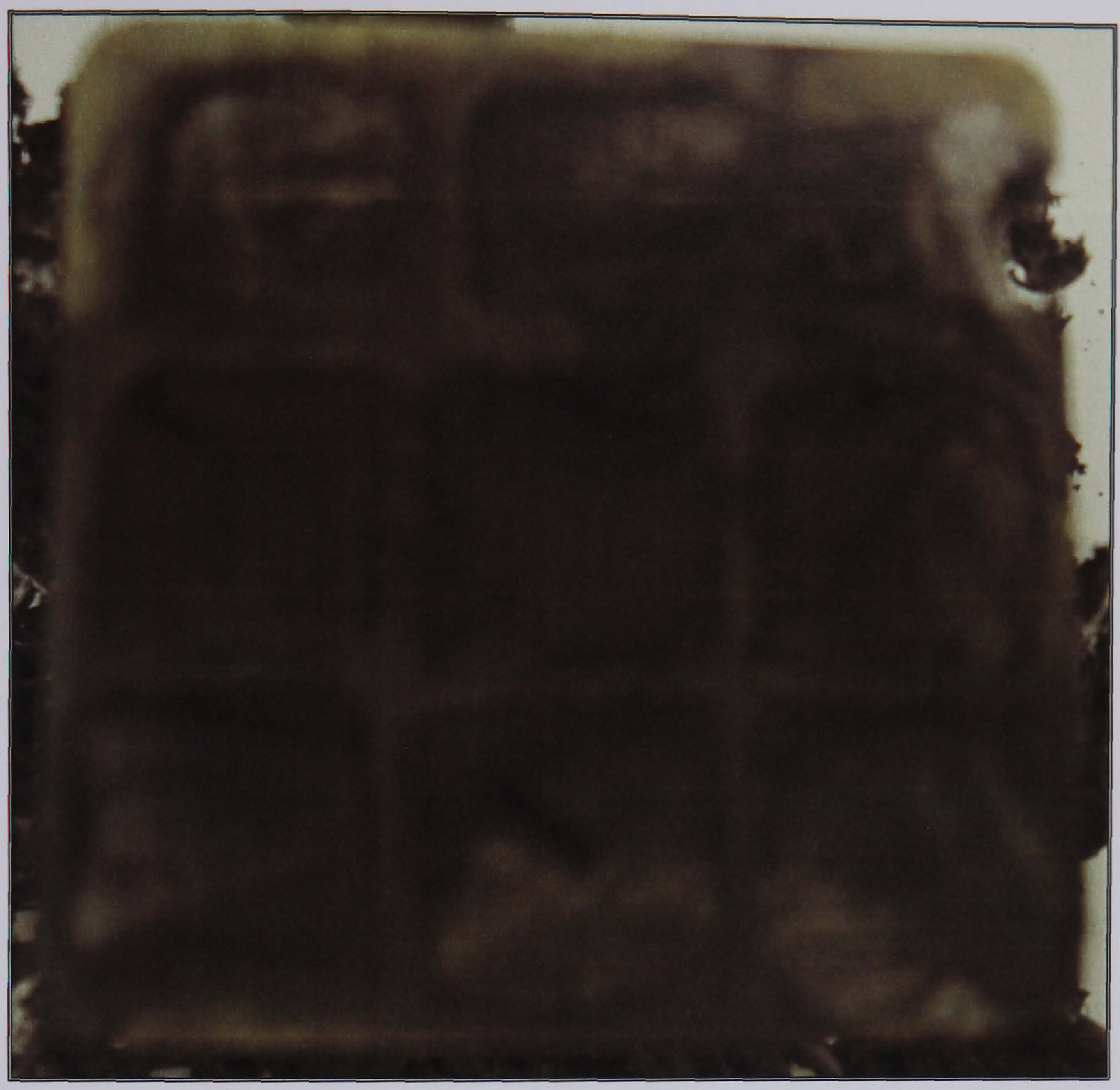
20 B



26 B

Sample Number	Measured Internal Wall thickness Range (Min-Max) mm	Measured External Wall Thickness Range (Min-Max) mm
20 B	1.8 – 2.2	0.9 – 1.1
26 B	2.0 – 2.3	1.1 – 1.4

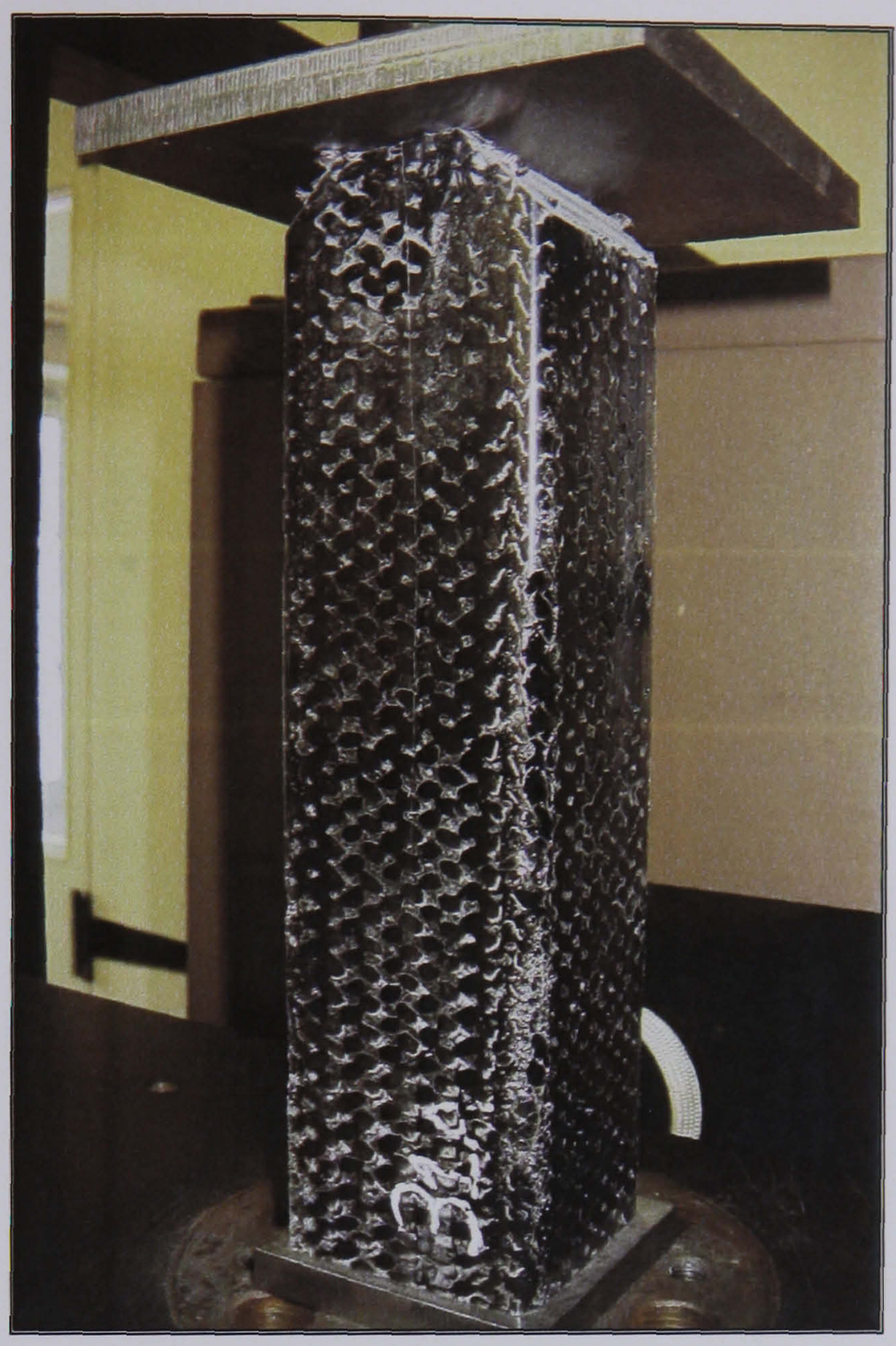
BEAM TYPE K



M51 A

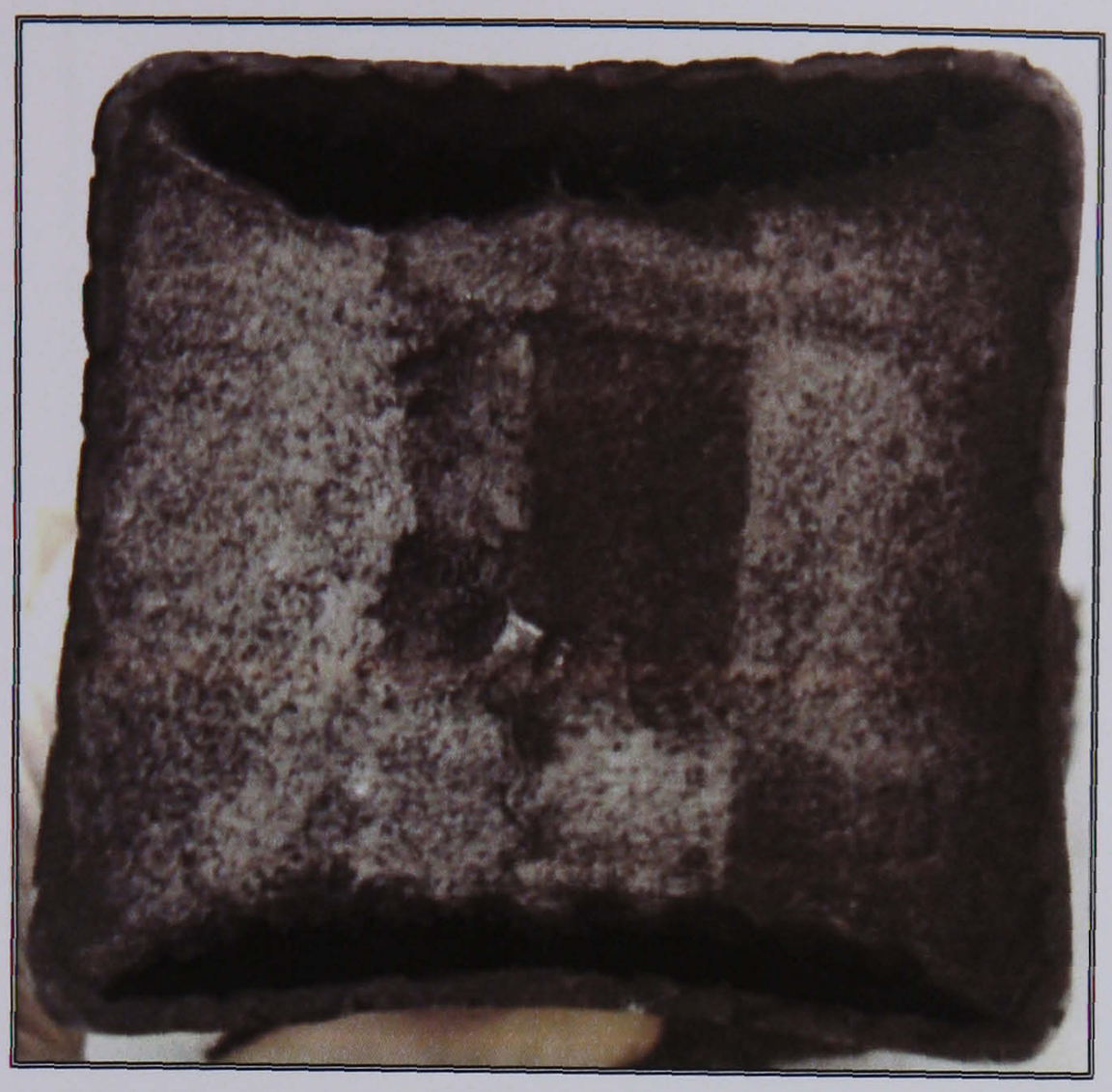
Sample Number	Measured Internal Wall thickness Range (Min-Max) mm	Measured External Wall Thickness Range (Min-Max) mm
M51A	1.7 – 3.0	1.2 – 3.2

BEAM TYPE M

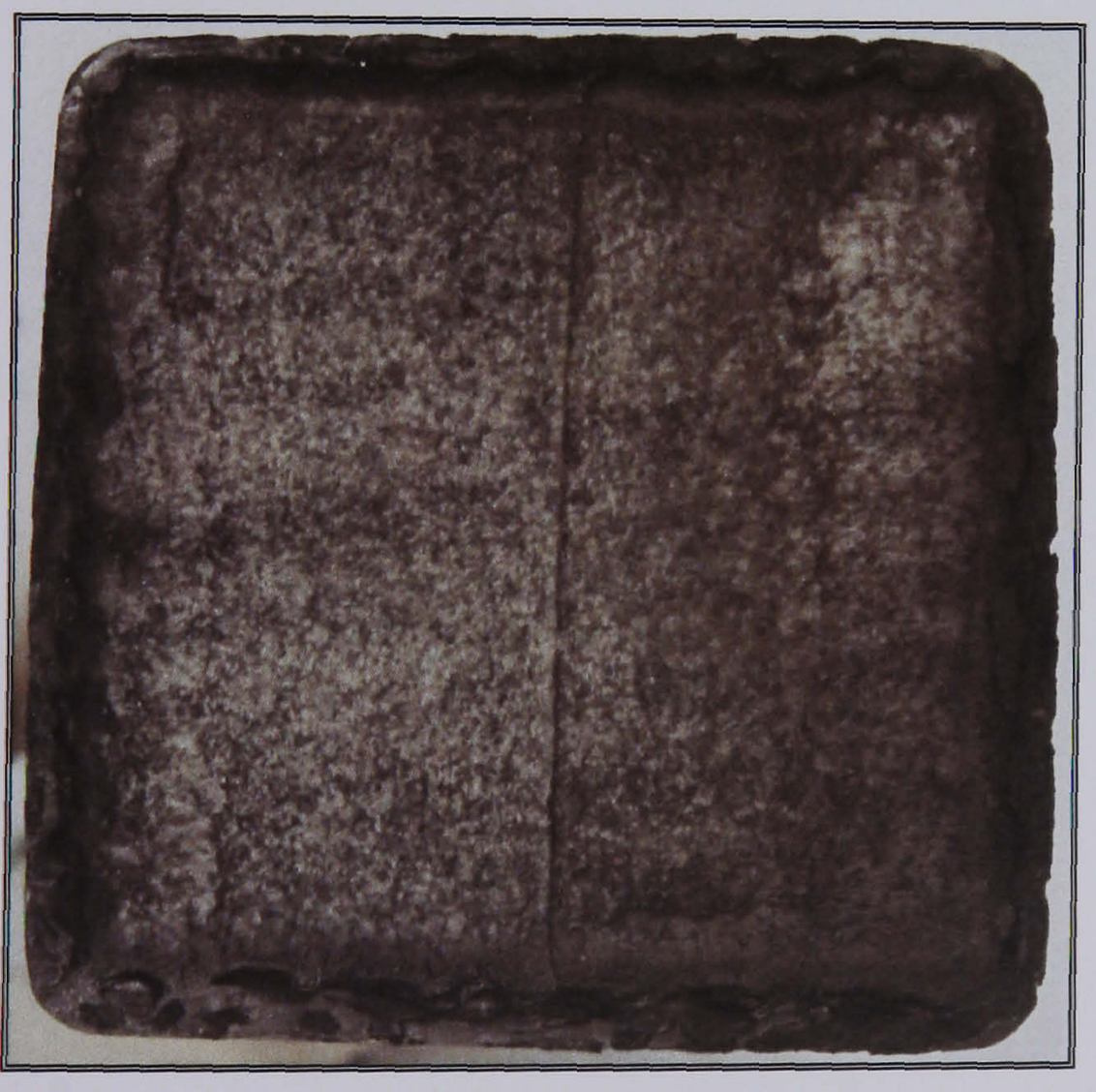


Sample Number	Measured Internal Wall thickness Range (Min-Max) mm	Measured External Wall Thickness Range (Min-Max) mm
31 B		1.6 – 1.9

BEAM TYPE N



34 C



35 A

Sample Number	Measured Internal Wall thickness Range (Min-Max) mm	Measured External Wall Thickness Range (Min-Max) mm
34 C		1.6 – 1.9
35 A		1.3 – 2.4
M46 B		1.2 – 1.8

BEAM TYPE O



M 47 B

Sample Number	Measured Internal Wall thickness Range (Min-Max) mm	Measured External Wall Thickness Range (Min-Max) mm
M47 B		3.9 – 4.1

Appendix E: Fibre, Resin and Foam data sheets

Tenax Fibers

Delivery programme and characteristics for Tenax® filament yarn

Type		**STS 5631**
Linear density [1]	(tex)	1600
Number of filaments	24000	
Twist	(t/m)	0
Filament diameter	(µm)	7
Running length per kg	(m/kg)	625
Package weight, net	(kg)	2 / 4 / 6 / 8

[1] Without sizing

Characteristics (typical values)

Density	(g/cm^3)	1,77
Tensile strength	(MPa)	4000
Tensile modulus	(GPa)	240
Elongation at break	(%)	1,5

Type codes for STS

STS is a special type suitable for modern industrial applications and it can be processed for all common fibre processing methods.

5631 = Type with ca. 1,0% Sizing based on polyurethane

For design purposes please request fibre specification.

Tenax Fibers GmbH, 42103 Wuppertal, Germany
Telefon: +49 (2 02) 32 - 23 39 Telefax: +49 (2 02) 32 - 23 60
Internet: www.tenax-fibers.com e-mail: sales@tenax-fibers.com

Tenax Fibers

Delivery programme and characteristics for Tenax® filament yarn

Type		HTA 5241	HTA 5131		HTA 5131 HTS 5631	
Linear density [1]	(tex)	67	200	400	800	1600
Number of filaments		1000	3000	6000	12000	24000
Twist	(t/m)	S15	0/Z15	0/Z10	0	0
Filament diameter	(µm)	7	7	7	7	7
Running length per kg	(m/kg)	15000	5000	2500	1250	625
Package weight, net	(kg)	0,2 / 0,5	1 / 2	2 / 4	2 / 4 / 6	2 / 4 / 6 / 8

[1] Without sizing

Characteristics (typical values)		HTA	HTS
Density	(g/cm^3)	1,76	1,76
Tensile strength	(MPa)	3950	4300
Tensile modulus	(GPa)	238	238
Elongation at break	(%)	1,7	1,8
Specific heat capacity	(J/kgK)	710	710
Thermal conductivity	(W/mK)	17	17
Coefficient of thermal expansion	(10^{-6}/K)	-0,1	-0,1
Specific electrical resistance	(Ω cm)	$1,6 \times 10^{-3}$	$1,6 \times 10^{-3}$

Type codes for HTA / HTS

HTA and HTS are the classic Tenax® high performance carbon fibre yarn types. These high tenacity (HT) fibres provide excellent mechanical laminate properties.

5241 = Type with ca. 2,5% Sizing based on epoxy resin
5131 = Type with ca. 1,3% Sizing based on epoxy resin
5631 = Type with ca. 1,0% Sizing based on polyurethane

Please contact our sales team any time, for choosing the right type.

Special types may have other type codes.

For design purposes please request fibre specification.

Tenax Fibers GmbH, 42103 Wuppertal, Germany
Telefon: +49 (2 02) 32 - 23 39 Telefax: +49 (2 02) 32 - 23 60
Internet: www.tenax-fibers.com e-mail: sales@tenax-fibers.com

arbon Fibre

Commercial documentation – N°AQ.866 - 9 - Date: September 2003

TORAYCA®

TYPE OF CARBON FIBRE T700S

Item	Property	Unit	Filaments	Nominal Value
TORAYCA® **Yarn Properties**	Tensile Strength Tensile Modulus Elongation	MPa (kgf/mm²) GPa (10^3 kgf/mm²) %		4900 (500) 230 (23.5) 2.1
	Density	g/cm³		1.80
	Yield	tex(g/1000m) tex(g/1000m)	12000 24000	800 1650
	Specific Heat Volume Resistivity 0 ° Coef. of Thermal Expansion 0 ° Thermal Conductivity	cal/g.°C $x10^{-3}\Omega$.cm $x10^{-6}$ °C^{-1} cal/cm.s.°C		0.18 1.6 -0.38 2.24×10^{-2}
	Cross Sectional Area	mm²	12000 24000	0.44 0.92
	Filament Diameter	µm		7
Composite Property (Resin System: 2500) (Measured Temp: RT)	0 ° Tensile Strength Tensile Modulus Elongation	MPa (kgf/mm²) GPa (10^3kgf/mm²) %		2550 (260) 135 (14.0) 1.7
	0 ° Compressive Strength Compressive modulus	MPa (kgf/mm²) GPa (10^3 kgf/mm²)		1470 (150) 127 (13.0)
	0 ° ILSS	MPa (kgf/mm²)		90 (9)

SOFICAR
Sales Office
3 avenue du chemin de Presles
94 410 Saint Maurice Cedex - France
Tel : 33 (0)1 45 11 12 80
Fax : 33 (0)1 48 85 62 92
E-mail : info@soficar-carbon.com

SOFICAR
Head Office & plant
Route de Lagor
64 150 Abidos - France
Tel : 33 (0)5 59 60 71 00
Fax : 33 (0)5 59 60 71 10
E-mail : info@soficar-carbon.com

Advanced Materials

Structural Composites

HUNTSMAN

MATRIX SYSTEMS FOR INDUSTRIAL COMPOSITES

DATA SHEET

Warm-curing epoxy systems based on Araldite® LY 3505* / Hardeners XB 3403* / XB 3404* / XB 3405*

Araldite LY 3505 is an epoxy resin
Hardeners XB 3403, XB 3404 and XB 3405 are based on aliphatic polyamines.

Applications

Industrial composites, repair of composites.

Properties

Laminating systems without reactive diluent. The reactivity of the systems may easily be adjusted to demands through the combination of the three hardeners of different reactivity. The long possible pot life facilitates the production of very large industrial parts. The systems are qualified by Germanischer Lloyd.

Processing

- Wet lay-up
- Filament Winding
- Resin Transfer Moulding (RTM)
- Pressure Moulding

Key data

Araldite LY 3505

Aspect (visual)	clear liquid	
Colour (Gardner, ISO 4630)	≤ 3	
Viscosity at 25 °C (ISO 12058-1)	6500 - 8000	[mPa s]
Density at 25 °C (ISO 1675)	1.15 - 1.20	[g/cm^3]
Flash point (ISO 2719)	> 200	[°C]
Storage temperature (see expiry date on original container)	2 - 40	[°C]

Hardener XB 3403

Aspect (visual)	transparent liquid	
Viscosity at 25 °C (ISO 12058-1)	5 - 20	[mPa s]
Density at 25 °C (ISO 1675)	0.95 - 1.0	[g/cm^3]
Flash point (ISO 2719)	124	[°C]
Storage temperature (see expiry date on original container)	2 - 40	[°C]

Hardener XB 3404

Aspect (visual)	clear, blue liquid	
Viscosity at 25 °C (ISO 12058-1)	20 - 40	[mPa s]
Density at 25 °C (ISO 1675)	0.95 - 1.0	[g/cm^3]
Flash point (ISO 2719)	121	[°C]
Storage temperature (see expiry date on original container)	2 - 40	[°C]

Key data

Hardener XB 3405

Aspect (visual)	clear, red liquid	
Viscosity at 25 °C (ISO 12058-1)	70 - 90	[mPa s]
Density at 25 °C (ISO 1675)	0.95 - 1.0	[g/cm^3]
Flash point (ISO 2719)	109	[°C]
Storage temperature (see expiry date on original container)	2 - 40	[°C]

* *In addition to the brand name product denomination may show different appendices , which allows us to differentiate between our production sites: e.g , BD = Germany, US = United States, IN = India, CI = China,etc. These appendices are in use on packaging, transport and invoicing documents. Generally the same specifications apply for all versions. Please address any additional need for clarification to the appropriate Huntsman contact.*

March 2004

Processing data

Mix ratio

Components	*Parts by weight*	*Parts by volume*
Araldite LY 3505	100	100
Hardener XB 3403	35	42
Araldite LY 3505	100	100
Hardener XB 3404	35	42
Araldite LY 3505	100	100
Hardener XB 3405	35	42

We recommend that the components are weighed with an accurate balance to prevent mixing inaccuracies which can affect the properties of the matrix system. The components should be mixed thoroughly to ensure homogeneity. It is important that the side and the bottom of the vessel are incorporated into the mixing process.

When processing large quantities of mixture the pot life will decrease due to exothermic reaction. It is advisable to divide large mixes into several smaller containers.

		[°C]	*[mPa s]*
Initial mix viscosity			
(Hoeppler, ISO 12058-1)	LY 3505/XB 3403	at 25	300 - 400
	LY 3505/XB 3404	at 25	550 - 800
	LY 3505/XB 3405	at 25	1000 - 1200
Pot life		*[°C]*	*[min]*
(Tecam, 100 ml, 65 % RH)	LY 3505/XB 3403	at 23	600 - 720
		at 30	430 - 510
	LY 3505/XB 3404	at 23	80 - 100
	LY 3505/XB 3405	at 23	26 - 36
Gel time		*[°C]*	*[min]*
(Hot plate)	LY 3505/XB 3403	at 60	105 - 125
		at 80	36 - 48
		at 100	14 - 18
	LY 3505/XB 3404	at 60	60 - 70
		at 80	11 - 18
		at 100	3 - 7
	LY 3505/XB 3405	at 60	18 - 26
		at 80	5 - 11
		at 100	1 - 6

The values shown are for small amounts of pure resin/hardener mix. In composite structures the gel time can differ significantly from the given values depending on the fibre content and the laminate thickness.

			[h]
Gelation at 23 °C			
(in thin layers: 0.4 - 0.7 mm)	LY 3505/XB 3403	Start	14 - 16
		End	19 - 21
	LY 3505/XB 3404	Start	5 - 7
		End	9 - 11
	LY 3505/XB 3405	Start	2 - 3
		End	4 - 5

Typical cure cycles

15 h at 50 °C
or 8 - 10 h at 60 °C
or 6 - 8 h at 80 °C

Optimum properties cannot be reached with room temperature cure.

The optimum cure cycle has to be determined case by case depending on the pro cessing and the economic requirements.

Recommendations to get shortest curing time	at 50 °C	with XB 3403 = 10 h	with XB 3404 = 7 h	with XB 3405 = 6 h
	at 60 °C	with XB 3403 = 8 h	with XB 3404 = 6 h	with XB 3405 = 4 h
	at 80 °C	with XB 3403 = 6 h	with XB 3404 = 3 h	with XB 3405 = 1 h

Properties of the cured, neat formulation

Glass transition temperature	*Cure:*	T_G	*LY 3505 XB 3403*	*LY 3505 XB 3404*	*LY 3505 XB 3405*
(IEC 1006, DSC, 10 K/min)	8 days 23 °C	[°C]	49 - 53	48 - 52	55 - 60
	1 day 23 °C + 15 h 50 °C	[°C]	63 - 68	64 - 69	68 - 73
	8 h 60 °C	[°C]	66 - 72	66 - 71	71 - 76
	6 h 80 °C	[°C]	75 - 80	75 - 80	86 - 91
	4 h 60 °C + 6 h 80 °C	[°C]	78 - 83	76 - 81	87 - 92
	8 h 100 °C	[°C]	81 - 86	77 - 82	85 - 89
Tensile test (ISO 527)		*Cure: 4 h 60 °C + 6 h 80 °C*	*LY 3505 XB 3403*	*LY 3505 XB 3404*	*LY 3505 XB 3405*
	Tensile strength	[MPa]	70 - 74	82 - 86	85 - 90
	Elongation at tensile strength	[%]	3.8 - 4.2	4.0 - 4.4	4.4 - 4.9
	Ultimate strength	[MPa]	46 - 50	73 - 78	83 - 89
	Ultimate elongation	[%]	10 - 13	5.2 - 5.8	5.0 - 6.2
	Tensile modulus	[MPa]	3180 - 3280	3400 - 3700	3500 - 3900
Flexural test (ISO 178)		*Cure: 7 days 23 °C*	*LY 3505 XB 3403*	*LY 3505 XB 3404*	*LY 3505 XB 3405*
	Flexural strength	[MPa]	85 - 93	100 - 110	90 - 100
	Elongation at flexural strength	[%]	2.4 - 2.8	3.3 - 4.0	2.2 - 2.6
	Ultimate strength	[MPa]	85 - 93	100 - 110	90 - 100
	Ultimate elongation	[%]	2.4 - 2.8	3.3 - 4.0	2.2 - 2.6
	Flexural modulus	[MPa]	3450 - 3600	3400 - 3550	3800 - 4000
		Cure: 24 h 23 °C + 15 h 50 °C	*LY 3505 XB 3403*	*LY 3505 XB 3404*	*LY 3505 XB 3405*
	Flexural strength	[MPa]	120 - 135	135 - 150	140 - 155
	Elongation at flexural strength	[%]	4.4 - 4.8	4.5 - 5.3	5.0 - 6.0
	Ultimate strength	[MPa]	64 - 72	125 - 150	125 - 140
	Ultimate elongation	[%]	11.0 - 13.0	5.5 - 7.5	7.0 - 8.5
	Flexural modulus	[MPa]	3400 - 3550	3550 - 3700	3600 - 3750
		Cure: 4 h 60 °C + 6 h 80 °C	*LY 3505 XB 3403*	*LY 3505 XB 3404*	*LY 3505 XB 3405*
	Flexural strength	[MPa]	110 - 130	125 - 145	135 - 155
	Elongation at flexural strength	[%]	4.8 - 5.5	5.0 6.0	5.2 - 6.2
	Ultimate strength	[MPa]	70 - 85	100 - 135	125 - 145
	Ultimate elongation	[%]	10.5 - 13.0	6.5 - 9.5	7.0 - 9.0
	Flexural modulus	[MPa]	3100 - 3300	3450 - 3600	3450 - 3650
Fracture properties Bend notch test (PM 258-0/90)		*Cure: 4 h 60 °C + 6 h 80 °C*	*LY 3505 XB 3403*	*LY 3505 XB 3404*	*LY 3505 XB 3405*
	Fracture toughness K_{1C}	[MPa√m]	0.95 - 1.05	0.8 - 0.95	0.8 - 0.9
	Fracture energy G_{1C}	[J/m²]	250 - 280	160 - 200	150 - 190
Water absorption (ISO 62)	*Immersion:*	*Cure: 4 h 60 °C + 6 h 80 °C*	*LY 3505 XB 3403*	*LY 3505 XB 3404*	*LY 3505 XB 3405*
	10 days H_2O 23 °C	[%]	0.38 - 0.42	0.25 - 0.30	0.30 - 0.35

Properties of the cured, reinforced formulation

Interlaminar shear strength
(ASTM D 2344)

Short beam: Laminate comprising 12 layers unidirectional E-glass fabric (425 g/m^2)
Laminate thickness t = 3.0 - 3.2 mm
Fibre volume content: 63 - 65 %

	Cure: 4 h 60 °C + 6 h 80 °C	*LY 3505 XB 3403*	*LY 3505 XB 3404*	*LY 3505 XB 3405*
Shear strength	[MPa]	53 - 57	59 - 62	54 - 58

Storage	Provided that Araldite LY 3505 and Hardeners XB 3403, XB 3404 and XB 3405 are stored in a dry place in their original, properly closed containers at the above mentioned storage temperatures they will have the shelf lives indicated on the labels. Partly emptied containers should be closed immediately after use.	
Handling precautions	Mandatory and recommended industrial hygiene procedures should be followed whenever our products are being handled and processed. For additional information please consult the corresponding product safety data sheets and the brochure "Hygienic precautions for handling plastics products" . Personal hygiene	
	Safety precautions at workplace	
	protective clothing	yes
	gloves	essential
	arm protectors	recommended when skin contact likely
	goggles/safety glasses	yes
	Skin protection	
	before starting work	Apply barrier cream to exposed skin
	after washing	Apply barrier or nourishing cream
	Cleansing of contaminated skin	
		Dab off with absorbent paper, wash with warm water and alkali-free soap, then dry with disposable towels. Do not use solvents
	Disposal of spillage	
		Soak up with sawdust or cotton waste and deposit in plastic-lined bin
	Ventilation	
	of workshop	Renew air 3 to 5 times an hour
	of workplaces	Exhaust fans. Operatives should avoid inhaling vapours
First aid	Contamination of the *eyes* by resin, hardener or mix should be treated immediately by flushing with clean, running water for 10 to 15 minutes. A doctor should then be consulted. Material smeared or splashed on the *skin* should be dabbed off, and the contaminated area then washed and treated with a cleansing cream (see above). A doctor should be consulted in the event of severe irritation or burns. Contaminated clothing should be changed immediately. Anyone taken ill after *inhaling* vapours should be moved out of doors immediately. In all cases of doubt call for medical assistance.	
Note	Araldite® is a registered trademark of Huntsman LLC or an affiliate thereof in one or more countries, but not all countries.	

Huntsman LLC
®Registered trademark

APPROVED TO ISO 9001

IMPORTANT: The following supersedes Buyer's documents. SELLER MAKES NO REPRESENTATION OR WARRANTY, EXPRESS OR IMPLIED, INCLUDING OF MERCHANTABILITY OR FITNESS FOR A PARTICULAR PURPOSE. No statements herein are to be construed as inducements to infringe any relevant patent. Under no circumstances shall Seller be liable for incidental, consequential or indirect damages for alleged negligence, breach of warranty, strict liability, tort or contract arising in connection with the product(s). Buyer's sole remedy and Seller's sole liability for any claims shall be Buyer's purchase price. Data and results are based on controlled or lab work and must be confirmed by Buyer by testing for its intended conditions of use. The product(s) has not been tested for, and is therefore not recommended for, uses for which prolonged contact with mucous membranes, abraded skin, or blood is intended; or for uses for which implantation within the human body is intended.

Advanced Materials

Structural Composites

HUNTSMAN

Provisional DATA SHEET

Toughened Epoxy Resin
Resin XU 3508* / Hardeners XB 3403* / XB 3486* / Aradur™ 22962* / Aradur™ 2954* / Hardener XB 3473*

Resin XU 3508 is a medium viscosity toughened epoxy resin.

Applications

Industrial composites

Properties

Laminating Resin XU 3508 has a good toughness effect combined with a low viscosity

Processing

- Wet lay-up
- Filament Winding
- Pressure Moulding
- Resin Transfer Moulding (RTM)

Key data

Resin XU 3508

Aspect (visual)	white liquid	
Viscosity at 25 °C (ISO 12058-1)	11000 - 13000	[mPa s]
Epoxy value	4.8 - 5.2	[ep/Kg]
Density at 25 °C (ISO 1675)	1.15 - 1.20	[g/cm^3]
Flash point (ISO 2719)	200	[°C]
Storage temperature (see expiry date on original container)	2 - 40	[°C]

Storage

Provided that Resin XU 3508 are stored in a dry place in his original, properly closed containers at the above mentioned storage temperatures they will have the shelf lives indicated on the labels.

Partly emptied containers should be closed immediately after use.

* *In addition to the brand name product denomination may show different appendices , which allows us to differentiate between our production sites: e.g , BD = Germany, US = United States, IN = India, etc.. These appendices are in use on packaging, transport and invoicing documents. Generally the same specifications apply for all versions. Please address any additional need for clarification to the appropriate Huntsman contact.*

July 2003

Processing data

Mix ratio *[pbw]*					
Resin XU 3508	100	100	100	100	100
Hardener XB 3403	30	-	-	-	-
Hardener XB 3486	-	30	-	-	-
Aradur 22962	-	-	22	-	-
Aradur 2954	-	-	-	30	-
Hardener XB 3473	-	-	-	-	23
Gel time *[min]* (hot plate)					
at 80 °C	30 - 36	-	-	-	-
at 100 °C	13 - 18	9 - 14	6 - 10	9 - 14	-
at 110 °C	-	-	-	-	-
at 120 °C	-	3 - 7	4 - 8	-	-
at 140 °C	-	-	-	2 - 4	23 - 30
at 160 °C	-	-	-	-	15 - 21
Pot life *[min.]* (Tecam, 100 ml)					
at 23 °C	600 - 720	380 - 480	100 - 150	320 - 380	1700 - 2000
Initial mix viscosity *[mPas]* (cone plate viscosimeter)					
at 25 °C	650 - 800	720 - 860	1800 - 2100	2600 - 3300	4400 - 5500

Properties of the cured, neat formulation

Resin XU 3508	Hardeners				
	XB 3403	**XB 3486**	**Aradur 22962**	**Aradur 2954**	**XB 3473**
Glass transition temperature (DSC, 10 K/min)					
Cure:	*8h 60 °C*	*16h 50 °C*	*4h 80 °C*	*1h 80 °C + 8h 160 °C*	*1h 120 °C + 2h 200 °C*
T_G [°C]	63 - 68	68 - 74	102 - 112	150 - 158	160 - 168
Cure	*4h 60 °C + 6h 80 °C*	*5h 100 °C*	*15 min 120 °C + 2h 150 °C*	*1h 80 °C + 8h 140 °C*	*2h 120 °C + 2h 140 °C + 2h 180 °C*
T_G [°C]	70 - 75	95 - 102	144 - 154	145 - 152	160 - 168
Cure cycle	*4h 60 °C + 6h 80 °C*	*5h 100 °C*	*15 min 120 °C + 2h 150 °C*	*1h 80 °C + 8h 140 °C*	*2h 120 °C + 2h 140 °C + 2h 180 °C*
Flexural test (ISO 178)					
Flexural strength [MPa]	100 - 125	110 - 125	120 - 135	125 - 135	110 - 125
Elongation at flexural strength [%]	4.5 - 5.5	5.8 - 6.8	7.0 - 8.5	6.8 - 7.8	5.8 - 6.8
Ultimate strength [MPa]	80 - 90	90 - 100	120 - 135	125 - 135	110 - 125
Ultimate elongation [%]	9.0 - 11.0	10.0 - 12.5	8.0 - 10.0	7.0 - 8.0	5.9 - 6.9
Flexural modulus [MPa]	2900 - 3100	2750 - 2950	2700 - 2900	2580 - 2780	2500 - 2700
Fracture properties Bend notch test (PM 258-0/90)					
Fracture toughness K_1 [MPa√m]	2.1 - 2.3	2.2 - 2.4	0.95 - 1.15	0.85 - 1.05	1.2 - 1.4
Fracture energy G_{1C} [J/m^2]	1250 - 1400	1500 - 1700	340 - 380	250 - 290	420 - 480
Water absorption (ISO 62)					
10 days H_2O 23 °C [%]	0.44 - 0.52	0.48 - 0.55	0.50 - 0.58	0.44 - 0.52	0.54 - 0.62

Handling precautions

Mandatory and recommended industrial hygiene procedures should be followed whenever our products are being handled and processed. For additional information please consult the corresponding product safety data sheets and the brochure "Hygienic precautions for handling plastics products" (Publ. No. 24264/e).

Personal hygiene

Safety precautions at workplace	
protective clothing	yes
gloves	essential
arm protectors	recommended when skin contact likely
goggles/safety glasses	yes
Skin protection	
before starting work	Apply barrier cream to exposed skin
after washing	Apply barrier or nourishing cream
Cleansing of contaminated skin	
	Dab off with absorbent paper, wash with warm water and alkali-free soap, then dry with disposable towels. Do not use solvents
Disposal of spillage	
	Soak up with sawdust or cotton waste and deposit in plastic-lined bin
Ventilation	
of workshop	Renew air 3 to 5 times an hour
of workplaces	Exhaust fans. Operatives should avoid inhaling vapours

First aid

Contamination of the *eyes* by resin, hardener or mix should be treated immediately by flushing with clean, running water for 10 to 15 minutes. A doctor should then be consulted.

Material smeared or splashed on the *skin* should be dabbed off, and the contaminated area then washed and treated with a cleansing cream (see above). A doctor should be consulted in the event of severe irritation or burns. Contaminated clothing should be changed immediately.

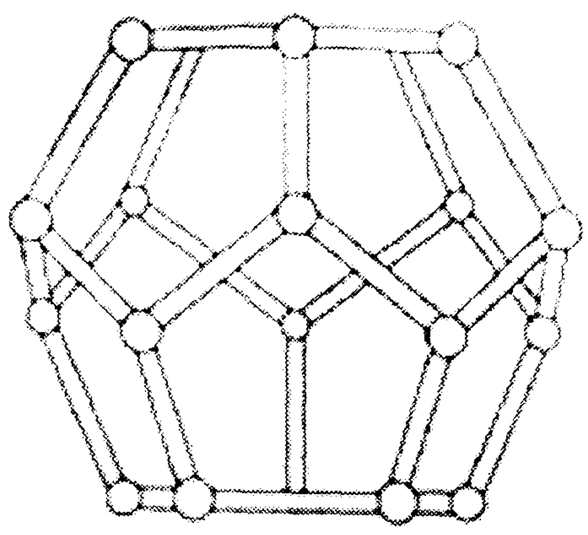
Anyone taken ill after *inhaling* vapours should be moved out of doors immediately.

In all cases of doubt call for medical assistance.

Vantico Ltd.
Advanced Materials
®Registered trademark

APPROVED TO ISO 9001

IMPORTANT: The following supersedes Buyer's documents. SELLER MAKES NO REPRESENTATION OR WARRANTY, EXPRESS OR IMPLIED, INCLUDING OF MERCHANTABILITY OR FITNESS FOR A PARTICULAR PURPOSE. No statements herein are to be construed as inducements to infringe any relevant patent. Under no circumstances shall Seller be liable for incidental, consequential or indirect damages for alleged negligence, breach of warranty, strict liability, tort or contract arising in connection with the product(s). Buyer's sole remedy and Seller's sole liability for any claims shall be Buyer's purchase price. Data and results are based on controlled or lab work and must be confirmed by Buyer by testing for its intended conditions of use. The product(s) has not been tested for, and is therefore not recommended for, uses for which prolonged contact with mucous membranes, abraded skin, or blood is intended; or for uses for which implantation within the human body is intended.



EM26

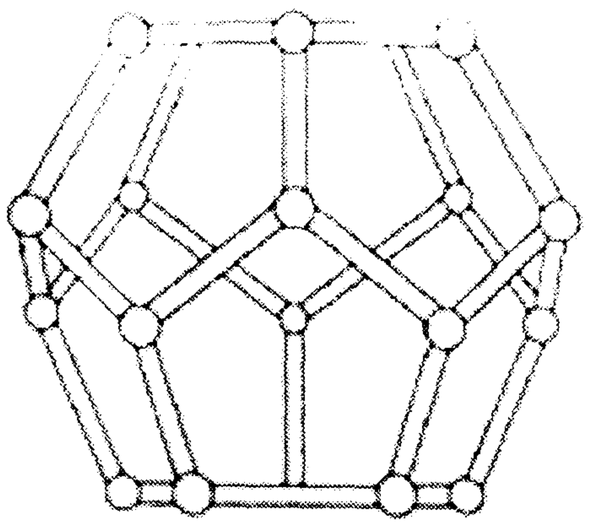
Supazote®

Lightweight supersoft foam
26 kg/m3

ZOTEGRAM

Supazote foam is a closed cell cross-linked copolymer foam available in sheet form. This data characterises the copolymer foam grade EM26 (26kg/m3). The material will thermoform into simple and complex shapes.

Density Skin/Skin (s/s)	EN ISO 845 1995 BS 4443 Pt1 : 2 1988 DIN 53420 1978	kg/m³	26
Recommended operating temperature range	Internal	Max °C	see note
		Min °C	
Compression stress - strain characteristics	EN ISO 3386/1 1997 BS 443 Pt1 : 5a 1988		
25% Compression	DIN 53572 1986	kPA	25
40% Compression		kPA	50
50% Compression		kPA	75
60% Compression		kPA	120
Compression set s/s thickness 72 hrs 50% compression 23°C, ½ hr recovery	EN ISO 1856 1996 BS 4443 Pt1 : 6b 1988 DIN 53572 1986	% set	45
48 hrs 20% compression 23°C, ½			13



EM26

Supazote®

Lightweight supersoft foam
26 kg/m3

ZOTEGRAM

Supazote foam is a closed cell cross-linked copolymer foam available in sheet form. This data characterises the copolymer foam grade EM26 (26kg/m3). The material will thermoform into simple and complex shapes.

Density Skin/Skin (s/s)	EN ISO 845 1995 BS 4443 Pt1 : 2 1988 DIN 53420 1978	kg/m³	26
Recommended operating temperature range	Internal	Max °C	see note
		Min °C	
Compression stress - strain characteristics	EN ISO 3386/1 1997 BS 443 Pt1 : 5a 1988		
25% Compression	DIN 53572 1986	kPA	25
40% Compression		kPA	50
50% Compression		kPA	75
60% Compression		kPA	120
Compression set s/s thickness 72 hrs 50% compression 23°C, ½ hr recovery	EN ISO 1856 1996 BS 4443 Pt1 : 6b 1988 DIN 53572 1986	% set	45
48 hrs 20% compression 23°C, ½			13

RECOMMENDED OPERATING TEMPERATURE RANGE

Supazote foam has been formulated for high dimensional stability and, at temperatures up to 80°C, linear shrinkage is typically 2% or less. However, the material will soften at lower temperatures and properties, such as compression set, will deteriorate significantly at temperatures over 50°C. A low temperature limit of -70°C is advised.